#### **Eastern Washington University**

#### **EWU Digital Commons**

**EWU Masters Thesis Collection** 

Student Research and Creative Works

Spring 2023

## Theoretical epidemiology analysis of Plague, Polio, and Covid-19 outbreak

Vivian J. Goshashy
Eastern Washington University

Follow this and additional works at: https://dc.ewu.edu/theses

#### **Recommended Citation**

Goshashy, Vivian J., "Theoretical epidemiology analysis of Plague, Polio, and Covid-19 outbreak" (2023). *EWU Masters Thesis Collection*. 858.

https://dc.ewu.edu/theses/858

This Thesis: EWU Only is brought to you for free and open access by the Student Research and Creative Works at EWU Digital Commons. It has been accepted for inclusion in EWU Masters Thesis Collection by an authorized administrator of EWU Digital Commons. For more information, please contact jotto@ewu.edu.

## THEORETICAL EPIDEMIOLOGY ANALYSIS OF PLAGUE, POLIO, AND COVID-19 OUTBREAK

A Thesis

Presented To

Eastern Washington University

Cheney, Washington

In Partial Fulfillment of the Requirements for the Degree

Master of Science in Applied Mathematics

By

Vivian J. Goshashy

Spring 2023

#### THESIS OF VIVIAN J. GOSHASHY APPROVED BY

	DATE:
ANDREW OSTER, GRADUATE STUDY COMMITTEE	
	DATE:
FRANK LYNCH, GRADUATE STUDY COMMITTEE	
	DATE:
KRISZTIAN MAGORI, GRADUATE STUDY COMMITTEE	

#### ABSTRACT

## THEORETICAL EPIDEMIOLOGY ANALYSIS OF PLAGUE, POLIO, AND COVID-19 OUTBREAK

by

Vivian J. Goshashy

Spring 2023

Infectious diseases have been a persistent challenge to global health throughout history, and they continue to pose a significant threat in the present day. With the emergence of new diseases and the reemergence of existing ones, understanding the transmission dynamics, and developing effective prevention strategies are critical for public health. Mathematical modeling has proven to be a valuable tool in studying infectious diseases, allowing researchers to simulate and analyze various scenarios to gain insights into disease spread and inform public health policies. This paper provides an overview of the different types of mathematical models utilized in infectious disease modeling, focusing on their application in studying the spread of complex diseases such as Plague, Polio, and Covid-19. Mathematical models can capture the intricacies of disease transmission by incorporating factors such as population demographics, disease characteristics, and intervention strategies. By quantifying these variables, researchers can simulate the dynamics of disease transmission and assess the impact of various interventions, such as vaccination campaigns, social distancing measures, or treatment protocols. To ensure the reliability of these models, statistical techniques are employed to validate their accuracy and assess their goodness of fit to real-world data. Model fitting involves comparing the simulated outputs with observed epidemiological data, allowing researchers to refine their models and improve their predictive capabilities. Moreover, understanding the stability of steady states in these models is crucial in predicting the long-term behavior of an outbreak. By analyzing the stability of these states, researchers can determine whether an outbreak will be self-limiting or persist within the population over time. By studying diseases like Plague, Polio, and Covid-19, this research aims to provide valuable insights into the spread of infectious diseases and contribute to the development of effective intervention strategies. The findings from this study can enhance our understanding of disease transmission dynamics and help inform public health efforts to prevent and control future epidemics. Ultimately, the goal is to minimize the impact of infectious diseases on populations worldwide and ensure the well-being of individuals and communities.

#### **ACKNOWLEDGEMENTS**

I am extremely grateful to Dr. Andrew Oster, Dr. Frank Lynch, and Dr. Krisztian Magori for their exceptional patience and valuable feedback. Their extensive knowledge and vast experience have been a tremendous source of encouragement for me, both academically and in my daily life. Additionally, I would like to express my appreciation to my colleagues for their unwavering support throughout my studies. I am also deeply thankful to all the members of the mathematics department, as their kind assistance and encouragement have made my time in the USA truly wonderful.

#### TABLE OF CONTENTS

	ABS	STRACT	iii
	ACI	KNOWLEDGEMENTS	V
	List of Figures		
	List	of Tables	X
Chapt	er	P	age
1	Int	roduction of Epidemiology Analysis	1
	1.1	Mathematical Modeling of Infectious Diseases	1
	1.2	Analyzing the classical SIR Model	5
	1.3	Model fitting	19
2	Ana	alysis of Plague Outbreak in Europe	22
	2.1	Overview of Plague Disease	23
	2.2	Mathematical Models	32
		2.2.1 Pneumonic Model	32
		2.2.2 Keeling-Gilligan RFT Model	33
		2.2.3 Human-Ectoparasite Model (HET model)	36
		2.2.4 Lynch-Oster RFT Model	40
	2.3	Result Methods	44
		2.3.1 Describing Mathematical Models fits	47
		2.3.2 Examining role of exposed group in Lynch-Oster model	50
	2.4	Discussion	53
3	Ana	alysis of the Hypothesis of Endemic Stability: Polio and	l
	Cox	vid-19	56

Chapte	e <b>r</b> 3.1	Hypot	hesis of Endemic Stability	<b>Page</b> 58
	3.2	Immu	nity: Polio	63
		3.2.1	Overview of Polio Disease	63
		3.2.2	Mathematical Models	68
		3.2.3	Results	81
	3.3	Absen	ce of Immunity and Partial Immunity: Covid-19	98
		3.3.1	Overview of Covid-19	98
		3.3.2	Mathematical Models	100
		3.3.3	Results	139
	3.4	Discus	ssion	175
		3.4.1	Immunity	175
		3.4.2	Absence of Immunity and Partial Immunity	177
4	Con	clusio	n	179
	Ref	erence	s	183
	Vita	a		190

## List of Figures

1.1	SIR Model Transitions	5
1.2	Equilibrium states of the SIR model	10
1.3	Simulation of the classical SIR model	14
1.4	Force of infection and Disease incidence (SIR model)	16
2.1	The Pneumonic model	33
2.2	The Keeling-Gilligan Rat-Flea model	34
2.3	The Human Ectoparasite model	37
2.4	The Lynch-Oster model	42
2.5	Plague mortality fitted models	49
2.6	Examine role of SEID	52
3.1	The relationship between age and disease incidence	59
3.2	Hypothesis variation	60
3.3	Flowchart of the Single Age Class Model with Immunity	71
3.4	Flowchart of the Age Structure Model with Immunity	76
3.5	Single Age Class with Immunity	84
3.6	Total Population of Children and Adults model with immunity	88
3.7	Age Structure Model with Immunity	91
3.8	Force of infection and Disease incidence for the immunity models	95

3.9	Flowchart of Single Age Class Model with Absence of Immunity	103
3.10	Force of Infection and Disease incidence in the $\mathrm{SI}\tilde{R}$ Model $$	108
3.11	Flowchart of Age Structure Model with Absence of Immunity	110
3.12	Flowchart of Age Structure Model with Absence of Immunity	
	without considering transition between age classes	113
3.13	Flowchart of Single Age Class Partial with Immunity model .	116
3.14	Flowchart of Age Structure with Partial Immunity model	120
3.15	Flowchart of Age Structure with Partial Immunity model with-	
	out considering the transition rate	123
3.16	Flowchart of Single Age Class Partial Immunity with births and	
	deaths	126
3.17	Flowchart of Age Structure Model Partial Immunity with Births	
	and Deaths	130
3.18	Impact of Infection Rate on Disease Spread in a Single Age	
	Class Model with Absence of Immunity	142
3.19	Exploring the Impact of Infection Rates on Covid-19 Dynamics:	
	Unveiling Outbreak Patterns in both children and adults	146
3.20	Examining the Influence of Infection Rates on Different Age	
	Groups in the Dynamics of Covid-19	148
3.21	Exploring Re-infection Dynamics: An Enhanced Model for Mul-	
	tiple Infections in COVID-19	152
3.22	The two-age class model with partial immunity no birth nd	
	death processes demonstrates a similar trend to the single age	
	class model, with consistent disease dynamics	156

3.23	Impact of partial immunity on disease dynamics in an age-	
	structured population model without birth and death processes.	
		157
3.24	Exploring the dynamics of the single age class model with par-	
	tial immunity, birth, and death processes unveils interesting in-	
	sights into the interplay between disease transmission, popula-	
	tion dynamics, and immunity	161
3.25	Age structure model with partial immunity and considering	
	birth and death dynamics provides comprehensive insights into	
	disease dynamics across different age groups	165
3.26	Age structure partial immunity model with birth and death	
	dynamics, revealing distinct patterns for children and adults in	
	COVID-19 susceptibility	167
3.27	Comparing Force of Infection in Single Age Class Models: Ab-	
	sence of Immunity vs. Partial Immunity with and without Birth	
	and Death Dynamics	169
3.28	Comparing Force of Infection in Age Structure Models: Absence	
	of Immunity vs. Partial Immunity with and without Birth and	
	Death Dynamics	172

## List of Tables

1.1	Units of the variables and parameters in the SIR model	7
2.1	Plague transmission parameters	39
2.2	Lynch-Oster model parameters	44
2.3	Plague mortality data during Second Outbreak	47
2.4	Plague models comparison	50
2.5	Examining the role of the exposed group	53
3.1	Units of the variables and parameters in the immunity based	
	models	80
3.2	Units of Variables and Parameters in Absence of immunity models.	114
3.3	Units of Variables and Parameters in Partial Immunity Models	
	with and without Births and Deaths	139

### Chapter 1

# Introduction of Epidemiology Analysis

## 1.1 Mathematical Modeling of Infectious Diseases

Infectious diseases have long been a major global health challenge, with new diseases constantly emerging and existing ones are resurging. From history, some of the earliest known infectious diseases include tuberculosis, leprosy, and malaria, which were prevalent in ancient times [1]. Further, in the 14<sup>th</sup> century, an estimated 25 million people in Europe died of the bubonic plague also known as the Black death [2]. In the 19th century, significant progress was made in the understanding and control of infectious diseases. The discovery of bacteria and viruses, and the development of vaccines and antibiotic, helped to prevent and treat many infectious diseases. Despite these advances, infectious diseases still remain a major health challenge, especially

in developing countries. For instance, we have observed new diseases emerging such as HIV/AIDS, Ebola, Polio, and Covid-19, which have negatively impacted the global economy [1] [3] [4] [5].

In the 1950s and 1960s, researchers developed models to understand the transmission dynamics of sexual transmitted infections such as syphilis and gonorrhea diseases and evaluated the impact of different prevention strategies [6]. These models were used to inform public health policies and to design clinical trials of new treatments. Further, these models were adapted and developed in the study of HIV/AIDS transmission in the 1970s and 1980s [6]. Today, scientists use mathematical models to study a wide range of infectious diseases and epidemiology.

Mathematical modeling is used to uncover patterns in epidemics, to extrapolate epidemic behaviors, and to study the effect of interventions such as immunization, quarantine, social distance, and hygiene measures. Mathematical modeling of infectious diseases uses mathematical equations to describe and analyze the spread and control of diseases within populations. These models are set to represent the different classes of individuals in a population such as susceptible, exposed, infected, recovered (asymptomatic or symptomatic), and dead. There are several main types of mathematical models. The most widely studied are SIR type models, which tracks the number of susceptible, infected, and recovered individuals in a populations over time and represents with system of ODEs. In addition, agent-based models are a class of models that simulate the behavior of individual agents such as people or animals and the interactions between them to model disease transmission [7].

In recent times, with the emergence of complex diseases like Covid-19

and intricate transmission patterns, advanced models such as SEID, SIRD, and SIRDSI are being employed to better understand the disease dynamics. The SEID model, for example, allows for the prediction of the number of individuals who are exposed but do not yet show symptoms and tracks the number of either dead or disease (symptomatic), while the SIRD model accounts for the possibility of asymptomatic and symptomatic transmission. The SIRDSI model incorporates the concept of immunity decay, where individuals who have recovered from the disease may become susceptible to infection again after a certain period of time. Furthermore, these models are adaptable to investigate the spread of other infectious diseases, such as plague and polio, which had caused major outbreaks in different regions, such as Europe and United States. By utilizing these models, we gain a deeper understanding of the transmission patterns of infectious diseases and develop strategies to control their spread. We then validate models using statistical techniques like Markov Chain Monte Carlo and look at their measures such as Bayesian Inference Criterion (BIC) and root mean squared error (RMSE) and allows for an assessment of their goodness of fit and comparison of their performance. Moreover, mathematical models are used to determine the stability of the steady states. Stability of the steady states provides information about whether an outbreak will be selflimiting or will persist in the population over time. Stability of steady states allows scientists to predict the long-term behavior of a disease outbreak. We will investigate the classical SIR model and determine the stability. This analysis is valuable for public health officials in determining if an outbreak is self-limiting. In such cases, they can focus on implementing short-term measures to reduce transmission and control the outbreak until it subsides. On the other hand, if an outbreak is predicted to become pandemic; then, they would need to focus on long-term interventions and measures to prevent the spread of the disease in the population.

This project aims to provide insights into the spread of infectious diseases and determining the most effective interventions to avoid an epidemic outbreak. This is going to be achieved by considering various mathematical models of a selection of infectious diseases and fitting them to the available data. However, these models are based on assumptions about disease transmission; thus, their accuracy depends on the quality of the data used to build them and the assumptions made. Our goal is that the findings from this research will enhance our knowledge of how infectious diseases spread and potentially aid in efforts to prevent their spread.

#### 1.2 Analyzing the classical SIR Model

The classical SIR model is a widely used mathematical model used to study the spread of infectious diseases in a population [8]. The model assumes that the population can be divided into three compartments: Susceptible (S), Infected (I), and Recovered (R), with the total population size N = S + I + R assumed to be constant, and individuals can move from one compartment to another over time. The classical SIR model is based on several key assumptions, individuals can only leave the susceptible group by being infected and infected individuals can leave the infected group if they recover from the disease and acquired immunity. Further, we assume that people in the population make random contact with one another, and there is a closed system such that the population neither increases nor decreases. Lastly, there is no vaccination [8] [9].



Figure 1.1: SIR Model Transitions - Illustration of inward and outward transitions in a classical SIR model. The model captures the movement of individuals between compartments, with inward transitions positively influencing the rate of change and outward transitions negatively impacting it.

#### System of ODEs and Initial Conditions

The rate of change of the three populations (S, I, R) in the model is described by a system of ordinary differential equations. The number of susceptible individuals at time t is denoted as S(t), the number of infected individuals as I(t), and the number of recovered individuals as R(t). The rate of change of these populations over time can be described by the following system of differential equations.

$$\frac{dS}{dt} = -\beta S(t)I(t)$$

$$\frac{dI}{dt} = \beta S(t)I(t) - \lambda I(t)$$

$$\frac{dR}{dt} = \lambda I(t)$$
(1.1)

The specific description of the SIR model is shown above where  $\beta$  represents the transmission rate and  $\lambda$  is the recovery rate. In our model, we would want to have I(t) = 0. This means that there is disease free equilibrium.

Our initial conditions are:

$$S(0) = S_0 > 0, I(0) = I_0 \ge 0, R(0) = 0$$
(1.2)

The classical SIR model has only three compartments; thus, the rates of change of these compartments must sum up to the total rate of change of the population. The law of conservation is then used to understand whether the total population is conserved or not. From the total populations size, we know that N = S + I + R. By taking derivative of both sides with respect to time, we get [8] [10]:

$$\frac{dN}{dt} = \frac{dS}{dt} + \frac{dI}{dt} + \frac{dR}{dt} = -\beta S(t)I(t) + \beta S(t)I(t) - \lambda I(t) + \lambda I(t) = 0 \quad (1.3)$$

The equation describes that the total rate of change of the population is equal to the sum of the rates of change of the three compartments. We observe that  $\frac{\partial N}{\partial t} = 0$ , this means that the total populations is conserved. The coservation law help us to understand the dynamics of the disease transmission and to identify factors that contribute to its spread [8].

Variable	Description	$\operatorname{unit}$
$\beta$	Transmission rate	people * days
$\lambda$	Recovered rate	$\frac{1}{\text{days}}$
t	Time	$\operatorname{days}$
S	Number of susceptible people	people
I	Number of infected people	people
R	Number of recovered people	people
N	Total number of people	people

Table 1.1: Units of the variables and parameters in the SIR model.

#### Dimensional Analysis

Here we want to reduce the number of parameters and make the model dimensionless. We focus on the Infected population, then the important parameter would be transmission rate which affects the qualitative behavior of the solutions. We assume that time is measured in days, then we use the differential equations 1.1 to determine the units carried by each of the variables and parameters in the model.

From the equation in the models, we observe that the left-hand side have dimensions of number of people per time. This is also true for every term in the equations. Further, we define new variables, x(t) as the fractional of the population in the susceptible class and y(t) as the fractional of the population in the infected class [8].

Now, we define arbitrary dimensionless variables,

$$x = \frac{S}{N}, y = \frac{I}{N}, \tau = \frac{t}{\frac{1}{\mu}} = t * \mu$$
 (1.4)

Using equation N = S + I + R, it follows that

$$\frac{S}{N} + \frac{I}{N} = \frac{N}{N} = x + y = 1$$

Next, we substitute equation 1.4 into the model equations,

$$S = xN, I = yN, t = \frac{\tau}{\mu} \tag{1.5}$$

This leads to,

$$\frac{d(xN)}{d(\frac{\tau}{\mu})} = -\beta(xN)(yN)$$
$$\frac{d(yN)}{d(\frac{\tau}{\mu})} = \beta(xN)(yN) - \lambda(yN)$$

We cancel the common factors N and  $\mu$  on both sides,

$$\frac{dx}{d\tau} = -\frac{\beta N}{\mu} xy$$

$$\frac{dy}{d\tau} = \frac{\beta N}{\mu} xy - \frac{\lambda}{\mu} y$$

We notice that the equation contains two remaining ratio of parameters that we denote by the notations

$$R_0 = \frac{\beta N}{\mu}$$
 and  $M_0 = \frac{\lambda}{\mu}$ 

We observe that these two are important quantities such that  $R_0$  is the basic reproductive number. Thus, we rewrite our equations by substituting new variables,

$$\frac{dx}{d\tau} = -R_0 xy$$

$$\frac{dy}{d\tau} = R_0 xy - M_0 y$$
(1.6)

#### Identifying Steady States

Steady states show the equilibria of the equations. To determine whether we have a disease-free equilibrium or a disease endemic state, we need to determine steady states of the model. Let us observe equations 1.6. For steady state to occur, we need  $\frac{dx}{dt} = 0$  and  $\frac{dy}{dt} = 0$ . Here we look at the equation above that involves y and we use this equation to determine when y = 0 and when  $y \neq 0$ . Therefore, using equations 1.6, we then have two steady states; disease free-equilibrium and disease endemic state. The two equilibrium points of the system are as follows [8]:

Here, we want I=0. Since, x+y=1 by conservation law, this leads to x=1-y. If we substitute x to  $\frac{dy}{d\tau}$  from equation 1.6, leads to

$$\frac{dy}{d\tau} = R_0(1-y)y - M_0y = y[(R_0 - M_0) - R_0y]$$

Steady states satisfy  $\frac{\partial y}{\partial \tau} = 0$ . Thus,  $y[(R_0 - M_0) - R_0 y] = 0$ .

**1.Disease-free equilibrium points:** A solution is observed where y = 0 and, due to conservation, x = 1. This solution corresponds to a pop-

ulation without any infected individuals, leading to I(t) = 0 and S(t) = N, where N denotes the total population size.

2. Disease Endemic equilibrium points: If the steady state of a classical SIR model has non-zero infected individuals, i.e.,  $I \neq 0$ , then the value of x at the steady state is equal to  $\frac{M_0}{R_0}$  due to the conservation of the total population size. Additionally, y at the steady state is equal to  $1 - \frac{M_0}{R_0}$ . This implies that the disease is widely spread in the population.

A steady state is biologically feasible only if the reproductive number of the disease, denoted by  $R_0$ , is greater than 1. In such a case, the disease is considered to be endemic, and the steady state with non-zero infected individuals is stable. On the other hand, if  $R_0 < 1$ , the only biologically feasible steady state is the disease-free state where  $x_0 = 0$ , and the disease is eradicated.

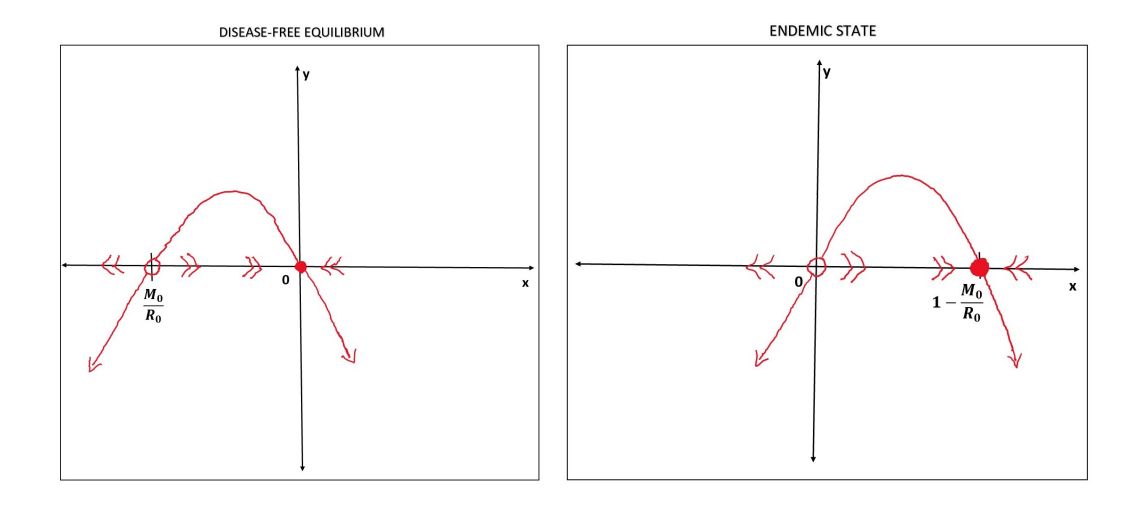


Figure 1.2: In the left hand side figure,  $R_0 < 1$  and  $M_0 > R_0$ , such that we have a disease-free equilibrium. The right hand side figure  $R_0 > 1$  and  $M_0 < R_0$ , the disease is at endemic state.

#### Stability Analysis

To assess the stability of a system, we examine the Jacobian matrix, defined as:

$$\mathbf{J}_{(x,y)} = egin{bmatrix} rac{df_x}{dt} & rac{df_y}{dt} \ rac{dg_x}{dt} & rac{dg_y}{dt} \end{bmatrix}$$

The functions f(x,y) and g(x,y) in the Jacobian matrix represent the rates of change of x and y with respect to time t. The Jacobian matrix helps us to analyze the local behavior of the system around a specific point. By calculating the determinant and trace of the Jacobian matrix, we can determine the stability of the system.

By calculating the determinant and trace of the Jacobian matrix, we can make determinations about the system's stability. The determinant reveals insights into the local stability of the system. If the determinant is positive, it suggests that the system is stable, indicating that small perturbations around the steady state will eventually converge back to it. Conversely, a negative determinant implies an unstable system, where perturbations may grow over time, leading to unpredictable behavior.

The trace of the Jacobian matrix is the sum of the diagonal elements and can be used to identify the type of stability, such as stable nodes or unstable saddles. For example, if the trace is negative and the determinant is positive the equilibrium point is a stable node, indicating that the system will converge towards that point from nearby initial conditions. Eigenvalues of the Jacobian matrix also provide insights into the stability of the system. The eigenvalues can be used to classify the equilibrium point as stable or unstable, and the sign of the real part of the eigenvalues determines the nature of the

stability, such as oscillatory or asymptotic. By analyzing the eigenvalues of the Jacobian matrix, we can gain a deeper understanding of the behavior of the system near the equilibrium point.

Using the system of equations from dimensionless equations, we have,

$$\mathbf{J}_{(x,y)} = \begin{bmatrix} -R_0 y & -R_0 x \\ R_0 y & R_0 x - M_0 \end{bmatrix}$$

#### 1. Disease-free equilibrium points

$$\mathbf{J}_{(x,y)} = \mathbf{J}_{(1,0)} = \begin{bmatrix} 0 & -R_0 \\ 0 & R_0 - M_0 \end{bmatrix}$$

we observe that

$$|J| = \mathbf{det}|J| = 0$$

with

$$\beta = tr(J) = R_0 - M_0 < 0$$

and  $\lambda = 0$ .

This indicates that the equilibrium point is a saddle node.

#### 2. Disease Endemic equilibrium points

Evaluating the Jacobian matrix at the equilibrium  $(\frac{M_0}{R_0}, \frac{R_0 - M_0}{R_0})$ , we find

$$\mathbf{J}_{(\frac{M_0}{R_0}, \frac{R_0 - M_0}{R_0})} = \begin{bmatrix} M_0 - R_0 & -M_0 \\ \\ M_0 - R_0 & 0 \end{bmatrix}$$

It follows that

$$|J| = \det|J| = -M_0^2 + M_0 R_0 < 0$$

with

$$\beta = tr(J) = M_0 - R_0 > 0$$

and 
$$\lambda_{1,2} = \frac{M_0}{2} - \frac{R_0}{2} \pm \frac{\sqrt{-(M_0 - r_0)(3M_0 + r_0)}}{2}$$
.

Therefore, this equilibrium point is a saddle node.

#### **Numerical Simulation**

The classical SIR model is commonly used to simulate the behavior of a population during a disease outbreak. In order for an outbreak to occur, at least one individual in the population must be infected with the disease. Transmission of the disease is believed to occur through close contact between individuals in the population. In this model, we assume that the population size is N=1000 people, the initial number of infected individuals is I(0)=1, the transmission rate is  $\beta=0.2(\frac{1}{days})$ , and the recovery rate is  $\lambda=\frac{1}{10}$  days.

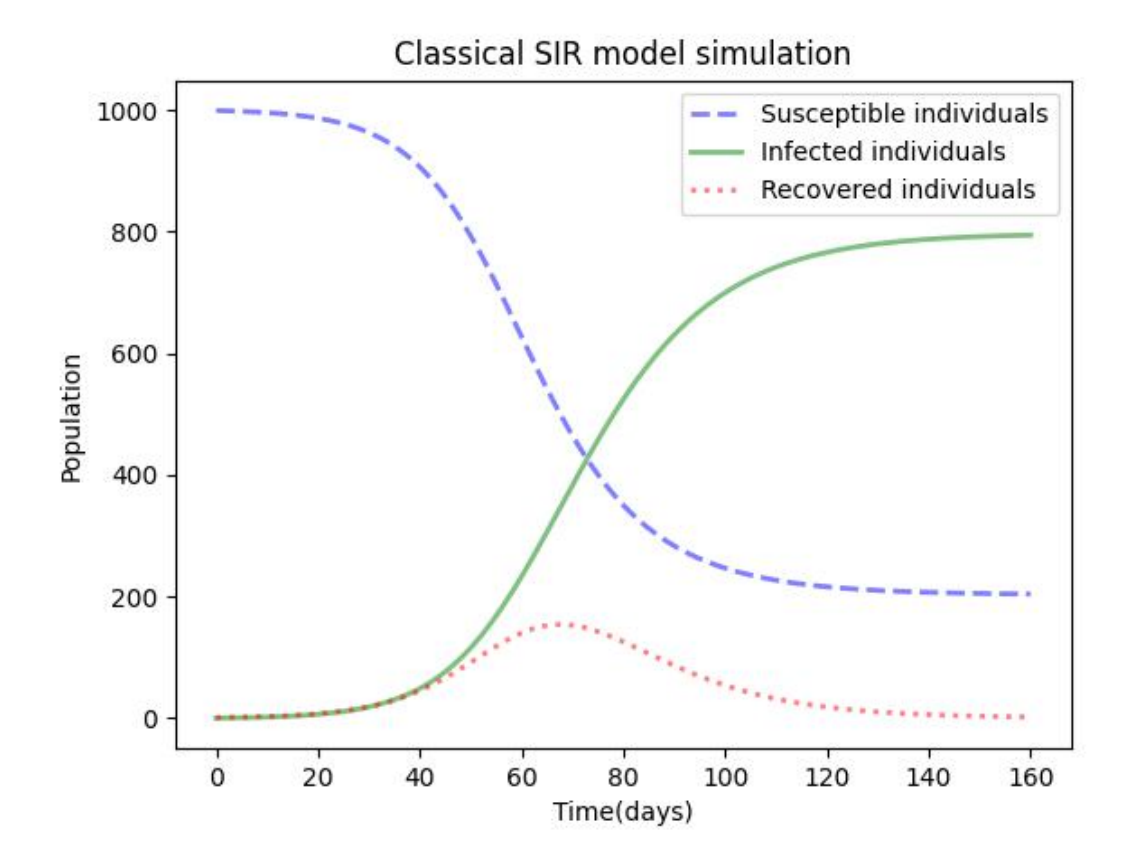


Figure 1.3: Simulation of the classical SIR model demonstrates the temporal evolution of susceptible, infected, and recovered individuals in a population. As time progresses, the number of susceptible individuals gradually decreases, while the number of infected individuals increases. The rate of deaths caused by the disease follows the trend of the infected population, at a slower pace. This simulation was conducted with a transmission rate  $(\beta)$  of 0.2  $\frac{1}{\text{day}}$  and a recovery rate  $(\lambda)$  of  $\frac{1}{10}$  days, reflecting the dynamics of the disease spread and recovery.

Figure 1.3 shows that as time progresses, the number of susceptible individuals in the population decreases while the number of infected individuals also increases. In addition, the number of recovered individuals also increases, although at a much slower rate than the number of infected individuals. This simulation provides insight into how each population group changes over time during an outbreak. Such information can be used to devise strategies to re-

duce the spread of the disease, with the ultimate goal of increasing the number of susceptible or immune individuals in the population.

It should be noted that the classical SIR model has limitations and assumptions. For instance, it assumes a homogeneous population, constant population size, and a fixed transmission rate. Despite these limitations, it remains a useful tool for understanding the dynamics of disease spread in populations.

#### Force of infection and Disease incidence

The force of infection (F) is an important epidemiological concept that measures the rate at which susceptible individuals acquire a disease within a population and is influenced by various factors such as the pathogen's virulence, host susceptibility, and effectiveness of control measures. Disease incidence is a measure of the frequency of new cases of a disease within a defined population over a specific period, providing insight into the occurrence and spread of infectious diseases and estimating the risk of acquiring the disease within the population.

The average force of infection, denoted as  $(\tilde{F})$ , is calculated by integrating the product of the transmission rate  $(\beta)$  and the number of infectious individuals (I) over a specific time period (T). This integral is then divided by the product of the total population size (N) and the duration of the time period (T). Essentially, it provides an average value of the force of infection over time.

$$\tilde{F} = \frac{\int_0^T (\beta I)dt}{NT} \tag{1.7}$$

Similarly, the average disease incidence, denoted as  $(\tilde{D})$ , is obtained by integrating the product of the recovery rate  $(\lambda)$  and the number of infectious individuals (I) over a specific time period (T). This integral is also divided by the product of the total population size (N) and the duration of the time period (T). It provides an average value of the disease incidence over the given time frame.

$$\tilde{D} = \frac{\int_0^T (\lambda I)dt}{NT} \tag{1.8}$$

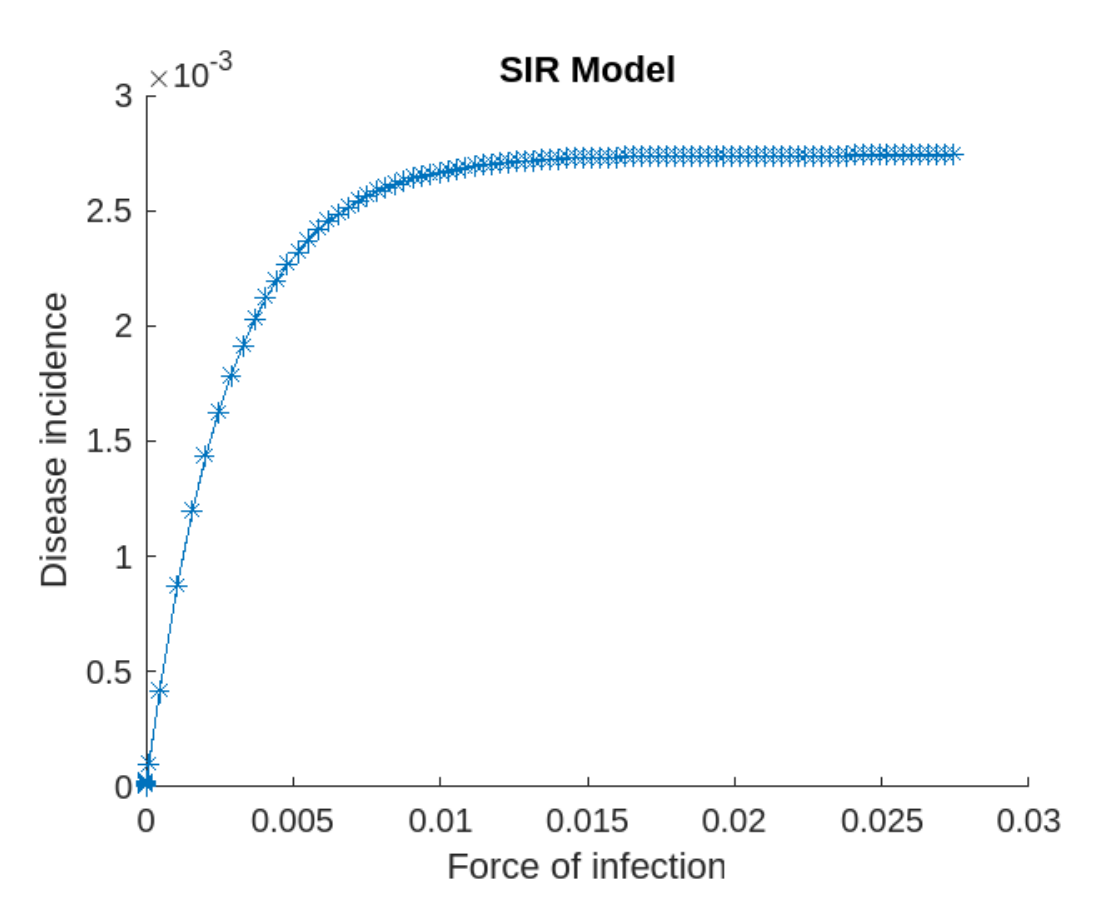


Figure 1.4: The force of infection (F) and disease incidence over time during a simulated disease outbreak using the classical SIR model. The total population size is 1000 individuals, with an initial infected population of 1 person. The recovery rate is set at 1/10, while the transmission rate varies between 0 and 100 with a time step of 1.

Over time, the dynamics of infection and disease incidence follow distinct patterns. Initially, when the transmission rate of a disease is low, both the force of infection (the rate at which susceptible individuals become infected) and disease incidence (the number of new cases) remain relatively low. This is because the disease is not spreading rapidly, and only a small portion of the population is affected.

However, as the transmission rate increases during a certain period of time, more individuals become infected, leading to a higher force of infection. This means that a larger proportion of susceptible individuals are being exposed to the disease, resulting in a relative increase in disease incidence. The number of new cases rises, reflecting a growing outbreak.

As the outbreak progresses, the force of infection and disease incidence may continue to increase, reaching a peak. The specific dynamics of the outbreak, such as the effectiveness of control measures or the development of natural immunity, will influence whether the increase in transmission eventually slows down.

If effective control measures are implemented or a significant portion of the population develops natural immunity. As a result, disease incidence reaches a plateau, where the number of new cases remains relatively constant over time. This plateau signifies a phase of the outbreak where the disease is no longer rapidly spreading, and the number of infected individuals remains fairly consistent.

Figure 1.4 illustrates these patterns, showcasing the relationship between the force of infection and disease incidence throughout the course of the outbreak. It visually demonstrates the initial low levels, the increase during

the outbreak, and the subsequent stabilization or decline depending on the control measures and immunity factors involved. This idea is going to be reintroduce in chapter 3 such that we examine criteria for endemic stability of Polio and Covid-19 disease.

#### 1.3 Model fitting

#### Markov-Chain Monte-Carlo Simulation (MCMC)

MCMC is a powerful Bayesian method used for estimating the distribution of parameters by randomly sampling them from a probabilistic space. This technique is particularly useful in epidemiology models where there are numerous unknown parameters. The distribution of parameters provides a mathematical representation of all possible values of parameters and their likelihood of occurrence [11] [12]. MCMC algorithms are iterative processes where the future state depends on the current state process. The sequence of events that are probabilistically related to one another, and the succession of these steps is known as a Markov Chain. probability [11] [13]. Markov Chains are used in MCMC to generate a sequence of parameter samples that represent the posterior distribution of the parameters. By sampling from the posterior distribution, we can estimate the most likely values of the parameters and quantify the uncertainty associated with these estimates [11].

The MCMC method enables the estimation of parameters such as means, variances, expected values, and exploration of the posterior distribution of Bayesian models. Monte Carlo simulations refer to a technique that involves sampling many random values from a posterior distribution of interest. This process involves repeatedly generating random numbers to observe how fixed parameters are estimated. Monte Carlo simulations provide an approximation of a parameter when it is impossible or prohibitively expensive to calculate it directly [12] [11].

In epidemiology, the MCMC technique is commonly utilized to fit de-

terministic models to observed data and estimate unknown parameters. Typically, these models have a time-step of one day or one week, and the likelihood of the observed data given the model parameters is evaluated as the product of Poisson random variables. The prior distributions are often uniformly distributed, and MCMC simulations are employed to derive the posterior distributions. However, MCMC algorithms are sensitive to their initial starting point, and they often require a burn-in or warm-up phase to explore a promising part of the search space. After this phase, prior samples can be discarded, and valuable samples can be collected.

In this process, Metropolis-Hastings's algorithms are used, which involve proposing a probability distribution to sample, then using an acceptance criterion to decide whether the new sample is accepted into the chain or discarded [13]. The acceptance criterion is how likely the proposal distribution differs from the true next-state probability distribution. Model convergence will be assessed using the Gelman-Rubin statistic, commonly used to determine if multiple chains of MCMC simulations have reached convergence and are sampling from the same posterior distribution [14]. The Gelman-Rubin statistic compares the within-chain variance to the between-chain variance of the MCMC samples. If the chains have converged, the within-chain variance should be similar to the between-chain variance. The statistic is calculated by taking the square root of the ratio of the average of the within-chain variances to the pooled variances across all chains. If the Gelman-Rubin statistic is close to 1, it indicates that the chains have converged and are sampling from the same posterior distribution [14].

#### Bayesian Information Criterion (BIC)

BIC is a model selection method that uses the likelihood function and is particularly useful in mathematical modeling when dealing with models that have many parameters. The BIC introduces a penalty term that is proportional to the number of parameters, helping to mitigate the risk of overfitting, specifically:

$$BIC = \ln(n) \times k - 2\ln(\hat{L}),$$

where  $\hat{L}$  represents the maximized value of the likelihood function of the model, n represents the number of data points, and k represents the number of free parameters that need to be estimated.

#### Mean Squared Error (RMSE)

The RMSE (Root Mean Square Error) is a commonly used metric for evaluating the predictive accuracy of quantitative models. It measures the dissimilarity between the predicted values generated by a model and the actual observed values in a dataset. Mathematically, the RMSE is defined as:

$$RMSE = \sqrt{\frac{\sum_{i=1}^{n} (\hat{y}_i - y_i)^2}{n}}$$

In this equation,  $\hat{y}_i$  represents the predicted values,  $y_i$  represents the observed values, and n represents the total number of observations in the dataset. By calculating the RMSE, we can determine how well a model fits the data.

### Chapter 2

# Analysis of Plague Outbreak in Europe

In this chapter, we delve into the dynamics of bubonic plague epidemics using several mathematical models, including the Pneumonic model, Lynch-Oster Rat Flea model, Keeling-Gilligan model, and Human Ectoparasite model. These models allow us to examine how the disease spreads among different populations, such as humans, rats, and fleas.

We begin by discussing the process of parameter estimation for these models. This involves estimating important parameters like transmission rates, carrying capacities, and death rates. To fit the models to observed mortality data from various cities, we employ Bayesian inference techniques. Through this fitting process, we obtain posterior distributions for the model parameters. To assess how well the models fit the observed data, we use metrics such as the Bayesian Information Criterion (BIC) and root mean squared error (RMSE). These metrics help us evaluate the models' ability to capture the observed data and provide a basis for model comparison.

This chapter emphasizes the significance of understanding the assumptions and limitations of the models. Each model has its own specific focus and assumptions, which may involve considering transmission through respiratory systems, flea ecology, contact networks, or rodents. By fitting these models to data from multiple cities, such as Givry, Florence, Eyam, Barcelona, Moscow, and Malta, we can compare the dynamics of plague epidemics across different locations and time periods. This comparison reveals variations in transmission rates and flea ecology, shedding light on the diverse aspects of the disease's spread.

Lastly, we discuss the findings presented in Dean et al.'s paper, which suggests that human ectoparasites were the primary vectors for plague during the second pandemic, including the Black Death. However, in this chapter, we introduce an additional model, the Lynch-Oster model, which explores the population dynamics of rats and fleas over time. By incorporating this model, we present a compelling argument that the pandemic was not solely caused by human ectoparasites but also by infected rats. This highlights the importance of considering multiple factors and populations in understanding the dynamics of bubonic plague epidemics.

#### 2.1 Overview of Plague Disease

#### **Background of Plague Outbreaks**

Plague is an extremely contagious disease that can result in severe illness and fatalities in both humans and animals. It primarily affects wild mammals and can lead to the death of vulnerable rodent species, cats, camels,

and other mammals when it spreads from its reservoir host species. Plague is caused by Yersinia pestis, a bacteria that is primarily found in small mammals and their fleas. The bacteria were first discovered during the 1894 pandemic that originated in China and spread to Hong Kong, where it was identified by a French Pastorian bacteriologist. The pandemic is thought to have occurred due to the spread of infected fleas over long distances, as they were carried by rats and humans along trade routes [15]. The fleas multiplied by feeding on their hosts, biting with increased frequency and agitation, and infested new hosts when the original hosts died. Commensal domestic black rats and brown sewer rats (Rattus rattus and Rattus norvegius) and their fleas (Xenopsylla cheopis) are considered the most important hosts and vectors involved in human outbreaks, but many other flea species can transmit plague [16].

Plague has caused three major outbreaks in human history, each with devastating mortality rates in various nations and continents. These pandemics had different origins and paths of spread. The first plague occurred in 541 AD, starting in central Africa and spreading to Egypt and the Mediterranean Sea. This plague is known as the Justinian plague. The second plague, known as The Black Death, occurred in the 14th century. It originated in Asia, spread to the Crimea, and then Europe and Russia. The Black Death was one of the deadliest pandemics in human history, causing an estimated 75 to 200 million deaths worldwide. It is believed to have originated from gerbils, where it was carried by fleas that infested black rats. The disease then spread to the Crimea, where it was first recorded in the early 1340s. From the Crimea, the Black Death spread rapidly along trade routes and sea ports, eventually reaching Europe and Russia [15].

The third plague began in the mid 19th century, originating in Yunnan,

China, and spreading to Hong Kong and India before spreading worldwide [15]. Advances in technology, such as the expansion of trade routes, allowed goods to be transported faster, which facilitated the establishment of Yersinia pestis cycles worldwide. Countries that were previously free of plague saw outbreaks, such as the United States, which had 61 cases between 1994 and 2003, and 13 cases and 2 deaths in 2006, as well as Madagascar and South America. During the 1990s and 2000s, scientists observed the reappearance of plague in several African countries. Between 2013 and 2018, the World Health Organization reported 2886 cases and 504 deaths in countries such as Madagascar, Uganda, and Tanzania. The recent increase in the number of cases is primarily due to poverty, resulting in poor housing, sanitation, and lack of public health services, which favor outbreaks of plague by increasing rodent populations. In warm climates, rodent flea fertility increases, leading to a rapid increase in the density of the rodent population and subsequent outbreaks of plague. Plague is categorized as a re-emerging disease; it reappears in different regions [15] [17].

#### Plague Types

Plague has similar symptoms to the flu, high fever, chills, malaise, and headache. The incubation period of plague is 2 to 3 days but may be as long as 6 days [15]. Further, symptoms of plague mostly depend on how the patient was exposed to the disease. There are three main clinical forms of plague depending on type of infection. These are,

#### 1. Bubonic plague

This type of plague, known as bubonic plague, is primarily transmitted through the bites of infected fleas vector carrying the bacterium Yersinia pestis. When an infected flea bites a person, the bacteria enter the body at the site of the bite and travel through the lymphatic system to the nearby lymph nodes, where they begin to replicate. As the bacteria multiply, the affected lymph nodes become inflamed and painful. Eventually, the lymph nodes can develop into open sores filled with pus [18] [2].

The symptoms of bubonic plague typically appear within the first week after infection, resulting in an incubation period of approximately 2 to 8 days [15]. Patients infected with bubonic plague may experience symptoms such as fever, headache, chills, weakness, and swollen and painful lymph nodes in the affected area. If left untreated with appropriate antibiotics, the bacteria can potentially spread to other parts of the body, leading to more severe forms of the disease.

It is important to note that while bubonic plague is primarily transmitted through flea bites, there are other forms of plague transmission as well, such as through respiratory droplets or direct contact with infected animals or their tissues. Each form of transmission may lead to different clinical presentations and manifestations of the disease. Early diagnosis and prompt treatment with antibiotics are crucial in managing and controlling bubonic plague. Timely intervention can help prevent the progression of the infection and reduce the risk of complications or the spread of the disease to other individuals.

2. Pneumonic plague Bubonic plague, if left untreated, can progress to a more severe form called pneumonic plague. Pneumonic plague occurs when the Yersinia pestis bacteria spread from the initial site of infection, such as the lymph nodes, to the lungs. Unlike bubonic plague, which is primarily transmitted through flea bites, pneumonic plague has the potential for person-to-person transmission through infectious respiratory droplets [2]. The incubation period for pneumonic plague is typically shorter, ranging from 1 to 3 days [18]. This rapid onset of symptoms distinguishes pneumonic plague from bubonic plague. Pneumonic plague has a higher mortality rate compared to bubonic plague, making it a more severe and life-threatening form of the disease.

When pneumonic plague is not promptly diagnosed and treated, it can lead to respiratory shock or failure, further exacerbating the severity of the condition. However, if pneumonic plague is detected early and appropriate antibiotic treatment is initiated within the first day of symptom onset, the recovery rates can be high. It is important to note that pneumonic plague is the only form of plague that can be transmitted directly from person to person through respiratory droplets. This mode of transmission poses a significant risk of rapid disease spread within communities or populations [17].

Efforts to control pneumonic plague involve early detection of cases, isolation and treatment of infected individuals, and the implementation of preventive measures to limit person-to-person transmission. In outbreak situations, public health interventions such as contact tracing, quarantine measures, and the administration of prophylactic antibiotics to close contacts may be necessary to prevent further spread of the disease [15].

#### 3. Septicemic plague

Septicemic plague is an extremely severe form of bacterial infection caused by Yersinia pestis. It can be transmitted to humans through the bloodstream, primarily as a result of mishandling infected animals or being bitten by fleas that carry the bacteria [2].

The symptoms of septicemic plague can vary, but commonly include fever, chills, extreme weakness, abdominal pain, shock, and bleeding into the skin and other organs. In severe cases, patients may experience tissue necrosis, which leads to the death of tissues and can result in blackening of affected areas, particularly in the extremities such as the toes, fingers, and nose [18].

#### Mechanisms of Spread

Plague is an endemic disease in various wildlife species. Rats and fleas are considered major hosts in carrying the plague between reservoirs and people. The transmission of plague primarily takes place in rural and semi-rural areas characterized by poor sanitation and high rodent populations. The disease can be transmitted to humans through the following means:

#### 1. Animal-Human Transmission

Humans can become infected with the plague through various means. One mode of transmission is by consuming infected animals, such as guinea pigs or camels, which serve as reservoirs for the disease [18]. Another way transmission can occur is through the handling of tissues or body fluids of infected animals. For example, if a hunter kills an infected rabbit without proper protection, the fleas on the rabbit may transfer to the hunter, resulting in plague transmission [19].

A range of animals can be affected by the plague, including rats, mice, squirrels, rabbits, prairie dogs, chipmunks, and camels in rural areas. In

1994, for instance, a sick camel in Saudi Arabia led to five human cases of plague and two deaths. The disease was transmitted to humans who had consumed the camel's meat. Similarly, in 2002, an individual who had hunted and skinned a sick wildcat contracted the plague disease [19]. Domestic animals like dogs and cats can also contract the plague by being bitten by infected fleas or by consuming rodents infected with the disease. These infected domestic animals can then transmit the disease to humans [18] [19]. Therefore, people who handle domestic animals such as cats and dogs are at a higher risk of exposure to the disease if the animals are infected. Transmission occurs when the infected animal's blood comes into contact with broken skin on the human body [17].

#### 2. Human-Human Transmission

In addition to the previously mentioned modes of transmission, plague can also spread through direct respiratory droplets. This occurs when an infected person coughs or sneezes, releasing droplets into the air that can be breathed in by susceptible individuals, leading to the transmission of the plague [2].

When an infected person coughs or sneezes, respiratory droplets containing the bacteria Yersinia pestis can be expelled into the surrounding environment. These droplets may contain viable bacteria and can travel through the air for a certain distance, depending on various factors such as air currents and environmental conditions. If a susceptible person is in close proximity to the infected individual or within the range of these respiratory droplets, they can inhale the contaminated droplets into their respiratory system, potentially leading to infection [15].

Respiratory transmission of the plague is of particular concern in crowded or close-contact settings, such as households, healthcare facilities, or densely populated areas. It highlights the importance of implementing measures to prevent the spread of respiratory droplets, such as maintaining good respiratory hygiene, practicing cough etiquette (covering the mouth and nose with a tissue or elbow when coughing or sneezing), and wearing appropriate personal protective equipment when caring for infected individuals.

#### 3. Flea-Human Transmission

Humans can contract the plague through flea bites, particularly in rural areas where wildlife rodent species are present. In these regions, warm climates, coupled with factors such as poor sanitation and high rodent populations, create an environment conducive to flea infestations. People in these areas are at an increased risk of being bitten by infected fleas, leading to the transmission of the plague [18].

Fleas serve as important vectors in the transmission of the plague. They can acquire the Yersinia pestis bacteria by feeding on infected animals, typically rodents, which act as reservoir hosts. Once the fleas become infected, they can transfer the bacteria to humans through their bites. In rural settings, where close contact between humans and wildlife rodents is more likely, the risk of flea bites and subsequent plague transmission is higher [2].

The transmission of plague through flea bites is influenced by various factors. For instance, individuals in rural areas may have their legs and feet exposed due to traditional clothing practices or lack of protective measures. This increases the chances of flea bites directly on the skin, providing an entry point for the bacteria. Additionally, warm climates in developing countries create an environment where fleas thrive, further increasing the risk of exposure to fleabites [19].

Prevention of flea bites is crucial in reducing the risk of plague transmission. Measures such as wearing protective clothing, using insect repellents, and maintaining good personal hygiene can help minimize exposure to fleas. Controlling rodent populations and implementing flea control strategies in both domestic and wildlife settings are also important in reducing the reservoir of infected fleas.

# 2.2 Mathematical Models

Mathematical modeling has proven to be a valuable tool in studying the transmission dynamics of plague during past epidemics. Earlier epidemiological models of the Black Death primarily focused on the spread of the disease through commensal rats during a single outbreak. However, in this study, we present a comparison of two models that consider both the rat-flea route and human ectoparasite transmission.

Our main objective is to gain a comprehensive understanding of the transmission dynamics of plague during European epidemics by applying these models to six outbreak scenarios from the Second Pandemic. By analyzing these outbreaks, we aim to identify the most appropriate model for each situation. Through this analysis, we can enhance our understanding of the intricate mechanisms of plague transmission and its impact on the dynamics of epidemics. By examining the different routes of transmission and their corresponding models, we can gain valuable insights into the factors influencing the spread of the disease and its variations across different outbreaks.

#### 2.2.1 Pneumonic Model

The pneumonic model in our study aims to depict the transmission dynamics of the plague disease from one human to another. This model is built upon the classical SIR framework, utilizing similar assumptions and employing a set of differential equations (2.1, 2.2, and 2.3) to describe the dynamics of the disease. The initial conditions for the model are defined by equation 1.2, providing the starting point for the simulation and analysis of plague transmission.

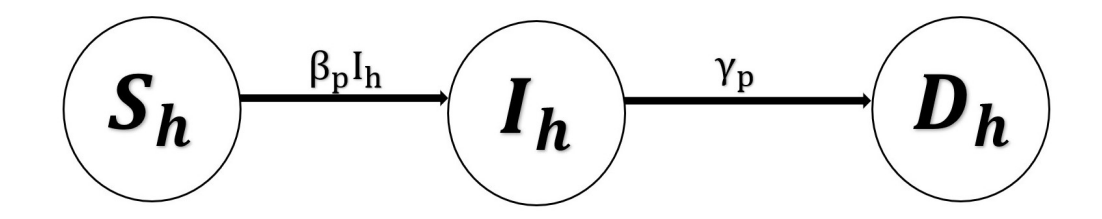


Figure 2.1: The pneumonic model is unique because it allows individuals to transition between different categories without considering recovery phase. This model specifically focuses on the human-to-human transmission of the bubonic plague, a highly infectious disease caused by the bacterium Yersinia pestis.

$$\frac{dS_h}{dt} = -\beta_p \frac{S_h I_h}{N_h},\tag{2.1}$$

$$\frac{dI_h}{dt} = \beta_p \frac{S_h I_h}{N_h} - \gamma_p I_h, \tag{2.2}$$

$$\frac{dD_h}{dt} = \gamma_p I_h \tag{2.3}$$

The pneumonic model has three compartments for humans:  $S_h$ ,  $I_h$ , and  $D_h$ . The total human population is  $N_h = S_h + I_h$ . Recovered individuals are not included in the model since untreated pneumonic plague has a very high fatality rate. The transmission of pneumonic plague from human to human occurs at a rate of  $\beta_p$ . The disease-induced mortality rate is  $\gamma_p$  per day and is equal to the inverse of the mean infectious period of pneumonic plague, which is about 2.5 days [2].

# 2.2.2 Keeling-Gilligan RFT Model

Keeling and Gilligan developed a metapopulation model to study the transmission dynamics of bubonic plague. This model incorporates 10 differential equations and focuses on the transmission of the disease from rodent epizootics to humans [20]. It provides a comprehensive representation of the disease's transmission dynamics, including the spillover effect. The spillover effect is the transmission of the plague from its natural reservoir hosts, such as rodents, to humans. It occurs when the bacterium Yersinia pestis, which is responsible for causing the plague, is transmitted from infected animals to humans, resulting in human cases of the disease.

By incorporating the spillover effect into their metapopulation model, Keeling and Gilligan were able to capture the complex dynamics of disease transmission between different populations. This comprehensive approach allows for a better understanding of how the plague spreads from rodent populations to human populations and provides insights into the factors that contribute to the disease's persistence and spread in different environments.

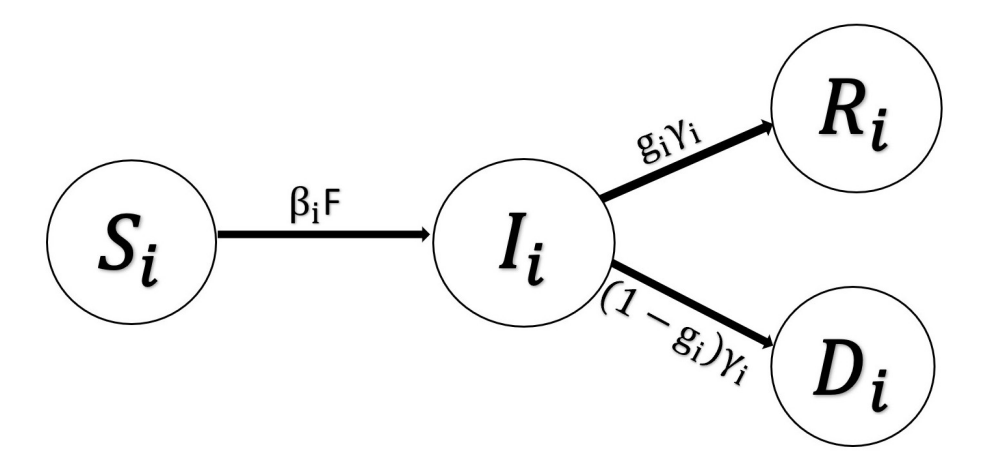


Figure 2.2: The model is based on the Keeling-Gilligan Rat-Flea-Transmission model, which takes into account both rat-flea and rat-human transmission. It involves a continuous flow of individuals moving in and out of different compartments, thereby providing a more detailed and comprehensive representation of the transmission dynamics.

$$\frac{dH}{dt} = r_f H (1 - \frac{H}{K_f}) \tag{2.4}$$

$$\frac{dF}{dt} = (1 - g_r)\gamma_r I_r H - d_f F \tag{2.5}$$

$$\frac{dS_i}{dt} = -\beta_i \frac{S_i F}{N_i} (1 - e^{-aN_i}) \tag{2.6}$$

$$\frac{dI_i}{dt} = \beta_i \frac{S_i F}{N_i} (1 - e^{-aN_i}) - \gamma_i I_i \tag{2.7}$$

$$\frac{dR_i}{dt} = g_i \gamma_i I_i \tag{2.8}$$

$$\frac{dD_i}{dt} = (1 - g_i)\gamma_i I_i \tag{2.9}$$

For each sub-category, namely rats and humans, there are four compartments, denoted by  $S_r$ ,  $I_r$ ,  $R_r$ , and  $D_r$  for rats and  $S_h$ ,  $I_h$ ,  $R_h$ , and  $D_h$  for humans. The rat population is assumed to be highly susceptible to the disease, and we start with an entirely susceptible population of black rats (Rattus rattus) [20]The infection is transmitted through infected fleas, which are represented by the variable F. The infection mechanism involves infected fleas randomly searching for a new rat host within a given time period. If an infected flea encounters a susceptible rat, there is a probability, denoted by  $\beta_r$ , that the rat becomes infected. The parameter a measures the efficiency of flea searching. Rats transition out of the infected class at a rate of  $\gamma_r^{-1}$ , and a fraction of them, denoted by  $g_r$ , survive and become resistant, while the rest die and release their infected fleas back into the environment.

The dynamics of the rat fleas are modeled by two variables, namely the average number of fleas per rat (H) and the number of free infectious fleas (F) that are actively searching for a host. In the absence of bubonic plague, the flea index H follows a logistic growth model, with a carrying capacity

of  $K_f$ . The increase in the average flea index due to free fleas finding new rat hosts is represented by the other term in the differential equation for H. When an infected rat dies, free infected fleas are released into the environment, releasing on average H fleas. Free fleas are assumed to die from starvation at a rate of  $d_f$  [20]. The model also focuses on the human population, which is divided into four compartments  $(S_h, I_h, R_h, \text{ and } D_h)$ , with a total population of  $N_h = S_h + I_h + R_h$ . The birth and death rates are assumed to be independent of population density [20].

## 2.2.3 Human-Ectoparasite Model (HET model)

The analysis of the model involves the use of seven differential equations to describe the spread of bubonic plague through a human ectoparasite vector, such as body lice or human fleas. Thus, transmission of bubonic plague via these vectors is effectively modeled [2].

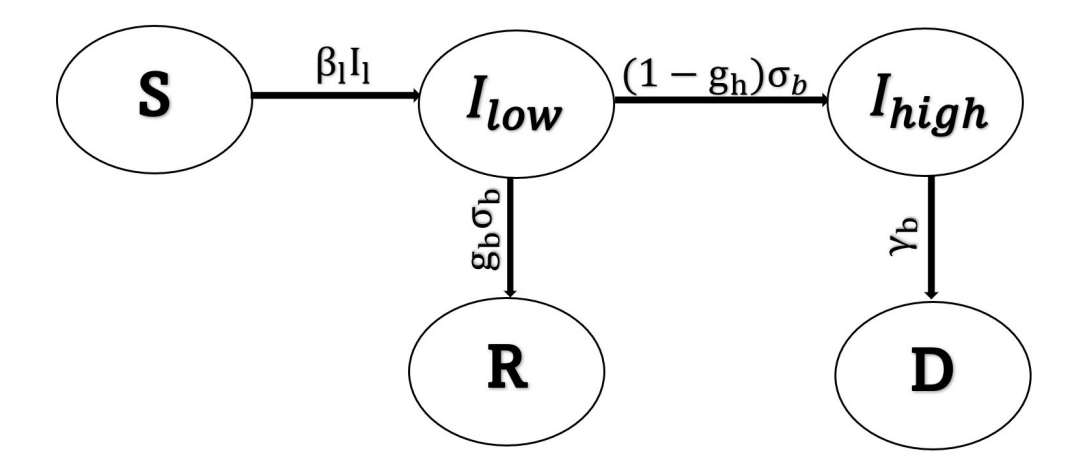


Figure 2.3: The Human-Ectoparasite SIIRD Model can be represented using a diagram that illustrates the flow of individuals in and out of each class. The diagram shows an inward flow that results in a positive rate of change, while an outward flow results in a negative rate of change. This flow diagram helps to visualize how the model accounts for the movement of human population between different categories, and how this movement contributes to the spread of bubonic plague.

$$\frac{dS_h}{dt} = -\beta_l \frac{S_h I_l}{N_h},\tag{2.10}$$

$$\frac{dI_{low}}{dt} = \beta_l \frac{S_h I_l}{N_l} - \sigma_b I_{low}, \qquad (2.11)$$

$$\frac{dI_{high}}{dt} = (1 - g_h)\sigma_b I_{low} - \gamma_b I_{high}, \qquad (2.12)$$

$$\frac{dR_h}{dt} = g_h \sigma_b I_{low}, \qquad (2.13)$$

$$\frac{dD_h}{dt} = \gamma_b I_{high},\tag{2.14}$$

$$\frac{dS_l}{dt} = r_l S_l (1 - \frac{N_l}{K_l}) - (\beta_{low} I_{low} + \beta_{high} I_{high}) \frac{S_l}{N_h}, \tag{2.15}$$

$$\frac{dI_l}{dt} = (\beta_{low}I_{low} + \beta_{high}I_{high})\frac{S_l}{N_h} - \gamma_l I_l$$
 (2.16)

The model incorporates five compartments for humans that vary over time: susceptible  $(S_h)$ , infectious with mild bacteremia  $(I_{low})$ , infectious with high bacteremia  $(I_{high})$ , recovered  $(R_h)$ , and deceased  $(D_h)$ . Additionally, there are two compartments for vectors: susceptible  $(S_l)$  and infectious  $(I_l)$ . The total living human population is determined by the sum of individuals in the susceptible, low infectious, high infectious, and recovered compartments, denoted as  $N_h = S_h + I_{low} + I_{high} + R_h$ . Plague transmission from vectors to humans occurs at a rate represented by  $\beta_l$ . Humans are mildly infectious for an average duration of 8 days. Individuals with mild bacteremia have a recovery rate of approximately 40%  $(g_h)$  in the case of untreated bubonic plague. Moribund humans transmit plague to vectors at a high rate  $(\beta_{high})$  for an average of 2 days [2].

The susceptible vector population grows at an intrinsic growth rate of  $r_l$  and is limited by the carrying capacity  $(K_l)$ , which is determined by the product of the parasite index and the number of human hosts  $(N_h)$ . The infection duration  $(\gamma_l)$  is, on average, 4.5 days for human fleas and 3 days for body lice [2]. The model assumes that infected human fleas and body lice do not recover, and the transmission of plague by human fleas is hypothesized to occur through early phase transmission, an alternative to the blocked transmission observed in rat fleas which refers to a temporary interruption of the flea's ability to transmit the Yersinia pestis bacteria to a new host. Due to the short duration of outbreaks, the model does not consider natural births and deaths in the human population [2].

Parameter	Value	Definition
Humans		
$eta_{low}$	U(0.001,0.05)	Transmission rate for bubonic plague from mildly infectious humans to body lice
$eta_{high}$	U(0.001,1)	Transmission rate for bubonic plague from highly infectious humans to body lice
$eta_{m p}$	U(0.001,1)	Transmission rate for pneumonic plague
$\beta_h$	U(0.001,0.2) (d)	Transmission rate for bubonic plague from rat fleas to humans
$\sigma_b^{-1}$	8.0 (d)	Average low infectious period for bubonic plague
$\gamma_b^{-1}$	2.0 (d)	Average high infectious period for bubonic plague
$\gamma_p^{-1}$	2.5 (d)	Average infectious period for pneumonic plague
$\gamma_h^{-1}$	10.0 (d)	Average duration of infection for bubonic plague
$g_h$ Lice (P. humanus	0.4	Probability of recovery from bubonic plague
humanus)		
*	0.11 (per d)	Natural lice growth rate
$egin{array}{c} r_l \ K_l \end{array}$	15.0 (per person)	Lice index at carrying capacity
$\beta_l$	0.05	Transmission rate for bubonic plague from body lice to humans
$\gamma_l^{-1}$	3.0 (d)	Average infectious period for bubonic plague
$\operatorname{Rats} \left( \operatorname{R.rattus} \right)$	0.0 (u)	Tiverage infectious period for bubolite plague
$\beta_r$	U(0.001,1)	Transmission rate for bubonic plague from rat fleas to rats
$\gamma_r^{-1}$	5.2 (d)	Average infectious period for bubonic plague
$g_r$	0.1	Probability of recovery from bubonic plague
Fleas (X. cheopis)	V	
$r_f$	0.0084 (per d)	Natural flea growth rate
$K_f$	6.0	Average number of fleas at carrying capacity
$d_f^{-1}$	5.0 (d)	Death rate of fleas
a	$\frac{3.0}{S_r(0)}$	Searching efficiency

Single numbers are fixed values and distributions (U=uniform) are priors [2].

Table 2.1: Utilizing parameters for the plague transmission from Dean et al. work to show comparison [2].

## 2.2.4 Lynch-Oster RFT Model

Logistic models play a crucial role in capturing the dynamics of rat and flea populations within the context of studying bubonic plague transmission. These models are employed to describe the changes and interactions that occur within these populations over time, providing a mathematical representation of their dynamics. By incorporating logistic equations into the modeling framework, we gain valuable insights into the overall transmission dynamics of bubonic plague.

The logistic model, a well-known mathematical framework, is particularly suitable for studying population dynamics when resources or environmental factors limit growth. It considers the carrying capacity of the environment, which represents the maximum population size that can be sustained. As the population approaches this limit, growth slows down, resulting in a more realistic representation of population dynamics.

In the context of bubonic plague, the logistic model allows for the exploration of how rat and flea populations interact and influence the transmission of the disease. Rats act as primary hosts for the bacteria Yersinia pestis, while fleas act as vectors that transmit the bacteria between rats and potentially to humans. Understanding the dynamics of these populations is crucial for comprehending the epidemiology and spread of bubonic plague.

By incorporating logistic equations into the models, we can study the growth and decline of rat and flea populations in response to factors such as resource availability, predation, and disease transmission. These equations provide a quantitative framework for examining how the population sizes of rats and fleas change over time, and how these changes can impact the overall transmission dynamics of bubonic plague.

$$\frac{dR_T}{dt} = \left(\frac{\beta_R}{K_R}\right) R_T (K_R - R_T) - \sigma R_C \tag{2.17}$$

$$\frac{dR_C}{dt} = \alpha \frac{F_C}{F_T} (R_T - R_C) - \frac{\beta_R}{K_R} (R_T)(R_C) - \sigma R_C - \gamma R_C$$
 (2.18)

$$\frac{dF_T}{dt} = \left(\frac{\beta_F}{K_F}\right) F_T (K_F - F_T) - \rho F_T \tag{2.19}$$

$$\frac{dF_C}{dt} = \lambda \frac{R_C}{R_T} (F_T - F_c) - \rho F_C \qquad (2.20)$$

In the given set of equations, the variables  $R_T$  and  $R_C$  represent the total population of rats and the population of rats that carry Y.pestis, respectively. These equations capture the dynamics of the rat population in relation to the transmission of plague. Similarly, the equations for the flea population follow a similar structure, where the variables  $F_T$  and  $F_C$  represent the total population of fleas and the number of contaminated fleas, respectively. These equations describe the dynamics of the flea population in the context of plague transmission.

Moving on to human dynamics, the SEIDR model (Susceptible, Exposed, Infected, Recovered, Dead) is employed. This model accounts for different compartments in the human population and how individuals transition between them based on the spread of the disease. Individuals move through these compartments as they become exposed to the disease, progress to an infectious state, die from the infection.

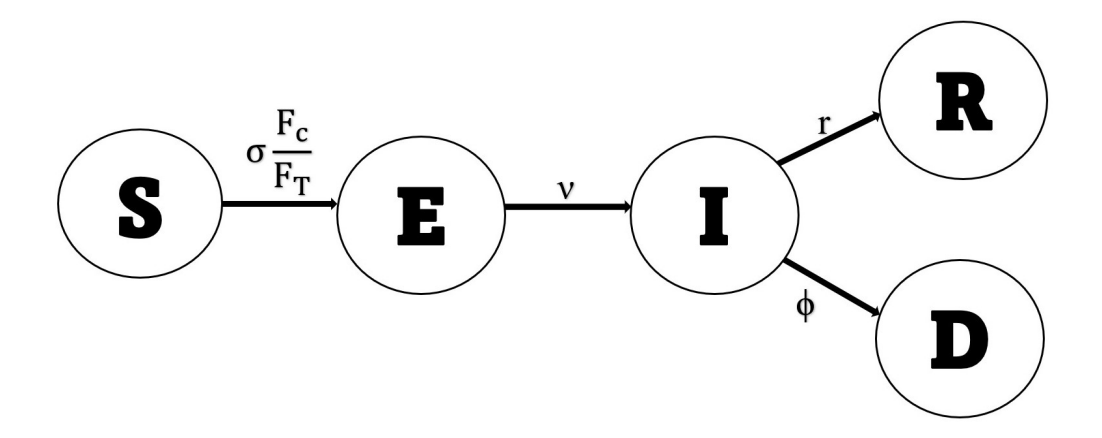


Figure 2.4: In the Lynch-Oster model, the focus is on the population dynamics of rats and fleas. The model accounts for the movement of individuals in and out of each class using the SEIDR model.

$$\frac{dS}{dt} = \beta(S + R_b) - \sigma S \frac{F_C}{F_T} - \mu S \tag{2.21}$$

$$\frac{dS}{dt} = \beta(S + R_b) - \sigma S \frac{F_C}{F_T} - \mu S \qquad (2.21)$$

$$\frac{dE}{dt} = \sigma S \frac{F_C}{F_T} - vE - \mu E \qquad (2.22)$$

$$\frac{dI}{dt} = vE - \phi I - rI \qquad (2.23)$$

$$\frac{dI}{dt} = vE - \phi I - rI \tag{2.23}$$

$$\frac{dR}{dt} = rI - \mu R_b \tag{2.24}$$

$$\frac{dD}{dt} = \phi I + \mu N_h \tag{2.25}$$

The SEIDR model is a compartmental model used to simulate the transmission dynamics of bubonic plague. It comprises nine compartments, including humans, rats, and fleas. The human compartments consist of susceptible individuals (S), exposed individuals (E), infected individuals (I), recovered individuals (R), and deaths (D). The rat compartments include total rat population  $(R_T)$ , contaminated rat population  $(R_C)$ , and flea compartments, including flea population  $(F_T)$ , contaminated flea population  $(F_C)$ , and deaths of rats. The model parameters include infection rates for rats and fleas ( $\beta_R$  and  $\beta_F$ , respectively), carrying capacities of rats and fleas ( $K_R$  and  $K_F$ ), transmission of the disease from contaminated rats to fleas ( $\alpha$ ), transmission rate of fleas from contaminated rats to susceptible rats ( $\lambda$ ), natural death rate of the rat population ( $\sigma$ ), and flea death rate ( $\rho$ ) [21].

The model equations describe the flow of individuals between compartments over time. Equations (2.17) and (2.18) represent the dynamics of the rat population, while equations (2.19) and (2.20) describe the dynamics of the flea population. Equation (2.21) represents the flow of susceptible humans into the exposed compartment, with the term  $\sigma S_{F_T}^{F_C}$  representing the transmission from infected fleas. Equation (2.22) describes the transition of exposed humans to the infected compartment with the parameter v being the transition rate. Equation (2.23) represents the flow of infected individuals into the recovered compartment at a rate r, and a death rate of  $\phi$  is assigned to infected individuals, resulting in the transition of infected individuals to the death compartment. Equation (2.24) represents the flow of recovered humans out of the recovered compartment, while Equation (2.25) describes the deaths of humans due to bubonic plague [21].

Parameter	Value	Definition
Human		
$\beta$	U(0.001,1)	Intrinsic birth rate
$\sigma$	U(0.001,1)	Chance of becoming infected from flea bite
$\mu$	U(0.001,1)	Intrinsic death rate
$v^{-1}$	U(0.25,10) (d)	Incubation period of the disease
$r^{-1}$	U(1, 100) (d)	Rate of recovery from bubonic plague
$\phi^{-1}$	U(1, 100) (d)	Death rate from bubonic plague
Rat		
$\beta_R$	U(0.1,1)	Intrinsic birth rate for rats
$K_R$	$1.5 \times N_h$	Carrying capacity for rats
$\delta$	U(0.001,1)	Death rate from bubonic plague
$\alpha$	U(0.001,1)	Infectivity of the plague from fleas to rats
$\gamma$	U(0.001,1)	Recovery rate for rats
Flea		
$eta_F$	U(10,100)	Intrinsic birth rate for fleas
$K_F$	$6 \times K_R$	Carrying capacity for fleas
ho	U(0.001,1)	Death rate from bubonic plague
λ	U(0.001,1)	Infectivity of the plague from rats to fleas

Table 2.2: Parameters for the Lynch-Oster model

# 2.3 Result Methods

By applying various plague models, including the Pneumonic model, Lynch-Oster RFT model, Keeligan Gilligan RFT model, and Human Ectoparasite model, to data from six different cities (Givry, Florence, Barcelona, Eyam, Malta, and Moscow), we can gain valuable insights into how plague epidemics evolve across different time periods and geographical locations. The dataset used in this analysis contains information on daily disease-induced mortality during the second outbreak in Europe, as outlined in Table 2.3. The dataset was sourced from a Royal Society paper [22]. The models' parameter values and initial conditions employed for the analysis are provided in Table 2.1 and 2.2, respectively.

Fitting these models to the data allows us to estimate the model parameters that best fit the data for each city, evaluate the goodness of fit of

the model for each city, and compare the dynamics of plague epidemics across cities. The goodness of fit metrics such as the Bayesian Information Criterion and root mean squared error will be used assess the accuracy of the model in predicting the observed data. Furthermore, comparing the model parameters and goodness of fit metrics across cities can reveal differences in the dynamics of plague epidemics, such as variations in transmission rates, and flea ecology. This information can inform public health policies and interventions for controlling and preventing plague outbreaks in different regions.

Bayesian inference is used to fit deterministic models to the observed data, estimating parameters that otherwise cannot be directly observed. The models are fitted to daily mortality with a time-step of 1 day. The probability of observing the data given the model parameters was calculated using a series of Poisson random variables. We estimate the transmission rates for each model and the initial size of the primary host population that was at risk or infected. Uniformly distributed priors were assumed, and posterior distributions were obtained using MCMC simulations with an adaptive Metropolis-Hastings algorithm. Convergence was assessed using the Gelman-Rubin statistic, and model comparison was performed using the Bayesian information criterion. The preferred model was the one with the lowest BIC value. The MCMC simulations were run for 180,000 iterations with a burn-in of 80,000 iterations and a thinning of 10. This means that 180,000 proposed values for the parameters of interest were generated and evaluated using the acceptance probability. However, the first 80,000 iterations were discarded as a burn-in period. In this particular case, a burn-in of 80,000 iterations is applied, meaning that the first 80,000 proposed parameter values are discarded. After the burn-in period, the remaining iterations (in this case, 100,000 iterations) are used to approximate

the posterior distribution and obtain estimates of the model parameters. The burn-in period is used to allow the Markov chain to reach its stationary distribution, where the distribution of the parameter values converges to the true posterior distribution. The first few iterations of the chain may not be representative of the true posterior distribution and discarding them helps to ensure that the final results are not biased. After the burn-in period, the remaining 100,000 iterations were thinned by a factor of 10. Thinning is used to reduce autocorrelation in the chain by skipping some of the proposed values. Autocorrelation occurs when the proposed values are highly correlated with each other, which can slow down convergence to the true posterior distribution. Thinning helps to reduce autocorrelation by keeping only every 10th proposed value, for example, and discarding the rest. We estimate the basic reproductive number was estimated in each model for the primary host using the next generation matrix method. Lastly, reporting error was also considered by incorporating a constant probability of reporting into the likelihood function, with different levels of underreporting (10%, 25%, and 50%) for each outbreak [2].

Overall, fitting plague models to data from multiple cities using statistical software packages such as "pymc" in Python can provide valuable insights into the dynamics of plague epidemics and inform public health policies and interventions. However, it is important to carefully interpret the results of the model fitting and consider the assumptions underlying the models to ensure that the results are valid and reliable.

Location	Date (MM/YYYY)	Population	Total recorded mortality
Givry, France	07/1348 - 11/1348	1,500	636
Florence, Italy	05/1400 - 11/1400	60,000	10,215
Barcelona, Spain	04/1490 - 09/1490	25,000	3,576
Eyam, England	06/1665 - 11/1665	350	197
Moscow, Russia	07/1771 - 12/1771	300,000	53,642
Island of Malta, Malta	04/1813 - 11/1813	97,000	4,487

Table 2.3: A summary of mortality data during the Second Pandemic in six major European cities. The Second Pandemic was a worldwide outbreak of bubonic plague that occurred during the mid-19th century and is estimated to have caused millions of deaths [2].

### 2.3.1 Describing Mathematical Models fits

This study utilized Bayesian Markov Chain Monte Carlo (MCMC) analysis to fit four transmission models to mortality data from the Second Pandemic outbreaks. The posterior means and 95% credible intervals for the estimated parameters in each model can be found in Figure 2.5 and Table 2.4.

Among the four models, the Human Ectoparasite model showed a superior fit to the observed mortality patterns in cities such as Givry, Florence, and Barcelona, as evidenced by lower Bayesian Information Criterion (BIC) values. Similarly, the Lynch-Oster model provided a better fit to the mortality data in cities like Moscow and Malta, where the presence of two peaks was observed. This finding aligns with Dean et al.'s paper, which also highlighted the irregularities in Moscow and Malta that were effectively captured by the Lynch-Oster model. Notably, the Lynch-Oster model also demonstrated a good fit for cities like Florence and Barcelona.

In the case of the Eyam outbreak, the Pneumonic model exhibited a lower BIC compared to the other models, indicating a better fit to the observed data. However, distinguishing between the models for smaller outbreaks such as Eyam and Givry is challenging due to the overlapping credible intervals, making visual differentiation difficult. Interestingly, the Keeligan-Gilligan model had the highest BIC value and demonstrated poor fit to the observed data among the four models, suggesting that it could not adequately capture the dynamics of bubonic plague transmission.

It is important to note that while the plague outbreak was analyzed using daily data, some parameter values in the Pneumonic model and Keeligan-Gilligan model were adjusted to replicate the results presented in Dean et al.'s paper. This adjustment aimed to ensure consistency between the simulated outcomes and the findings of the previous study, maintaining the integrity of the analysis.

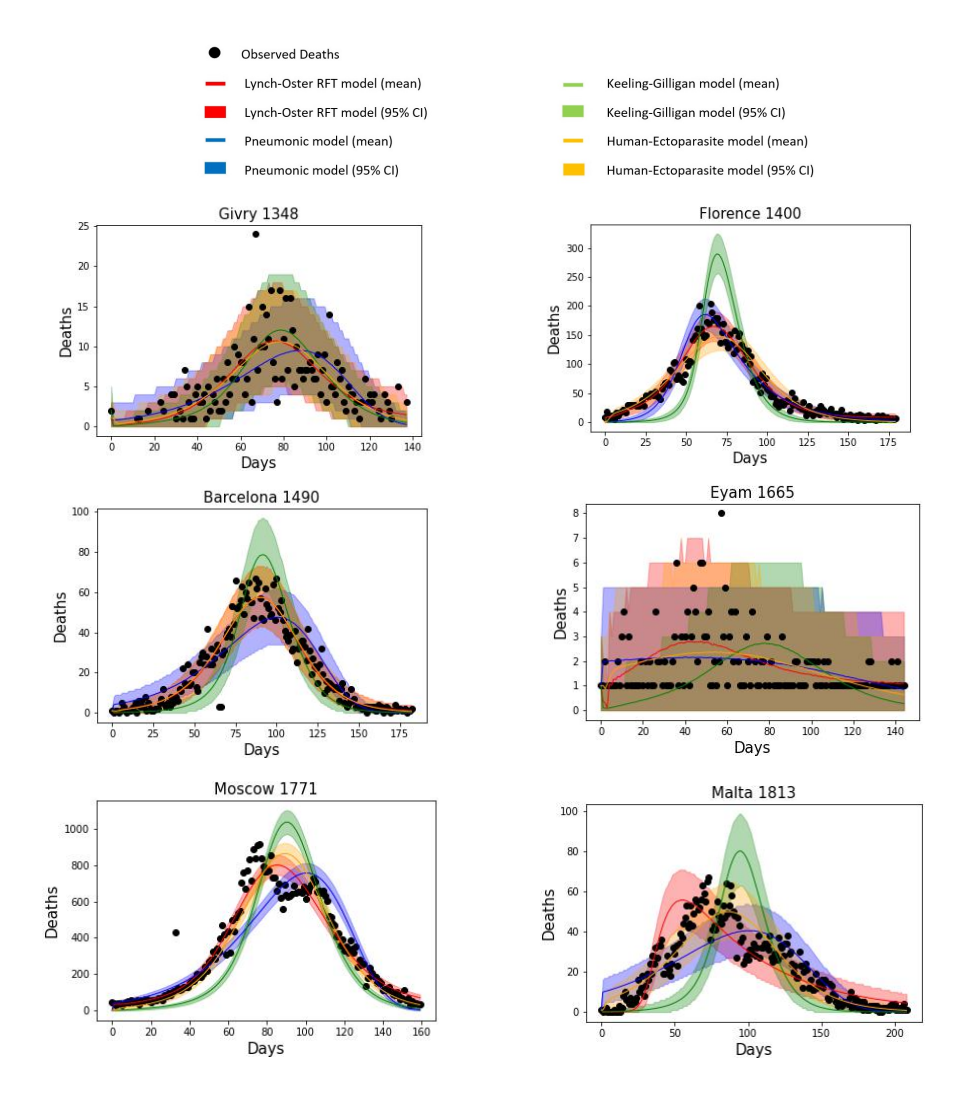


Figure 2.5: The mortality data from the Second Pandemic outbreaks is being fitted to four models of plague transmission: Lynch-Oster (red), Pneumonic (blue), Keeling-Gilligan (green), and Human-Ectoparasite (orange). The observed data is displayed as black dots, while the fitted models are represented by mean values with 95% credible intervals. These models are being applied to mortality data from six European cities, offering insights into the dynamics of plague transmission in different time periods.

City	Year	Model	BIC	$\Delta \mathrm{BIC}$	RMSE
Givry	1348	Pneumonic Model	1332.4867	54.7370	3.2642
		Keeling-Gilligan	1292.0497	14.4008	3.0912
		Lynch-Oster RFT	1326.3366	48.5877	2.9553
		Human-Ectoparasite	1277.7489	0	3.0652
Florence	1400	Pneumonic Model	3453.4082	674.7627	31.3240
		Keeling-Gilligan	13410.7304	10632.0849	21.3570
		Lynch-Oster RFT	4771.4387	1992.7932	11.7413
		Human-Ectoparasite	2778.6455	0	15.5567
Barcelona	1490	Pneumonic Model	2480.6936	434.0678	8.1350
		Keeling-Gilligan	3087.5268	1040.901	10.6453
		Lynch-Oster RFT	2110.0267	63.4009	4.8484
		Human-Ectoparasite	2046.6258	0	4.8730
Eyam	1665	Pneumonic Model	1189.9853	0	1.0084
		Keeling-Gilligan	1324.1347	134.1521	1.1387
		Lynch-Oster RFT	1219.6203	29.6350	1.0445
		Human-Ectoparasite	1194.5295	4.5442	1.1252
Moscow	1771	Pneumonic Model	7856.1234	3667.1689	116.2605
		Keeling-Gilligan	18778.3554	14589.4009	172.0217
		Lynch-Oster RFT	4188.9545	0	70.6026
		Human-Ectoparasite	5620.3103	1431.3558	89.6410
Malta	1813	Pneumonic Model	3066.4463	627.361	10.6540
		Keeling-Gilligan	7348.4848	4909.3995	20.4968
		Lynch-Oster RFT	2439.0853	0	6.1668
		Human-Ectoparasite	2547.3111	108.2258	7.8805

Table 2.4: Comparison of transmission models and posterior estimates for different plaque models and outbreaks

# 2.3.2 Examining role of exposed group in Lynch-Oster model

In this section, we explore the impact of including an additional exposed compartment in the Lynch-Oster model. This compartment accounts for the delay period between exposure and the onset of infectiousness. We examine whether this addition improves the model fit. The SEIRD model, which incorporates the exposed compartment and a compartment for individuals who have died from the disease, is compared to a simplified SIRD model without the exposed compartment. Our aim is to assess the influence of the

exposed compartment on the duration of the epidemic and the spread of the disease, while considering the possibility of overfitting.

Comparisons were made between the Lynch-Oster model and other models, including the Human Ectoparasite model, the Pneumonic model, and the Keeligan-Gilligan model, using the Bayesian Information Criterion (BIC). The results revealed that the Lynch-Oster model exhibited relatively lower BIC values, indicating a better fit and providing stronger support for the transmission dynamics of the outbreaks. Figure 2.6 and Table 2.5 present the results, showing that the two models generally yield similar outcomes. However, in Moscow, the SEIRD model had a slightly higher BIC value, and for Malta, the SEIRD model demonstrated a slightly better fit. Overall, the comparison did not indicate any evidence of overfitting due to the inclusion of the exposed group in the Lynch-Oster model.

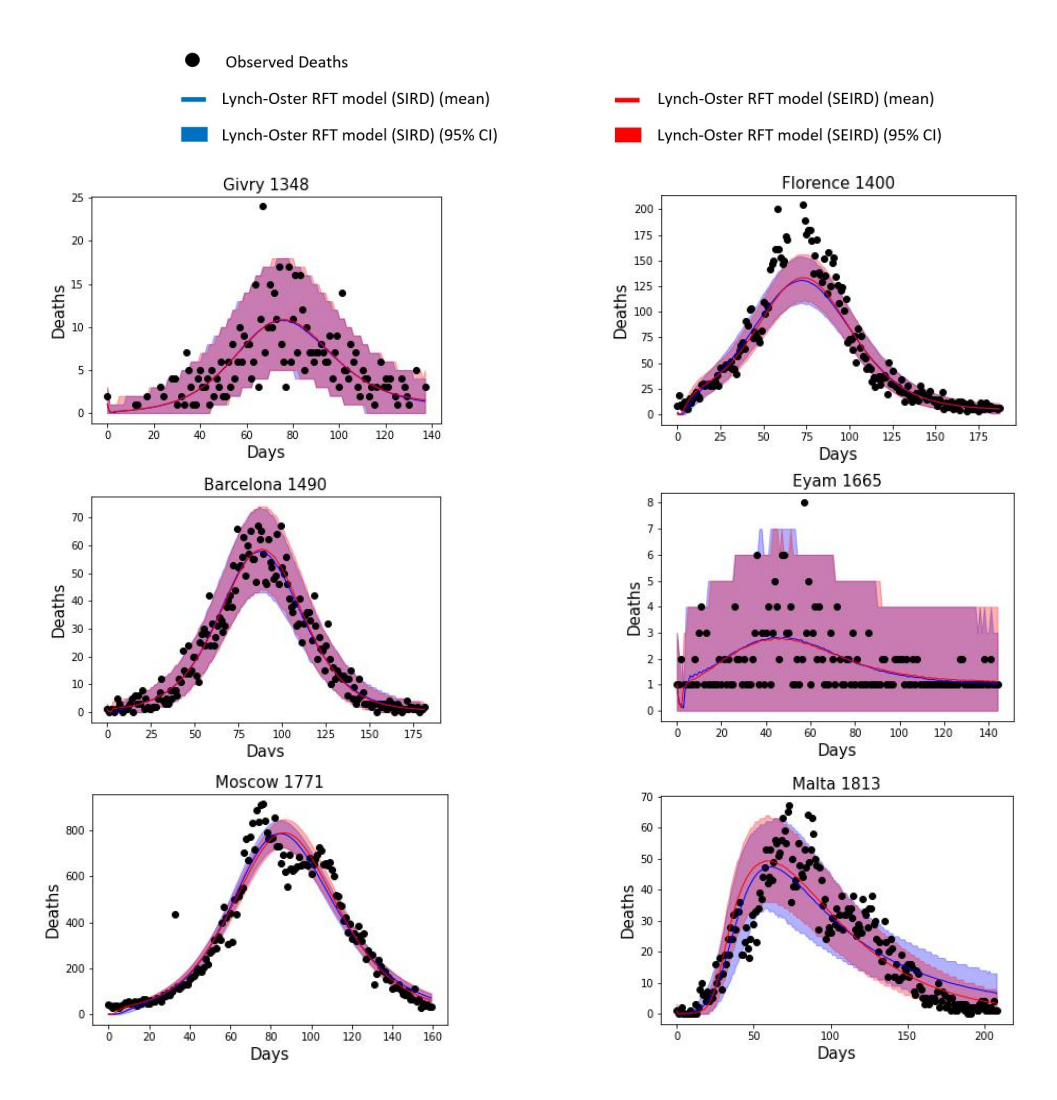


Figure 2.6: Fitting the SIRD that examines the role of exposed group and SEID in lynch-oster model of plague transmission to mortality during second pandemic outbreaks. The observed human mortality data (black dots) and the fit (mean and 95% credible interval) of the two models for plague transmission [SIRD (blue) and SEIRD (red)] for six plague outbreaks

City	Year	Model	BIC	$\Delta \mathrm{BIC}$	RMSE
Givry	1348	SIRD	1321.6421	0	2.9401
		SEIRD	1322.3741	0.832	2.9553
Florence	1400	SIRD	5003.8469	0	11.6460
		SEIRD	5055.1415	51.2946	11.7413
Barcelona	1490	SIRD	1992.9112	0	4.8474
		SEIRD	2004.5422	11.631	4.8484
Eyam	1665	SIRD	1212.9198	0	1.0438
		SEIRD	1222.0041	9.0843	1.0445
Moscow	1771	SIRD	5009.6170	201.9172	73.9805
		SEIRD	4807.6998	0	70.6026
Malta	1813	SIRD	2438.8950	2.2840	6.1577
		SEIRD	2463.6110	0	6.1668

Table 2.5: In order to examine the role of the exposed group in the Lynch-Oster model for different plague outbreaks, we compared the fit of the SIRD and SEIRD models using the BIC measure.

# 2.4 Discussion

The findings of our study support the notion that both rodent and human transmission contributed to the spread of bubonic plague during the Second Pandemic. The Lynch-Oster RFT model, which incorporates both modes of transmission, demonstrated a superior fit to the observed mortality patterns compared to other models considered. This suggests that rodents, particularly rats, may have played a significant role in the transmission dynamics of the disease.

The inclusion of an exposed compartment in the Lynch-Oster model, representing the delay period between exposure and infectiousness, did not result in substantial improvements in model fit or overfitting. This indicates that the simpler version of the model, without the exposed compartment (SIDR model), provided comparable results in certain cases, such as Eyam and Givry. These findings suggest that the inclusion of an exposed compart-

ment may not always be necessary to accurately capture the transmission dynamics of bubonic plague during the Second Pandemic.

However, it is important to acknowledge the limitations and uncertainties associated with modeling infectious diseases. Our study was based on specific assumptions and available data, which may introduce inherent biases. Different modeling approaches and parameterizations may yield alternative results, and therefore, the choice of model should consider not only the goodness of fit but also biological plausibility and prior knowledge about the disease.

The contradiction with Dean et al.'s paper highlights the complexity of modeling plague transmission and underscores the need for further research. Divergent findings among studies may arise due to variations in data sources, model assumptions, or methodological approaches. To gain a more comprehensive understanding of the transmission dynamics during the Second Pandemic, additional data are needed. This includes information on ecological factors that affect rodent populations, the dynamics of ectoparasites, and detailed historical records that provide insights into human behavior and movement patterns.

In conclusion, our study suggests that both rodent and human transmission likely played a role in the spread of bubonic plague during the Second Pandemic. The Lynch-Oster model, which incorporates both modes of transmission, demonstrated a better fit to the observed mortality data compared to other models considered. Nevertheless, further research and data collection are necessary to validate and refine these findings. By addressing the remaining uncertainties in modeling plague transmission, we can enhance our understanding of this historical pandemic and improve our preparedness for

future outbreaks of similar infectious diseases.

# Chapter 3

# Analysis of the Hypothesis of Endemic Stability: Polio and Covid-19

This chapter explores the concept of endemic stability, which refers to a situation where a population maintains a high prevalence of infection while experiencing a low incidence of clinical disease. To enhance our understanding of endemic stability, we utilize sophisticated models that consider various factors, such as immunity, partial immunity, and the absence of immunity dynamics.

Our models are specifically designed to investigate endemic stability using both single and two age classes. In the two-age class model, we focus on distinguishing between children and adults within the population. By separately analyzing these two distinct age groups, we can gain a more comprehensive understanding of how endemic stability manifests in different segments of the population.

To accurately represent real-world scenarios, our models incorporate the dynamics of immunity, including birth and natural deaths, while tracking the progression of individuals who have been infected with the disease. By studying the transition from infection to recovery, we enhance our comprehension of how the disease spreads within the population and evaluate the long-term implications of achieving endemic stability. For example, these models can be applied to analyze the dynamics of diseases like polio, where understanding the progression from infection to recovery is crucial.

Furthermore, our models incorporate partial immunity and account for the absence of immunity dynamics, which are essential for accurately capturing the interplay between susceptible individuals, infected individuals, and those who have recovered from previous infections but may still be susceptible to subsequent infections. This aspect is particularly relevant for analyzing diseases such as COVID-19, where immunity may decline over time, potentially leading to reinfection.

By utilizing these advanced modeling techniques, our primary objective is to gain insights into the necessary conditions and factors that contribute to the establishment of endemic stability. Through hypothesis testing and analysis, we aim to uncover the underlying mechanisms and prerequisites for maintaining a population with a high prevalence of infection while minimizing the incidence of clinical disease. This research will contribute to a better understanding of disease dynamics and provide valuable insights for effectively managing and controlling endemic diseases.

# 3.1 Hypothesis of Endemic Stability

In this section, we examine the hypothesis introduced by the authors of "Endemic stability, a veterinary idea applied to human public health" [23] and apply it to the analysis of Polio and Covid-19. Although the concept of endemic stability was initially developed in veterinary medicine to explain tick-borne diseases in cattle, it has also been extended to human infectious diseases such as malaria and rubella.

One of the key concerns discussed in the paper is the potential unintended consequences of reducing the force of infection through interventions like insecticide-treated nets for malaria control. The authors draw parallels with veterinary medicine, where interventions targeting tick-borne diseases have been associated with increased mortality rates. To address this concern, the authors propose a mathematical model that can be generalized to all diseases exhibiting endemic stability.

If this proposed model holds true, it could have significant implications for public health interventions aimed at controlling infectious diseases. Understanding the dynamics of endemic stability and its potential consequences could help inform decision-making and optimize the design and implementation of interventions to ensure the most effective and safe outcomes.

According to the authors, there are two necessary criteria for endemic stability: (1) the disease is more likely or severe in older individuals, and (2) initial infection reduces the likelihood of subsequent infections or the likelihood that subsequent infections will lead to disease [23]. They use a simple model to illustrate endemic stability, which involves an equation for the age-specific disease incidence.

$$\frac{dI}{dt} = \lambda S$$

such that,

$$I_a = \lambda pae^{-\lambda a},$$

where  $\lambda$  is the force of infection, pa is the probability that infection at aged a causes disease (where  $pa \leq 1$ ), and p is a constant greater than zero that determines the shape of the age-specific incidence curve.

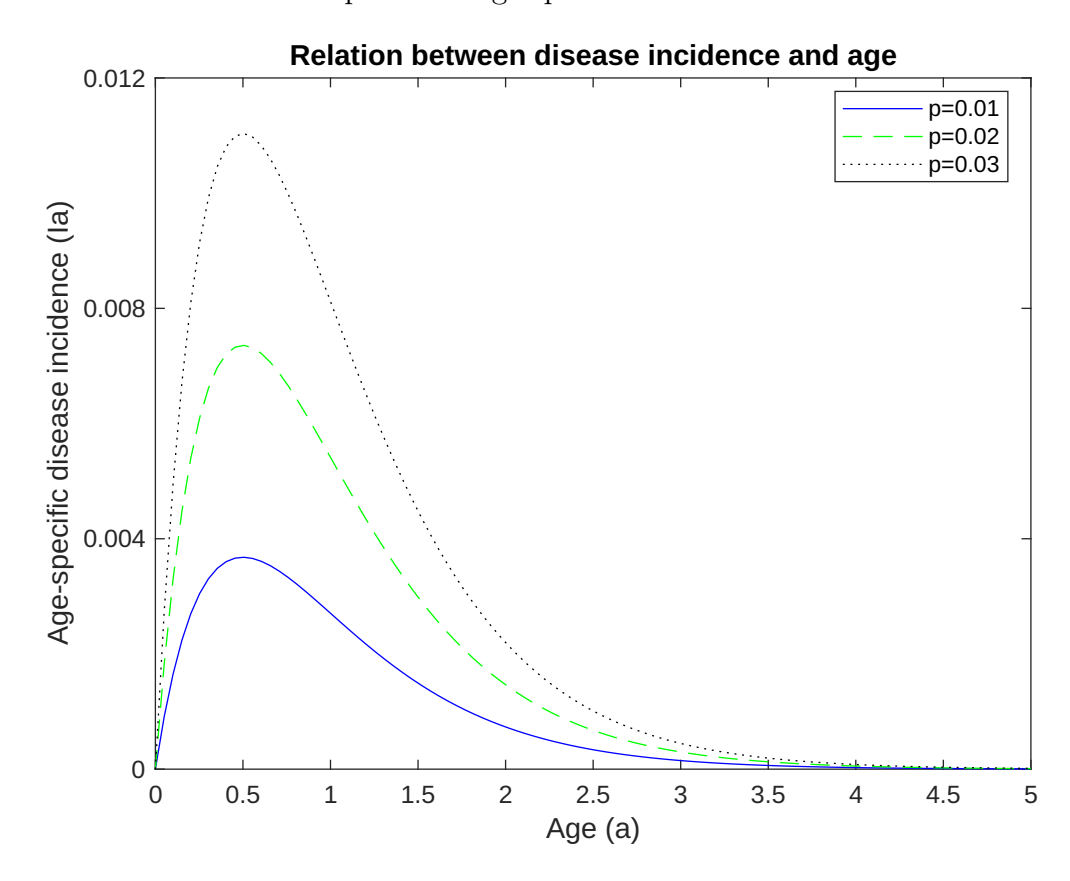


Figure 3.1: The relationship between age and disease incidence can be described by the force of infection, denoted as  $\lambda$ , where a value of  $\lambda = 2$  indicates a high likelihood of infection. The likelihood of an infection causing disease can be varied by 0.01, 0.02, and 0.03 to observe its impact on the force of infection.

The authors further derive an index of the overall disease incidence as a

function of  $\lambda$  for  $a_1 = 0$ ,  $a_2 = 2$ , and different values of p (power of infection). The overall disease incidence is given by:

$$\int_{a=a_1}^{a=a_2} \lambda pae^{-\lambda a} = \frac{p}{\lambda} - 2pe^{-2\lambda} - \frac{pe^{-2\lambda}}{\lambda}.$$

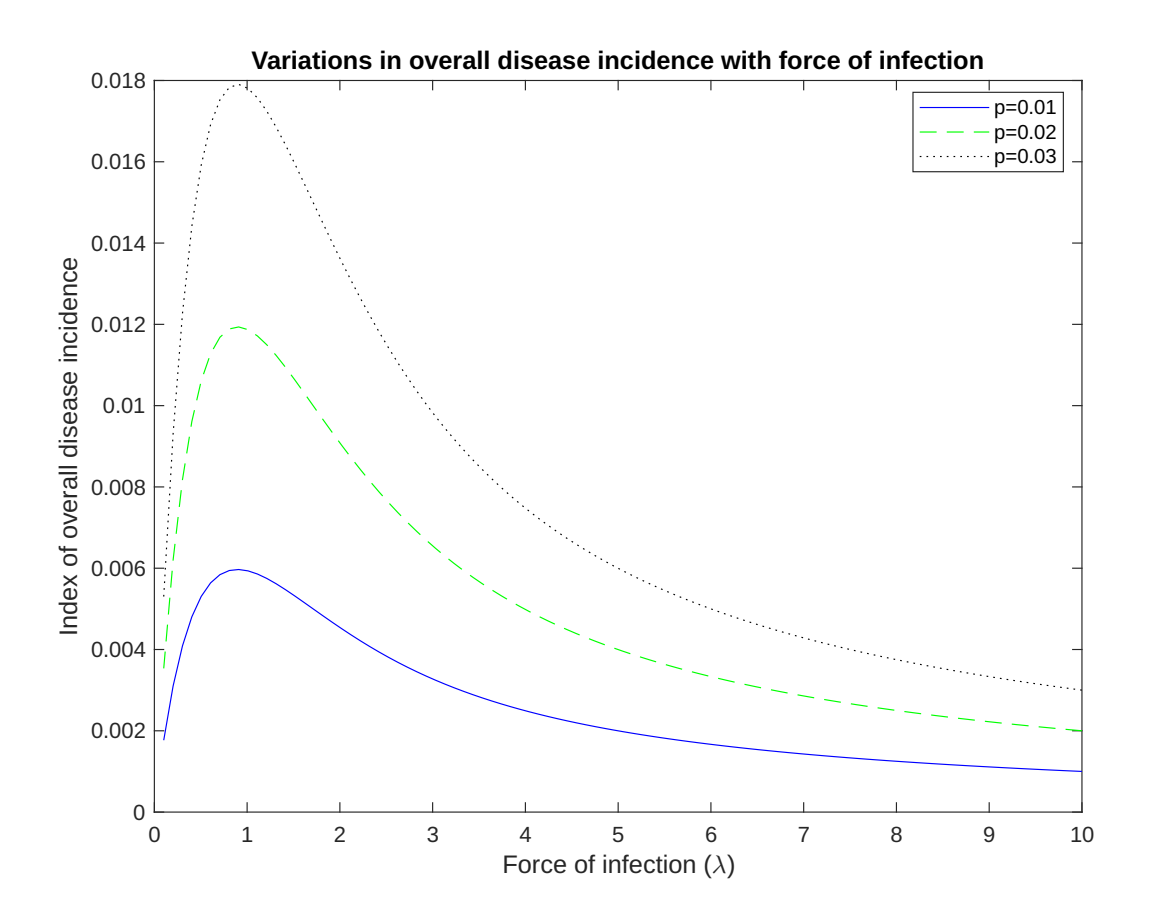


Figure 3.2: Variation in overall disease incidence with force of infection.

The model presented in Figure 3.2 provides insightful observations regarding endemic stability and its association with disease incidence and the force of infection. The model illustrates that as the force of infection increases, the overall disease incidence initially rises. At an intermediate level of infection, it reaches a peak, and subsequently, it declines at higher levels of the force

of infection. This pattern signifies that when the infection rate is high, there is a substantial population of infected individuals. Consequently, when the power of infection is low, only a small number of individuals become symptomatic, resulting in a lower peak of disease incidence observed in the solid blue curve. Conversely, with an increased power of infection, a relatively higher number of individuals are expected to experience the disease, as demonstrated by the dotted black curve.

The implications drawn from the model suggest that implementing partial control measures when the force of infection is already high (positioned to the right of the peak in disease incidence) may lead to an unexpected outcome. Instead of reducing disease incidence, partial control measures could potentially result in an increase in clinical disease within the population. This finding emphasizes the importance of carefully considering the consequences of partial control measures in the context of endemic stability.

These model results have significant implications for public health interventions. When dealing with diseases that exhibit endemic stability, it is crucial to adopt a comprehensive approach in designing and implementing interventions. Simply reducing the force of infection without implementing comprehensive measures may not lead to the desired reduction in clinical disease. Therefore, a holistic and strategic approach is necessary to effectively manage, and control diseases characterized by endemic stability.

The primary objective of this study is to conduct a comprehensive investigation and evaluation of two hypotheses proposed in the paper "Endemic stability - a veterinary idea applied to human public health" [23] The first hypothesis suggests that the power of infection (p) increases with age, indicating

a higher likelihood of infection progressing to a symptomatic state as individuals advance in age. The second hypothesis proposes that the power of reinfection  $(p^r)$  is lower than that of primary infections (p), indicating a decreased probability of clinical disease among individuals who have previously been infected. The second hypothesis also suggests that  $\lambda^r < \lambda$ , which we do not examine in this study.

To test the first hypothesis, we utilize both single and two age class SIRD (Susceptible-Infectious-Recovered-Diseased) models with a specific focus on immunity dynamics. These models will allow us to explore the consequences of the power of infection differing across different age groups.

Furthermore, we will extend the SIRD model to include scenarios of both absence of immunity and partial immunity to investigate the second hypothesis. This expanded model will enable us to analyze the power of reinfection  $(\pi^r)$  in comparison to primary infections  $(\pi)$ .

The findings and results obtained from these models will be carefully analyzed and compared to assess the validity of the hypotheses. By examining the conditions under which these hypotheses hold, our study aims to gain a deeper understanding of the underlying mechanisms contributing to endemic stability.

## 3.2 Immunity: Polio

### 3.2.1 Overview of Polio Disease

### **Background of Polio**

Polio is caused by the highly contagious Poliovirus, which belongs to the Picornaviridae family and is a type of Enterovirus. The virus mainly affects the motor neurons, which are responsible for transmitting messages between the muscles and the brain [24]. Humans are the only natural hosts of Poliovirus, although it can also infect monkeys if injected directly into their central nervous system (CNS). When ingested orally, the virus multiplies in the gut lining and then spreads to the bloodstream, eventually invading the CNS and replicating in the motor neurons [25]. The incubation period for poliovirus ranges from 2 to 35 days, and the virus is typically shed in stool 3 to 5 days after infection. It is believed that the virus may spread through the afferent nerve pathways in the brain, leading to damage and destruction of the anterior horn cells in the spinal cord and resulting in limb paralysis [26]. Polio is a life-threatening disease that can cause permanent disability.

Polio is an ancient disease that has been around for over 1000 years [24]. The earliest identifiable reference to paralytic poliomyelitis dates back more than 3500 years to an Egyptian stone engraving depicting a young man crippled by the disease [24]. In the 1800s, polio was relatively uncommon and spread at a low rate. During the 1890s, developed countries saw significant advancements in their standard of living, which some researchers believe made it easier for the virus to spread and lead to epidemics. Improved hygiene practices may have made more people susceptible to the virus, as fewer individuals

were exposed to it at a young age. In the past, poor sanitation meant that infants were highly exposed to polio, but their immune systems were aided by maternal antibodies that quickly defended against the virus.

The emergence of polio can be traced back to the year 1916 when the first cases were reported in New York City, United States. During that outbreak, there were more than 27,000 reported cases of polio, and tragically, it resulted in over 6,000 fatalities [26]. However, the development of effective vaccines in the mid-20<sup>th</sup> century helped reduce the incidence of polio, and the global polio eradication initiative launched in 1988 further reduced wild poliovirus cases by over 99%. As a result, the majority of countries in the world declared themselves polio-free, but Pakistan and Afghanistan remained endemic for wild poliovirus [27]. Despite these efforts, there have been recent outbreaks of wild poliovirus in countries such as Malawi, Afghanistan, and Pakistan.

Polio is a highly contagious disease that primarily affects children under the age of 5 years old but can also infect unvaccinated or partially vaccinated adults. There are three types of poliovirus, namely types I, II, and III, and individuals who are not fully vaccinated are at a higher risk of contracting any of these three types. In September 2022, an unvaccinated adult in New York was found to have contracted poliovirus, and a paralyzed 3-year-old girl was found with wild polio in Malawi. Tests confirmed that the virus was similar to the type circulating in Singh province in Pakistan, indicating that the circulation of poliovirus from endemic countries has not stopped [28]. These recent cases underscore the importance of continued efforts to eradicate polio and ensure vaccination coverage to prevent further outbreaks.

### **Polio Transmission**

Poliovirus is a contagious disease that spreads through contact with infected stool, water droplets from coughs or sneezes of an infected person, and contaminated water or food [24]. The virus multiplies in the intestine and can invade the nervous system, causing paralysis, especially in areas with poor sanitation [26]. The virus tends to propagate more rapidly among the nonimmune population during the summer seasons in temperate regions [26].

Most cases of polio present as mild illnesses symptoms, with only about 1% - 2% of infected individuals becoming paralyzed [24]. Paralytic polio occurs when the virus enters the bloodstream and attacks nerve cells, and in some cases, infected individuals may develop throat and chest paralysis [24]. Infected persons can spread the virus to others immediately before and up to two weeks after symptoms appear.

### Symptoms and Recovery of Polio Disease

According to the Centers for Disease Control and Prevention (CDC), around 72 out of 100 people who contract poliovirus do not display any visible symptoms, while 1 out of 4 individuals may experience flu-like symptoms, such as fever, fatigue, headache, vomiting, stiffness in the neck, and pain in the limbs, which typically last between 2 to 5 days [29]. However, individuals with weakened immune systems may develop more severe symptoms that affect the brain and spinal cord, such as paresthesia, meningitis, and paralysis [30].

The virus enters the body through the mouth, multiplies in the intestine, and can invade the nervous system [24]. In up to 90% of cases, polio infection causes no symptoms or mild symptoms that go unnoticed [29]. Some patients may recover completely from initial symptoms, which usually last between 2 to 10 days. However, in a small proportion of cases, the virus can cause paralysis, often of the legs, which can be permanent and may occur as quickly as within a few hours of infection. Approximately 5 - 10% of those who experience paralysis due to polio may die from immobilization of their breathing muscles [30]. Even children who fully recover from polio infection may experience new muscle pain, weakness, or paralysis as adults, usually between the ages of 15 to 40 years [29].

### Vaccination of Polio Disease

Poliovirus exposure or infection can provide immunity, but it is not a guaranteed protection against all three types of poliovirus. It is possible for a person to be exposed to or infected with one type of the virus and still contract another type.

There are two types of polio vaccines: the inactivated poliovirus vaccine (IPV) and the oral poliovirus vaccine (OPV). IPV was developed by Jonas Salk in the 1950s and is administered by injection in the leg or arm, depending on the age of the patient. OPV was developed by Albert Sabin and is given orally. The introduction of IPV in the 1950s led to a significant decrease in polio cases, and by 1994, most developed countries had eliminated polio. By 2000, Western countries had declared themselves polio-free, demonstrating the significant role of the vaccine in eradicating poliovirus [31].

Both types of vaccines have been shown to be highly effective against all three types of poliovirus. However, they work differently. IPV provides serum immunity to all types of poliovirus and protects against paralysis. OPV also provides serum immunity to all types of poliovirus and protects against paralysis, but it also prevents the virus from spreading to the nervous system. The oral polio vaccine (OPV) elicits an immune response within the intestinal mucous membrane, which serves as the main location for the replication of the poliovirus. Almost all children (99 out of 100) who receive all the recommended doses of IPV will be protected from polio. To be fully vaccinated, a person needs to receive all the recommended doses of either IPV or OPV [30].

### 3.2.2 Mathematical Models

This chapter focuses on studying the dynamics of disease spread in relation to polio, with a particular emphasis on considering population factors such as birth and death processes. We examine both single and two age SIRD (Susceptible-Infectious-Recovered-Diseased) models to explore the presence of endemic stability and gain a deeper understanding of the conditions that give rise to this phenomenon. Additionally, we aim to investigate the hypothesis that the power of infection  $(\pi)$  increases as age class advances, suggesting a higher probability of infection progressing to a symptomatic state with increasing age.

Based on data provided by the CDC (Centers for Disease Control and Prevention), we observe that approximately 70% of children infected with polio remain asymptomatic, while only around 5% develop paralysis. This information indicates that children have a lower risk of experiencing paralysis when infected with polio, suggesting a lower power of infection compared to adults. An important observation is that individuals who contract polio at a young age tend to recover quickly and acquire immunity. On the other hand, adults who have not previously been infected are more susceptible to paralysis if they contract the virus.

To account for the heterogeneity within the population, we incorporate an immunity model. This model takes into consideration that not all individuals have the same likelihood of becoming infected with polio, particularly at a young age. Some individuals may never experience an infection, while others may contract the virus later in life. By considering these variations, we obtain a more realistic understanding of the disease dynamics and the potential for endemic stability.

Moving on to the construction of the single age class model, our aim is to delve further into these immunity dynamics and analyze the necessary conditions for the presence of endemic stability. By examining the interactions between susceptible, infectious, recovered, and diseased individuals, we can assess how the disease spreads and persists within the population. Through this analysis, we strive to uncover the contributing factors and parameters that influence the establishment of endemic stability in the context of polio.

### A. Single Age Class Model with Immunity

In our analysis, we are utilizing a single age class model that considers the entire population and incorporates the occurrence of births and deaths. This model follows the SIRD (Susceptible-Infectious-Recovered-Diseased) flow, which represents the possible transitions individuals can undergo during the course of the disease. The model consists of four compartments: Susceptible (S), Infectious (I), Recovered (R), and Diseased (D). These compartments represent the different states an individual can be in with respect to the disease.

The flow of the model, as depicted in Figure 3.3, illustrates the transitions between the compartments. Initially, individuals in the population are classified as susceptible (S), meaning they are at risk of contracting the disease. When a susceptible individual comes into contact with an infectious individual, they become infected and move to the infectious compartment (I), where they have the potential to transmit the disease to others.

Over time, individuals in the infectious compartment may recover from the disease and move to the recovered compartment (R), indicating that they have developed immunity and are no longer capable of transmitting or getting the disease. However, some individuals in the infectious compartment may experience more severe outcomes and move to the diseased compartment (D), representing those who have suffered from the disease and are not able to recover.

To account for the occurrence of births and deaths within the population, we incorporate birth and death rates into the model. The birth rate represents the rate at which new individuals enter the population, while the death rate represents the rate at which individuals in the population pass away due to natural causes.

The mathematical equations shown in (3.1, 3.2, 3.3, and 3.4) govern the transitions between the compartments and capture the dynamics of the disease, births, and deaths within the population. By analyzing these equations and simulating the model, we can study the behavior of the system, explore the impact of births and deaths on the spread of the disease, and investigate the conditions necessary for achieving endemic stability.

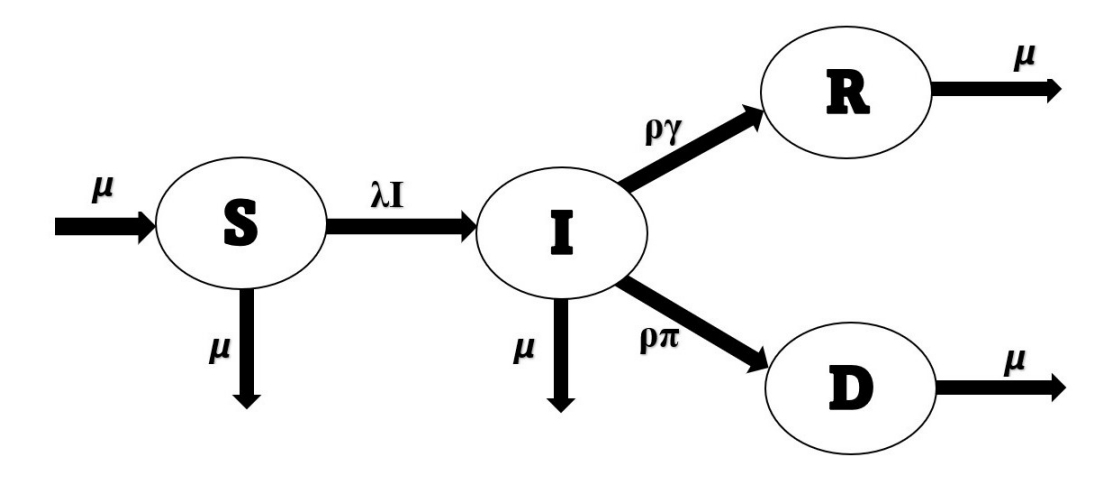


Figure 3.3: This visual representation showcases the movement of individuals between compartments (Susceptible, Infected, Recovered, and Diseased) in the single age class model with immunity. The arrows represent the flow of individuals, while the associated rates illustrate the probabilities of transitioning between compartments. The model takes into account the effects of births and natural deaths, allowing for a thorough analysis of disease dynamics and its interplay with population changes. By examining these transitions, the model offers valuable insights into the progression of diseases and the impact of immunity on population health.

$$\frac{dS}{dt} = \mu N - (\mu + \lambda \frac{I}{N})S, \tag{3.1}$$

$$\frac{dI}{dt} = \lambda S \frac{I}{N} - \rho(\gamma + \pi)I - \mu I,$$

$$\frac{dR}{dt} = \rho \gamma I - \mu R$$
(3.2)

$$\frac{dR}{dt} = \rho \gamma I - \mu R \tag{3.3}$$

$$\frac{dD}{dt} = \rho \pi I - \mu D \tag{3.4}$$

The system of equations comprises four differential equations that characterize the behavior of the single age class SIRD model incorporating birth and death processes. The total population is represented by the sum of the compartments: N = S + I + R + D

The rate of change of susceptible individuals (S) over time (t) is determined by a balance between the birth rate and total population  $(\mu N)$ , the impact of disease transmission over the entire population  $(\lambda_N^I)$ , and natural death  $(\mu S)$  within the susceptible population.

The rate of change of infected individuals (I) with respect to time (t) is influenced by the infectious rate  $(\lambda_N^I)$ , the likelihood of infection progress to asymptomatic state  $(\rho \gamma I)$ , likelihood of infection progress to symptomatic state  $(\rho \pi I)$ , and deaths  $(\mu I)$ . This equation captures the flow of individuals transitioning into the infectious state through disease transmission, their recovery (asymptomatic), progression to disease (symptomatic), and the impact of natural death.

The rate of change of recovered individuals (R) with respect to time (t) is determined by the likelihood of infection progress to asymptomatic state  $(\rho \gamma I)$  and deaths  $(\mu R)$ . It represents the flow of individuals recovering from the disease and those who have passed away due to natural death.

Lastly, the rate of change of diseased individuals (D) over time (t) is influenced by the likelihood of infection progress to symptomatic state  $(\rho \pi I)$  and deaths  $(\mu D)$ . This equation accounts for the flow of individuals who have experienced the disease and subsequently passed away from natural death.

These equations describe the interplay and transitions between the different compartments (susceptible, infected, recovered, and diseased) while incorporating the effects of births, deaths, disease transmission, recovery (asymptomatic), and disease (symptomatic) within the population. By solving these equations, we can analyze the dynamics of the disease, examine the impact of various parameters on the system, and explore the conditions required for endemic stability.

# Examining Force of infection and Disease incidence of Single Age Class model with Immunity

To further analyze the dynamics of the model, we can calculate important epidemiological measures such as the force of infection and disease incidence. The force of infection represents the rate at which susceptible individuals become infected, and it is given by:

$$F = \int_0^T (\lambda I) dt$$

We normalize the force of infection by dividing it by the product of the total population (N) and the length of the time period (T) gives us the average force of infection as shown in Equation 3.5.

$$\tilde{F} = \frac{\int_0^T (\lambda I)dt}{NT} \tag{3.5}$$

On the other hand, the disease incidence measures the number of new cases that become symptomatic within a given time period. It is calculated by integrating the product of the disease-induced mortality rate  $(\rho \pi)$  and the number of infected individuals (I) over the time period, and then normalizing it by dividing by the product of the total population (N) and the length of

the time period (T) as shown in equation 3.6

$$\tilde{D} = \frac{\int_0^T (\rho \pi I) dt}{NT} \tag{3.6}$$

### **Identifying Steady States**

To analyze the steady states of the SIRD with immunity model, we focus on two equilibrium points: the disease-free equilibrium and the disease-endemic equilibrium.

At the disease-free equilibrium, where the infected population (I) is zero, such that susceptible population  $(S) = (\rho(\gamma + \pi) + \mu)\frac{N}{\lambda}$ . This equilibrium represents the eradication of the disease, where no individuals are infected.

The disease-endemic equilibrium occurs when the infected population is non-zero. To find this equilibrium, we solve for the value of I by setting  $\frac{\partial S}{\partial t} = 0$ . This leads to the equation:

$$\mu N - \mu S - \lambda \frac{I}{N} S = 0$$

Simplifying and substituting the value of S, we have:

$$\mu N - \mu \rho \frac{N}{\lambda} (\gamma + \pi) - \mu^2 \frac{N}{\lambda} - I(\rho(\gamma + \pi) + \mu) = 0$$

Solving for I, we obtain the steady state at the disease-endemic equilibrium:

$$I = \frac{\mu N - \frac{\mu \rho}{N} (\gamma + \pi) - \mu^2 \frac{N}{\lambda}}{\rho (\gamma + \pi) + \mu}$$

Therefore, we assume that  $I^* = I$ , then force of infection is redefine as:

$$F \approx \lambda I^* = \lambda \frac{\mu N - \frac{\mu \rho}{N} (\gamma + \pi) - \mu^2 \frac{N}{\lambda}}{\rho(\gamma + \pi) + \mu}$$

Additionally, the disease incidence rate is redefined as:

$$D \approx \rho \pi I^* = \rho \pi \frac{\mu N - \frac{\mu \rho}{N} (\gamma + \pi) - \mu^2 \frac{N}{\lambda}}{\rho (\gamma + \pi) + \mu}$$

### B. Age Structure Model with Immunity

In this chapter, we extend our analysis to a two-age class model that takes into account the population division between children (0 - 2 years) and adults (2+ years). This model incorporates the occurrence of births and deaths and follows the SIRD flow, allowing for transitions between the different age classes. The compartments in this model are represented by variables  $S_c, I_c, R_c, D_c$  for children and  $S_a, I_a, R_a, D_a$  for adults.

Figure 3.4 illustrates the structure of the model and its corresponding parameters. Similar to the single age class model, adults give birth to newborns who are initially classified as susceptible, placing them at risk of contracting the disease. After two years, children transition to the adult age class and become more susceptible to developing symptoms when infected with the virus.

In this two-age class model, we assume that the birth and death rates are equal, indicating that the population is experiencing a balance between births and deaths. The mathematical equations shown in (3.7, 3.8, 3.9, 3.10, 3.11, 3.12, 3.13, and 3.14) govern the transitions between the compartments and capture the dynamics of the disease, births, and deaths within the population.

By utilizing this two-age class model and considering the interplay be-

tween children and adults, we can gain a deeper understanding of how the disease spreads and impacts different age groups. The equations provide a framework for studying the disease dynamics, birth and death rates, and the transitions between compartments.

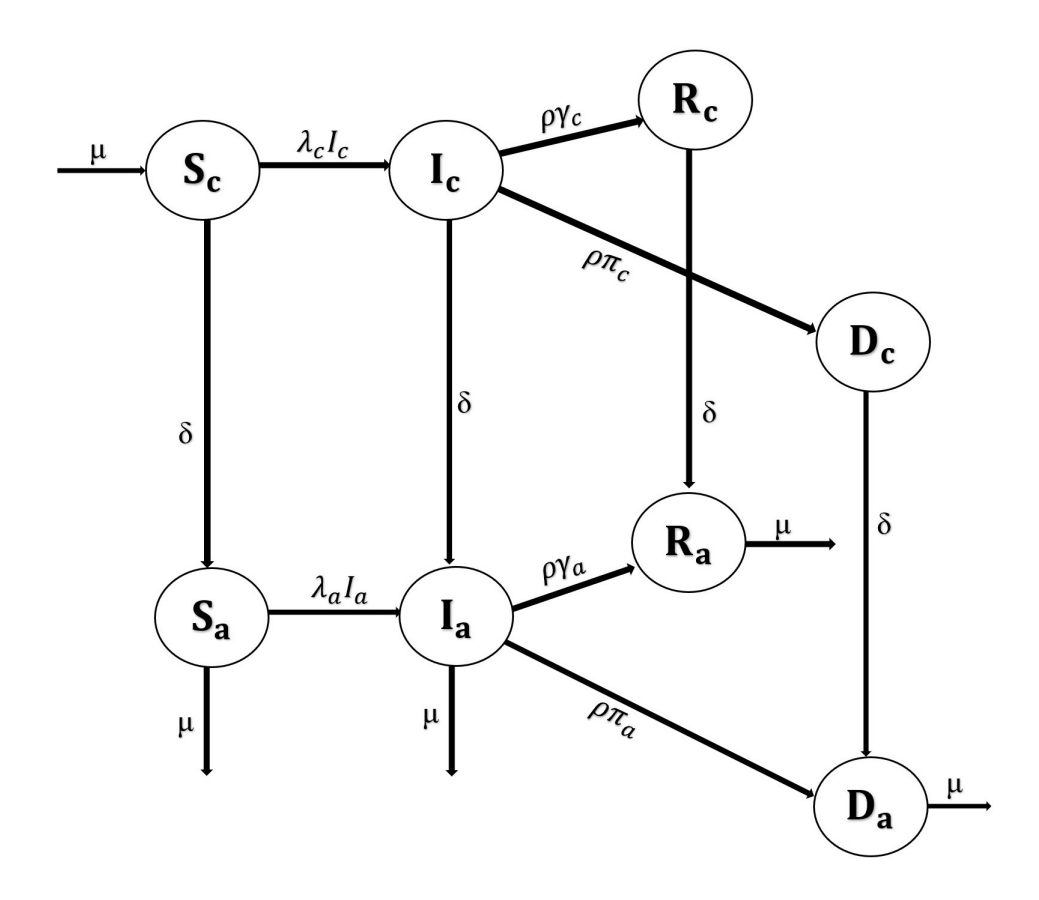


Figure 3.4: This illustrative flowchart displays the transitions between compartments (Susceptible, Infected, Recovered, and Diseased) in the age structure model with immunity. The arrows symbolize the movement of individuals, and the associated rates represent the probabilities of transitioning between compartments. Additionally, the model incorporates the effects of births and deaths on the population, contributing to a more accurate representation of disease dynamics and its interplay with population dynamics. By examining these transitions, the model enables an in-depth analysis of disease spread and the impact of age-specific factors on population health.

$$\frac{dS_c}{dt} = \mu N - \lambda \frac{I_c}{N} S_c - \mu S_c - \delta S_c \tag{3.7}$$

$$\frac{dS_a}{dt} = -\lambda \frac{I_a}{N} S_a - \mu S_a + \delta S_c \tag{3.8}$$

$$\frac{dI_c}{dt} = \lambda \frac{I_c}{N} S_c - \rho (\gamma_c + \pi_c) I_c - \mu I_c - \delta I_c$$
(3.9)

$$\frac{dI_a}{dt} = \lambda \frac{I_a}{N} S_a - \rho (\gamma_a + \pi_a) I_i - \mu I_a + \delta I_c$$
(3.10)

$$\frac{dR_c}{dt} = \rho \gamma_c I_c - \mu R_c - \delta R_c \tag{3.11}$$

$$\frac{dR_a}{dt} = \rho \gamma_a I_a - \mu R_a + \delta R_c \tag{3.12}$$

$$\frac{dD_c}{dt} = \rho \pi_c I_c - \mu D_c - \delta D_c \tag{3.13}$$

$$\frac{dD_a}{dt} = \rho \pi_a I_a - \mu D_a + \delta D_c \tag{3.14}$$

The given system of equations represents a disease spread model in a population consisting of two age classes: children and adults. It incorporates four compartments for each age class: susceptible population  $(S_{c,a})$ , infected population  $(I_{c,a})$ , recovered population  $(R_{c,a})$ , and diseased population  $(D_{c,a})$ . The total population is divided into children  $(N_c)$  and adults  $(N_a)$ , with the overall population denoted as  $(N = N_c + N_a)$ .

This model extends the previous single age class model by introducing the transition rate between age classes. Specifically, individuals transition from the child age class to the adult age class when they reach the age of two, governed by the transition rate  $\delta$ . Consequently, the population of children decreases while the population of adults increases.

By incorporating separate age classes and their transitions, this model provides a more comprehensive understanding of disease dynamics in the population. It allows us to analyze the influence of age-specific factors on disease spread, recovery, and infection rates. However, this model assumes that new births depend on the entire population, including children being able to give birth. This assumption deviates from reality. To address this limitation, we refine the model to better mimic the real world.

In our refined model, we consider that new births depend only on the adult population. Additionally, we assume that children do not experience deaths at a young age, meaning the death rate for children is set to zero. Furthermore, we assume that the birth rate is equal to the adult death rate  $(\mu = \delta \frac{N_c}{N_a})$ , which is determined by the transition rate between age classes and the ratio of the children population  $(N_c)$  to the adult population  $(N_a)$ . These refinements make the model more realistic and aligned with real-world dynamics.

$$\frac{dS_c}{dt} = \mu N_a - \lambda \frac{I_c}{N} S_c - \delta S_c$$

$$\frac{dS_a}{dt} = -\lambda \frac{I_a}{N} S_a - \mu S_a + \delta S_c$$

$$\frac{dI_c}{dt} = \lambda \frac{I_c}{N} S_c - \rho (\gamma_c + \pi_c) I_c - \delta I_c$$

$$\frac{dI_a}{dt} = \lambda \frac{I_a}{N} S_a - \rho (\gamma_a + \pi_a) I_i - \mu I_a + \delta I_c$$

$$\frac{dR_c}{dt} = \rho \gamma_c I_c - \delta R_c$$

$$\frac{dR_c}{dt} = \rho \gamma_a I_a - \mu R_a + \delta R_c$$

$$\frac{dD_c}{dt} = \rho \pi_c I_c - \delta D_c$$

$$\frac{dD_a}{dt} = \rho \pi_a I_a - \mu D_a + \delta D_c$$

# Examining Force of infection and Disease incidence of Age structure model with Immunity

The calculation of the force of infection and disease incidence in the twoage class model takes into account the dynamics of both children and adults within the population. These metrics provide insights into the transmission intensity and disease burden in each age class.

The force of infection (F) represents the rate at which susceptible individuals become infected. It is calculated by summing the contributions of infected individuals from both age classes over a specific time interval. The force of infection can be determined by integrating the product of the transmission rate  $(\lambda_{c,a})$  and the number of infected individuals  $(I_{c,a})$  over time:

$$F = \int_0^T (\lambda_c I_c + \lambda_a I_a) dt$$

To further assess the transmission intensity and the risk of infection within the population in a standardized manner, we can normalize the force of infection to obtain the average force of infection. This measure provides a relative assessment of the overall transmission intensity, accounting for the population size.

The average force of infection  $(\tilde{F})$  is obtained by dividing the integral of the force of infection (F) over a specific time interval by the product of the population size (N) and the duration of the observation period (T):

$$\tilde{F} = \frac{\int_0^T (\lambda_c I_c + \lambda_a I_a) dt}{NT}$$
(3.15)

Similarly, the disease incidence  $(\tilde{D})$  quantifies the rate of new disease

(symptomatic) cases in the population. It accounts for the contributions of symptomatic infections in both age classes over a specific time interval. The disease incidence is calculated by integrating the product of the disease-induced mortality rate ( $\rho \pi_{c,a}$ ) and the number of infected individuals ( $I_{c,a}$ ) over time:

$$\tilde{D} = \frac{\int_0^T \rho(\pi_c I_c + \pi_a I_a) dt}{NT}$$
(3.16)

Here, N represents the total population size, and T denotes the total duration of the observation period.

Variable	Description	unit
λ	Infection rate of susceptible population	1 people*days
$\mu$	Birth and Death rate	1 1
$\pi$	Likelihood of infection progress to symptomatic state (Power of infection)	days
$\gamma = (1 - \pi)$	Likelihood of infection progress to asymptomatic state	$\begin{array}{c} \overline{\text{days}} \\ \underline{I} \\ \text{days} \end{array}$
ho	Timescale that Infections are contagious	days
$\delta$	Transition rate between age groups	$\frac{1}{\text{days}}$
t	Time	days
S	Number of susceptible people	people
I	Number of infected people	people
R	Number of recovered (asymptomatic) people	people
D	Number of disease (symptomatic) people	people
N	Total number of people	people

Table 3.1: This table presents the units associated with the variables and parameters utilized in age structure model with immunity SIRD (Susceptible-Infected-Recovered-Disease) models. The variables, representing population compartments such as susceptible (S), infected (I), recovered (R), and disease (D), are measured in absolute quantities or proportions. The parameters, including infection rates, power of infection, and birth and death rates, possess specific units that may vary depending on the particular disease and context being modeled.

### 3.2.3 Results

In our study, we extensively investigate two models: the single age class model and the two-age class model. These models play a crucial role in providing us with valuable insights into the dynamics of disease transmission and progression. While they differ in their structural design, they share common parameter values and initial conditions, enabling us to make meaningful comparisons and obtain a comprehensive understanding of the behavior of infectious diseases.

One of the key aspects we focus on is the hypothesis that children have a lower likelihood of progressing to symptomatic infection compared to adults. To thoroughly examine this hypothesis, we analyze both the single age class model and the two-age class model. By incorporating age-specific parameters and considerations, we can explore how disease dynamics differ between children and adults.

In the single age class model, we investigate the progression of infection within a homogeneous population, where all individuals are treated as a single group without distinction based on age. This model allows us to study the overall dynamics of the disease and its impact on the population as a whole. By comparing the likelihood of symptomatic infection between different age groups within this model, we can gain initial insights into the potential differences in disease severity.

However, to gain a more comprehensive understanding of the role of age in disease dynamics, we also employ the two-age class model. This model divides the population into two distinct age groups: children and adults. By considering the interactions and transmission dynamics between these age groups, we can specifically examine how the disease behaves differently among children and adults. This model allows us to assess the varying susceptibility, infection rates, and recovery patterns based on age, providing more nuanced insights into the hypothesis.

Through the exploration of both models, we aim to uncover valuable information regarding the hypothesis that children have a lower likelihood of progressing to symptomatic infection compared to adults and determine necessary conditions for endemic stability. By incorporating age-specific parameters and observing the disease dynamics in different age groups, we can evaluate the validity of this hypothesis and gain a deeper understanding of the role of age in shaping the progression and severity of infectious diseases like Polio.

### Single age class model results analysis

In our investigation of the single age class model with immunity, we aim to understand the impact of different infection rates: 0.1 and 2.0. Following infection, individuals have two possible outcomes: they either become asymptomatic or progress to a symptomatic state. The likelihood of infection progressing to the asymptomatic state is 0.95, while the likelihood of progressing to the symptomatic state is 0.05. To ensure population balance, we set the birth and mortality rates to approximately 0.005, maintaining a stable equilibrium between population growth and loss. The simulation duration spans 10 years, providing us with an opportunity to examine the dynamics of immunity over time. During this period, we assume a contagious timescale of 0.15, representing the duration in which individuals are infectious and capable of transmitting the disease to others. Further, we assume that the model does not have any vaccinated individuals in the population.

To apply these models to a real-world scenario, we specifically focus on the city of San Francisco, utilizing population data from 2021. Based on available information, the population of San Francisco in 2021 was approximately 815,201 individuals. By considering this population size, we assume an initial infected population of around 100 individuals, with no individuals classified as recovered or diseased at the beginning of the simulation.

By incorporating these parameters and adapting the models to the context of San Francisco, we can simulate and analyze the spread of the disease, track the progression of immunity, and gain valuable insights into the potential for endemic stability within the city. This approach allows us to assess the effects of different transmission rates on disease dynamics.

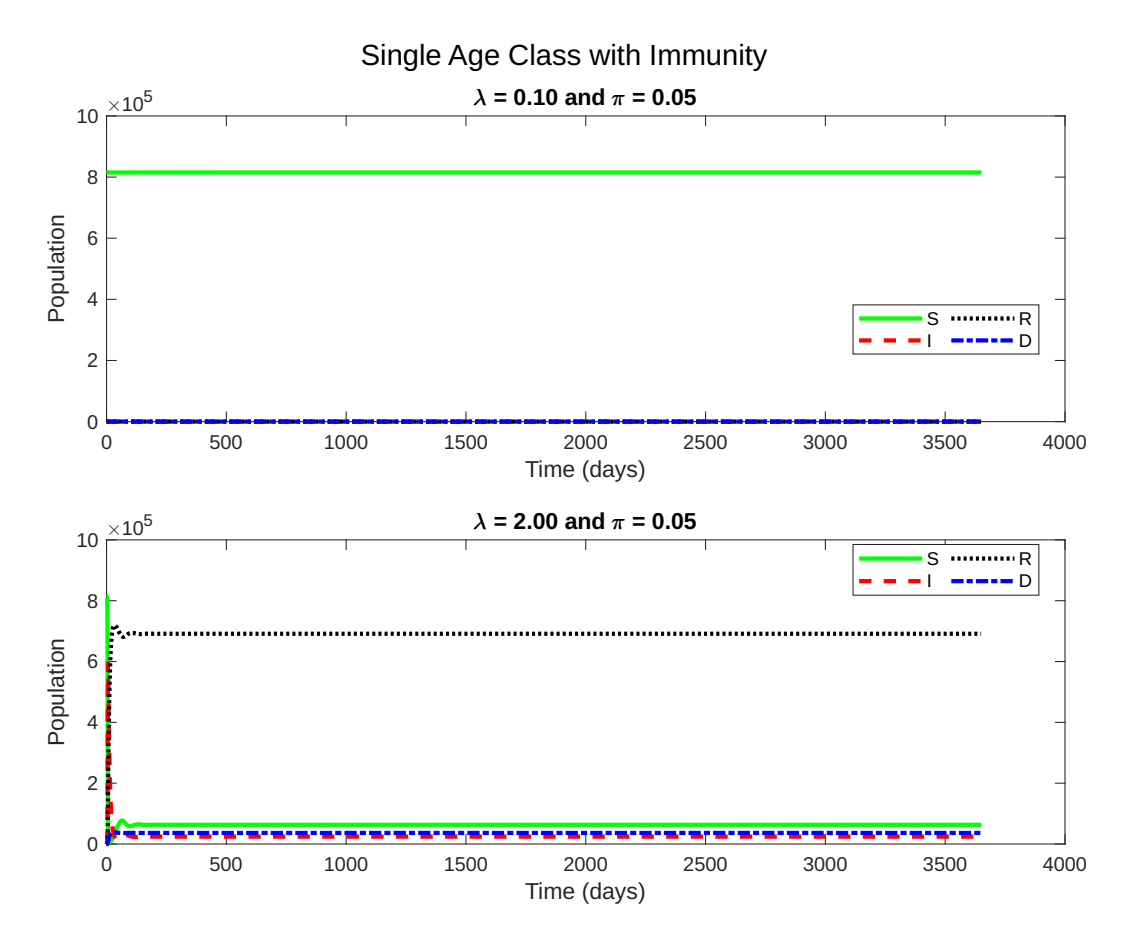


Figure 3.5: The single age class model incorporating immunity provides valuable insights into the dynamics of infectious diseases, particularly when applied to the analysis of polio. To contextualize our findings, we utilize population data from San Francisco, which has a total population of 815,201 individuals. By simulating the model over a 10-year period, we observe the emergence of a steady state, indicating a state of equilibrium in the disease dynamics. In our analysis of polio, we examine two scenarios: one with a low infection rate of 0.1 and another with a high infection rate of 2.0. When the infection rate is low, the disease incidence remains at a minimal level. This suggests that the impact on public health is relatively low, with only a small proportion of the population being affected by the disease. However, in the case of a high infection rate, the disease spreads rapidly throughout the population. This leads to a substantial increase in the number of infections and a larger population of individuals experiencing symptoms of the disease. Despite the initial surge in cases, we observe the emergence of a steady state, indicating the presence of endemic stability.

Our observations indicate that when the infection rate is very low, the

overall impact on the population is minimal. Infected individuals tend to recover quickly, resulting in a low number of infections and no symptomatic cases. However, as the infection rate increases, we observe a higher number of infections occurring within a shorter timeframe, followed by a higher likelihood of infection progress to asymptomatic state. Nevertheless, the number of individuals experiencing symptomatic disease remains relatively small, with approximately 36,388 individuals affected.

Considering equal birth and death rates in our model, we find that the susceptible population initially decreases rapidly as more individuals become infected, recovered (asymptomatic), and disease (symptomatic). However, over time, the susceptible population gradually increases due to new births, while the number of infected individuals decreases and reaches a steady state at approximately 24,260 individuals. This trend continues until a balance is achieved. Although the susceptible population does not reach zero, it becomes significantly smaller over time, resulting in a final susceptible population size of approximately 63,180 individuals.

Our analysis reveals that higher infection rates lead to a larger number of infections and recoveries (asymptomatic) individuals, while the susceptible population gradually increases but remains relatively small due to a balance between births and deaths. Moreover, the model reaches a steady state where there is no significant increase or decrease in population size for each age group. The presence of a high infection rate with a low number of symptomatic cases indicates that polio has reached endemic stability in the population.

To gain a more comprehensive understanding of disease dynamics, we also explore a two-age class model. This model introduces the concept of

age groups, specifically children and adults, allowing us to analyze how age influences disease transmission and progression. By incorporating age-specific parameters and considering the interactions between different age groups, we can gain valuable insights into the dynamics of disease spread and the impact of age-related factors on endemic stability.

By studying the two-age class model, we can examine how age-specific differences in susceptibility, infection rates, and likelihood of infection progress to asymptomatic and symptomatic state shape the spread of the disease. This approach enables us to assess the varying effects of age on disease dynamics and identify age-related factors that contribute to the establishment of endemic stability. Understanding the impact of age on disease transmission and progression is crucial for developing effective strategies to control and manage infectious diseases in different populations.

### Two age class

In our study of the two-age class model with immunity, we investigate different transmission rates similar to the single age class model. However, we introduce a distinction between children and adults by assigning different power of infection values for each group. Specifically, we assume that the power of infection for children ( $\pi_c$ ) is lower than that for adults ( $\pi_a$ ), with  $\pi_c = 0.005$  and  $\pi_a = 0.05$ . This differentiation allows us to examine how the level of infection contributes to the stability of the disease within each age group.

Furthermore, we account for the likelihood of infection progressing to the asymptomatic state, considering the differences between children and adults. For children, we set the likelihood to be approximately 0.995, indicating a high probability of progressing to the asymptomatic state. In contrast, for adults, we consider a value of 0.95, reflecting a slightly lower likelihood of progressing to the asymptomatic state.

To simulate the age transition from children to adults, we introduce a transition rate of approximately 0.001 for individuals transitioning from the children age group to the adults age group. However, in this model, there is no age transition from adults to the elderly.

For our simulation in the context of San Francisco, we utilize population data from 2021. According to available information, the population of children aged 0 to 2 years old in San Francisco was approximately 23,996, while the adult population was around 791,205. These population figures serve as the basis for initializing the model, while we maintain similar initial conditions for the other compartments as in the single age class model.

By incorporating these parameters and population data, our goal is to gain insights into the dynamics of the disease and assess its potential for endemic stability in a two-age class population. This model allows us to explore the impact of different transmission rates, age-specific power of infection, and the likelihood of progressing to the asymptomatic state, providing a more nuanced understanding of the disease dynamics within distinct age groups.

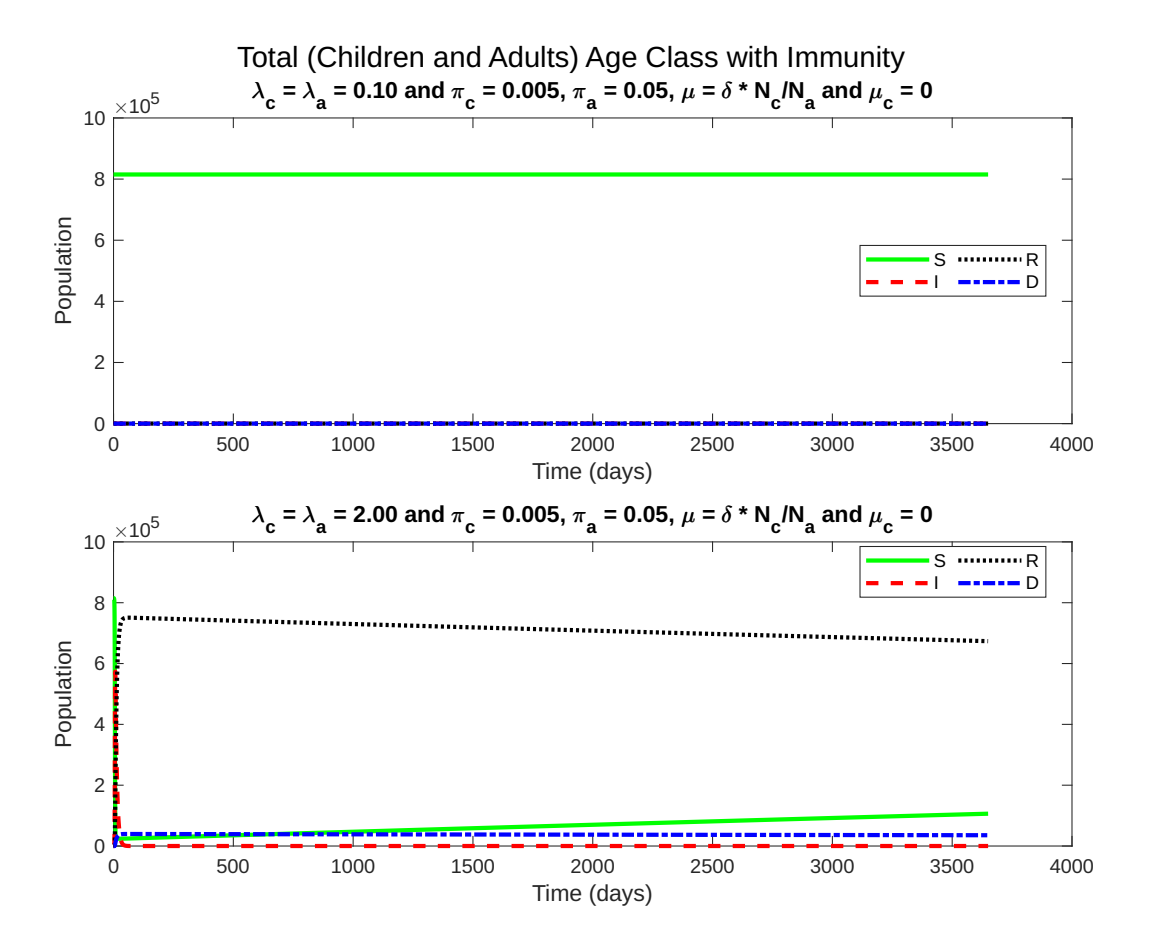


Figure 3.6: The figure illustrates the age structure model with immunity, incorporating the consideration of birth and death rates based on the modified simulation. In this modified simulation, it is assumed that only adults are capable of giving birth, represented by  $\mu_c = 0$ , while the death rate for adults,  $\mu$ , is determined by the equation  $\mu = \delta * \frac{N_c}{N_a}$ , where  $\delta$  represents the overall death rate, and  $N_c$  and  $N_a$  denote the population sizes of children and adults, respectively. The simulation results align with the previous observations when the infection rate is low, indicating the absence of an outbreak. Consequently, the susceptible population remains unchanged, as the impact of the disease is minimal. However, as the infection rate increases, an outbreak occurs, leading to a significant rise in infections within the population. Notably, as the outbreak progresses, the infected population eventually reaches zero, indicating that individuals have acquired immunity and the spread of polio has been effectively halted. This suggests that the population has developed resistance to the disease, leading to its eradication within the population. These findings emphasize the importance of considering age-specific factors and the incorporation of birth and death rates in disease modeling. By incorporating these elements, we can observe the impact of different demographic factors on disease transmission and the eventual attainment of immunity and disease eradication.

The simulation results from the modified model, which incorporates adjustments to new births occurring only among adults, reveal a significant transformation in disease dynamics. This modification leads to notable changes in the trajectory of the disease and its eventual outcome.

In the modified model, when examining the impact of low infection rates, we observe a similar pattern as in the single age class model. With minimal infection rates, the disease has a negligible impact on the population, resulting in a relatively stable susceptible population size. The number of new infections remains low, thereby maintaining a lower overall disease burden.

However, as we increase the infection rate, a distinct shift in dynamics becomes apparent. The higher infection rate leads to a more pronounced outbreak scenario characterized by a rapid increase in the number of infections within the population. The outbreak progresses rapidly, affecting a larger portion of the population before eventually reaching a peak and subsiding.

What becomes particularly intriguing in the modified model is the subsequent trend observed as the outbreak progresses. Unlike in the previous model, here we witness a decline in the number of infected individuals over time, eventually reaching zero. This signifies a significant shift towards disease eradication within the population. The decline in the infected population suggests that a substantial portion of the population has acquired immunity through previous exposure to the disease. However, it's important to note that in this model, we do not observe a steady state.

This outcome reflects the effectiveness of the population's immune response in halting the spread of polio. With a larger proportion of individuals being immune, the transmission of the disease is interrupted, resulting in the eradication of polio within the population. The eradication of polio in this refined model demonstrates the potential for successful disease control and prevention strategies, such as widespread vaccination campaigns and immunization efforts. By achieving high levels of immunity within the population, we can effectively halt the transmission of infectious diseases and work towards their eradication.

It's crucial to emphasize that the modified model shows a more favorable outcome in terms of disease control and eradication compared to the previous model, which exhibited endemic stability. Endemic stability indicates the potential for recurring outbreaks over time. These contrasting results highlight the significance of accurately representing demographic factors and birth and death rates when studying disease dynamics, as they can greatly influence the trajectory and eventual outcome of infectious diseases within a population. However, the primary goal is to achieve endemic stability, which requires identifying the necessary conditions. One approach to achieving endemic stability is by increasing the infection rate. It was observed that when the infection rate reaches or exceeds 5.3, there are still infected individuals present in the population, indicating the achievement of endemic stability. This approach is applied consistently across all models where endemic stability is not initially present.

# $\begin{array}{c} \text{Immunity} \\ \text{Children} \\ \lambda_c = \lambda_a = 0.10 \text{ and } \pi_c = 0.005, \pi_a = 0.05, \mu = \delta^* \text{N}_c/\text{N}_a \text{ and } \mu_c = 0 \\ 25 \\ 0 \\ 0 \\ 500 \\ 1000 \\ 1500 \\ 2500 \\ 3 \\ 2000 \\ 2500 \\ 3000 \\ 2500 \\ 3000 \\ 2500 \\ 3000 \\ 3500 \\ 4000 \\ 3500 \\ 4000 \\ 3500 \\ 4000 \\ 3500 \\ 4000 \\ 3500 \\ 4000 \\ 3500 \\ 4000$

Age structure model

Figure 3.7: The figure illustrates the simulation results of an age structure with immunity model, considering that new births depend on the adult population and setting the death rate for children to zero. The simulations are conducted for both children and adults, allowing us to observe the impact of different infection rates on the outbreak dynamics within each age group. When the infection rate for children is low, as well as when it is high, no outbreak is observed in the simulations. This suggests that children are less likely to become susceptible and develop symptoms of the disease, regardless of the infection rate. However, it is important to note that this does not imply the eradication of polio in the population. Instead, it indicates that children have a lower susceptibility and are less likely to show symptoms compared to adults. In contrast, when the infection rate for adults is low, no outbreak occurs, aligning with the previous observations. However, when the infection rate for adults is increased, an outbreak is observed in the simulations. This emphasizes that adults are more susceptible to the disease and can experience a higher risk of infection and symptoms when the transmission rate is higher. Interestingly, the simulation results for the age structure with immunity model closely resemble those of the total age structure simulation. This suggests that while the infected population may appear to reach zero, indicating a potential eradication of the disease, it is more likely that children who were less affected by the disease during their childhood may become susceptible and develop symptoms when they reach adulthood.

This analysis focuses on the relationship between new births and the adult population, as well as the assumption of a zero death rate for children.

The results of the simulation provide interesting insights into the dynamics of

polio infection in different age groups.

In the simulation, it is observed that the results for the children population are consistent regardless of whether the infection rate is low or high. This suggests that polio does not cause significant outbreaks among children and that they are less likely to become symptomatic when infected. This can be attributed to factors such as their immune response or previous vaccination, which provide a level of protection against the disease. Consequently, the impact of polio on the children population remains minimal throughout the simulation.

In contrast, the simulation results for the adult population reveal distinct patterns depending on the infection rate. When the infection rate is low, similar to the observations in the previous analysis, polio does not have a substantial impact on the adult population. The number of symptomatic cases remains low, indicating that the disease does not spread widely among adults in this scenario.

However, when the infection rate is high, an outbreak occurs in the adult population. In this scenario, a larger proportion of adults become infected, resulting in an increased number of symptomatic cases. Additionally, some individuals may develop asymptomatic infections and subsequently acquire immunity. This suggests that when the infection rate for polio is high, adults are more likely to experience symptoms compared to children. The higher number of symptomatic cases among adults may be attributed to factors such as weaker immune responses or a higher susceptibility to the disease.

Interestingly, the simulation also indicates the eradication of polio in the adult population. The number of infected individuals decreases to zero, indicating that the disease has been effectively controlled and eliminated. However, this does not guarantee long-term eradication, as the simulation suggests that children who were never infected with polio during their younger years remain susceptible as they transition into adulthood. If polio were to re-emerge or be reintroduced into the population, these previously uninfected individuals would be more likely to become symptomatic and contribute to the spread of the disease among adults.

In the age structure model, we have observed that the disease has been successfully eradicated. However, our main objective is to ensure that the model achieves endemic stability. Therefore, it is crucial to explore the conditions required to reach this state. One of the factors examined was the increase in the infectious rate, aiming to have infected individuals within the population. It was noted that when the infection rate is equal to or greater than 5.3, there are still infected individuals present in the population, thereby achieving endemic stability.

### Force of infection and Disease incidence

In the analysis of the force of infection and disease incidence, we focus on examining the average force of infection and disease incidence and making a comparison between the single age class and two-age class models. The aim of this analysis is to gain insights into the conditions necessary for the disease to reach an endemic state in the population.

By comparing the single age class and two-age class models, we can assess how different modeling approaches capture the dynamics of the force of infection and disease incidence. The single age class model assumes a homogeneous population, while the two-age class model incorporates age-specific parameters and compartments to account for variations in susceptibility, transmission, and recovery rates between different age groups. By comparing the results of these two models, we can gain insights into the influence of age-specific dynamics on the force of infection and disease incidence.

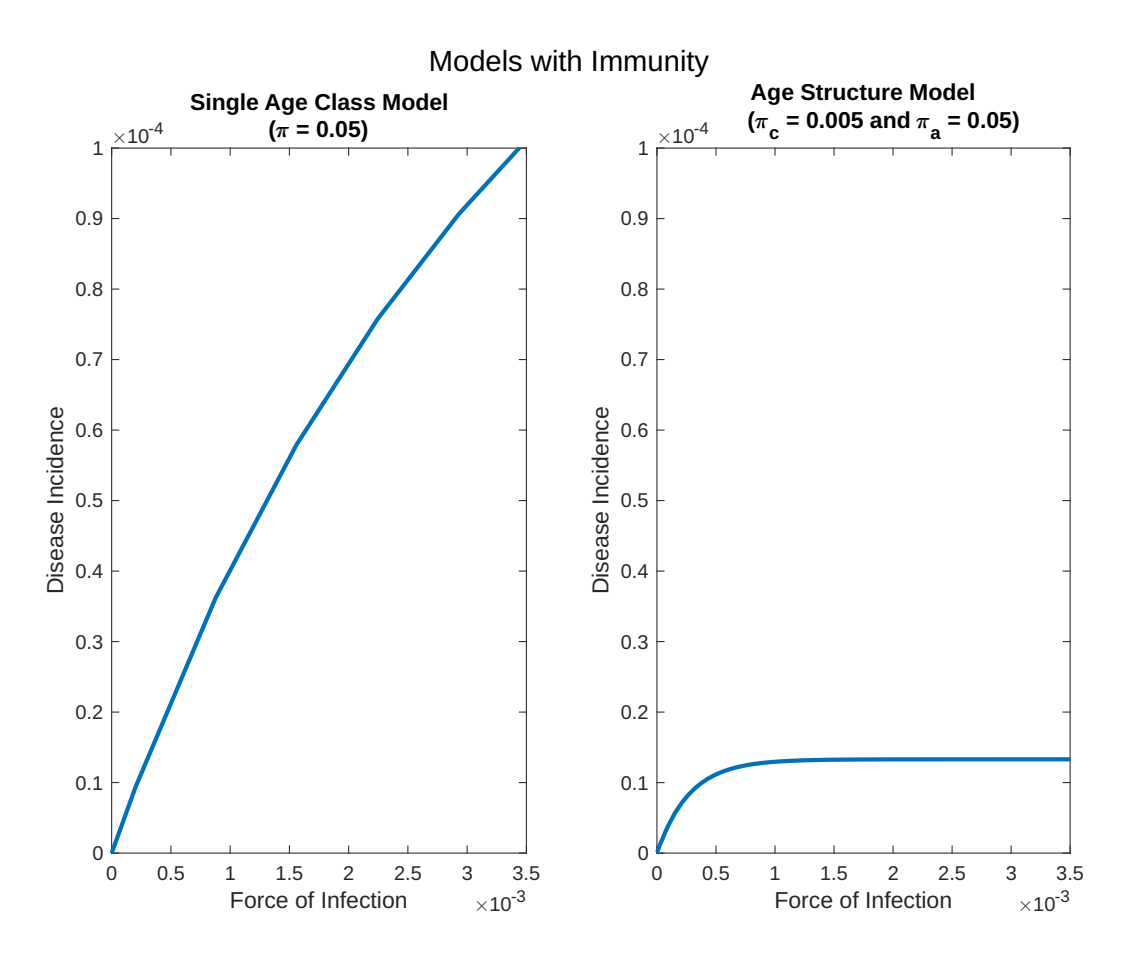


Figure 3.8: This study conducts a comparative analysis of force of infection and disease incidence dynamics in single age class and two-age class models with immunity. By varying the transmission rate from 0.0 to 2.0, we observe a notable decrease in disease incidence in the two-age class model. This reduction can be attributed to the incorporation of age-specific parameters and population structures, which enhance the model's accuracy in capturing realworld dynamics. In the age structure analysis, we consider the scenario when  $\mu = \delta \frac{N_c}{N_a}$  and  $\mu_c = 0$ , considering child births originating from adults. This enables us to assess the impact of intergenerational transmission within the population. By integrating these age-specific parameters and population structures, the two-age class model offers a more comprehensive understanding of disease dynamics, leading to a lower disease incidence compared to the single age class model. This highlights the importance of considering age heterogeneity and demographic factors when studying disease spread and control strategies.

In our study investigating the dynamics of polio transmission, we con-

ducted experiments using both a single age class model and an age structure model to understand the relationship between the force of infection, disease incidence, and age-specific factors.

In the single age class model, we consistently observed that increasing the infection rate resulted in a rise in the force of infection and disease incidence. This indicated that higher infection rates increased the likelihood of susceptible individuals becoming infected and developing symptoms. The relationship between infection rate and disease incidence showed an upward trend, indicating that as infections increased, the number of symptomatic cases also increased. However, at a certain threshold of infection rate, we noticed that the disease incidence reached a plateau. This suggested that the rate of new infections stabilized, resulting in a relatively constant level of symptomatic cases over time.

Moving to the age structure model, we expanded our analysis to incorporate age-specific factors and their impact on disease dynamics. By considering birth and death rates that account for age-specific parameters, such as the proportion of children and the lower likelihood of children dying from the disease, we introduced a more realistic representation of the population.

Interestingly, with the inclusion of age-specific factors, we found that the disease incidence reached a plateau more rapidly compared to the scenario without considering age-specific considerations. The presence of children, who were assumed to be more likely to be asymptomatic compared to adults, played a significant role in shaping disease incidence levels. When we manipulated the size of the children's population, we observed notable differences in overall disease incidence. This shift in the disease incidence peak was attributed to the

fact that infected children had a higher likelihood of remaining asymptomatic, leading to a lower number of symptomatic cases. This finding aligned with the understanding that children are more susceptible to polio and less likely to become symptomatic than adults.

Throughout our investigation, we focused specifically on the context of polio. The results from our study highlighted the complex interplay between transmission rates, age-specific factors, and disease spread. By considering the age structure and incorporating age-specific parameters, we gained valuable insights into the differential contributions of different age groups to disease transmission and the occurrence of symptomatic cases.

# 3.3 Absence of Immunity and Partial Immunity: Covid-19

# 3.3.1 Overview of Covid-19

The SARS-CoV-2 virus is responsible for causing Covid-19, an infectious disease as identified by the World Health Organization (WHO). Initially identified in 2019 in Wuhan City, Hubei Province, China, as an outbreak of respiratory illness, it rapidly spread globally and was declared a pandemic in 2020 due to its high rate of infection and the significant impact it had on public health and economies worldwide. Covid-19, also commonly referred to as Coronavirus disease, belongs to the family of novel coronaviruses [32].

## SARS-CoV-2 Transmission

The SARS-CoV-2 virus is a severe acute respiratory syndrome coronavirus that primarily spreads through respiratory droplets and particles released into the air when an infected person breathes, talks, coughs, sneezes, or engages in activities that involve the release of respiratory secretions. These droplets can be inhaled by others in close proximity or deposited on surfaces that can be touched by individuals, leading to potential transmission through contact [33].

### Symptoms and Measures

Symptoms of Covid-19 typically manifest within a range of 2 to 14 days after infection, although it is important to note that an infected person can be contagious to others for up to 2 days before symptoms appear [33].

The contagious period can last for 10 to 20 days, varying depending on factors such as an individual's immune response and the severity of their illness. While most people experience mild to moderate illness and recover without needing special treatment, certain populations, such as those with weakened immune systems, older adults, and individuals with underlying medical conditions, are at higher risk of developing severe illness [32].

The impact of Covid-19 has been devastating, with millions of deaths reported worldwide. In addition to the immediate health consequences, the disease has caused lasting health problems in some survivors, including respiratory complications, cardiovascular issues, and other long-term effects that are still being studied and understood by medical professionals.

To mitigate the spread of the virus, various preventive measures have been recommended. These include staying at home and self-isolating when feeling sick, wearing properly fitted masks in public spaces, practicing respiratory etiquette by covering the mouth and nose when coughing or sneezing, avoiding touching surfaces whenever possible, maintaining good hand hygiene by frequently washing hands with soap and water or using alcohol-based hand sanitizers, following social distancing guidelines, and adhering to local guidance and regulations regarding gatherings and public health measures.

It is important to note that while individuals may recover from Covid-19, there is a risk of subsequent infections as the disease does not necessarily confer long-lasting immunity. This means that individuals can become susceptible to reinfection after recovering from the initial illness. As a result, vaccination campaigns have played a crucial role in combating the virus, with the goal of reducing the severity of the disease, preventing hospitalizations and deaths, and ultimately achieving herd immunity to protect vulnerable populations. Vaccines have been developed and approved for emergency use in many countries, following rigorous testing and evaluation to ensure their safety and efficacy.

## 3.3.2 Mathematical Models

In this section, we delve into the study of models that investigate the intriguing phenomenon of absence or partial immunity. It is not uncommon for individuals who have previously recovered from a disease or infection to become susceptible to it again, even though they had developed some level of immunity initially. This absence of immunity implies that their immune system no longer provides adequate protection against the disease or infection, leaving them vulnerable to illness once more.

To begin our analysis, we investigate the hypothesis that the power of infection increases as individuals progress in age. This suggests that the likelihood of infection progressing to a symptomatic state becomes higher as age class increases. We can express this as the power of infection for children, denoted by  $\pi_c$ , being significantly smaller than the power of infection for adults, denoted by  $\pi_a$ .

Additionally, we examine the power of infection for subsequent infection, denoted by  $\pi^r$ , and compare it to the power of infection for primary infections, denoted by  $\pi$ . The aim here is to explore whether there is a decrease in the probability of subsequent infection among individuals who have previously been infected. If the power of infection for subsequent infection is lower than that of primary infections, it suggests a reduced likelihood of

individuals being re-infected after recovering from the initial infection.

To achieve a comprehensive understanding of these aspects of infectious diseases, we explore both single models and age-structured models. Single models focus on studying the dynamics of infection and immunity in a homogeneous population, assuming that everyone has the same level of susceptibility and recovery. On the other hand, age-structured models account for the heterogeneity of populations by dividing individuals into different age classes, recognizing that different age groups may exhibit varying levels of susceptibility and recovery.

By investigating these models, we aim to shed light on the intricate dynamics of subsequent infection and age-related susceptibility in the context of Covid-19.

# A. Single Age class model with Absence of Immunity

The single age class model used in this analysis is similar to the previously discussed immunity model. It consists of four compartments representing different states individuals can be in during the disease prevalence: susceptible (S), infected (I), recovered (R), and diseased (D). However, unlike the immunity model that considered birth and death rates to maintain population balance, this model focuses on the phenomenon of absence of immunity.

When an individual recovers from the disease, instead of acquiring longlasting immunity, they become susceptible to the infection again. This implies a transition from the recovered (R) and diseased (D) compartments back to the susceptible (S) compartment, reflecting the loss of immune protection and the potential for reinfection. By incorporating the absence of immunity mechanism, we can observe the flow of individuals between compartments in the population over time.

The mathematical equations (3.17, 3.18, 3.19, and 3.20) governing the transition between these compartments capture the dynamics of the disease in the single age class model. These equations describe the rates of change for each compartment and determine how individuals move between susceptible, infected, recovered, and diseased states. Simulating these equations allows us to study the system's behavior and explore the impact of the absence of immunity.

The model simulation enables the investigation of conditions required for achieving endemic stability, where the disease persists in the population over the long term. By analyzing the system's dynamics and studying its stability properties, we can gain insights into the factors contributing to sustained disease transmission and its population-level impact.

Figure 3.9 visualizes the flow of individuals between compartments in the single age class model, illustrating the transitions and interactions among susceptible, infected, recovered, and diseased populations. This visualization aids in understanding the disease dynamics and the role of absence of immunity in shaping infection spread and persistence.

Through this analysis, we aim to deepen our understanding of the impact of absence of immunity and explore the conditions necessary for establishing and maintaining endemic stability in the single age class model.

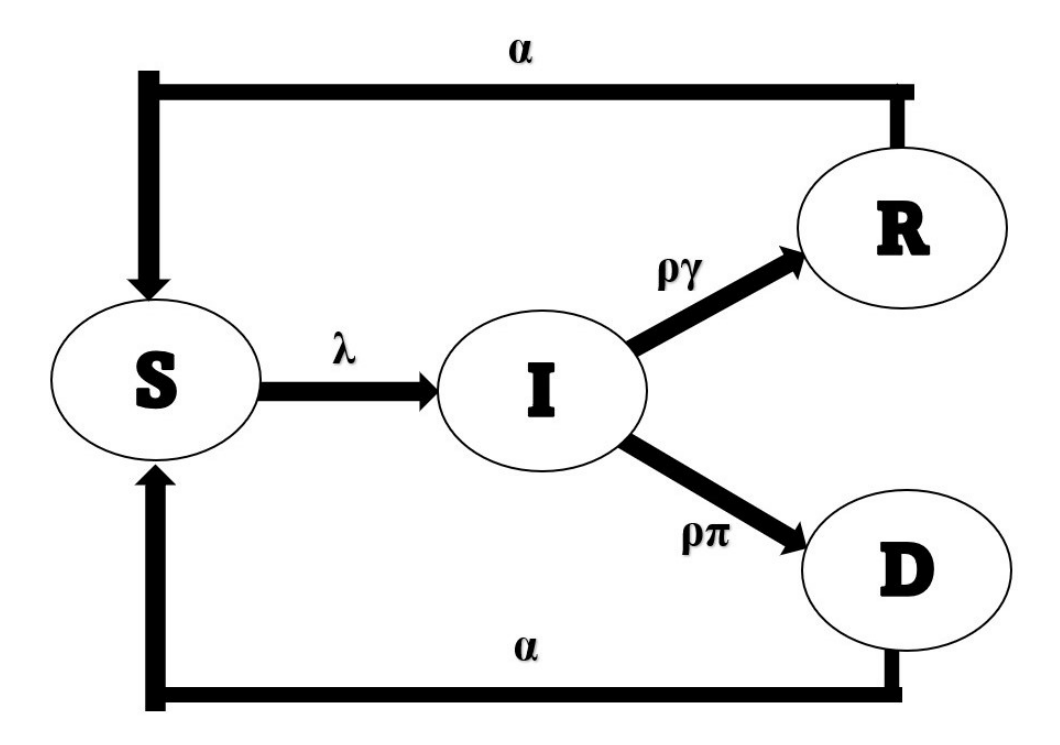


Figure 3.9: This informative diagram presents a schematic representation of the single age class model, focusing on disease transmission and progression within a population comprising a single age group. In this model, the absence of immunity is assumed, meaning individuals remain continuously susceptible to the disease. By visualizing the transitions between compartments (Susceptible, Infected, Recovered, and Diseased), the diagram provides a valuable insight into the dynamics of disease within a homogeneous population.

$$\frac{dS}{dt} = -\lambda S \frac{I}{N} + \alpha (R+D), \qquad (3.17)$$

$$\frac{dI}{dt} = \lambda S \frac{I}{N} - \rho(\gamma + \pi)I, \qquad (3.18)$$

$$\frac{dR}{dt} = \rho \gamma I - \alpha R \qquad (3.19)$$

$$\frac{dD}{dt} = \rho \pi I - \alpha D \qquad (3.20)$$

$$\frac{dR}{dt} = \rho \gamma I - \alpha R \tag{3.19}$$

$$\frac{dD}{dt} = \rho \pi I - \alpha D \tag{3.20}$$

The set of equations (3.17) - (3.20) describe a single-age SIRD (Susceptible-

Infectious-Recovered-Disease) model for infectious diseases. Equation (3.17) represents the rate of change of susceptible individuals, indicating how the number of susceptible individuals changes over time. It considers the infection rate of the disease, represented by  $\lambda$ , which determines how easily the disease spreads. The term  $\lambda S \frac{I}{N}$  captures the rate at which susceptible individuals become infected, proportional to the product of the number of susceptible individuals (S) and infectious individuals (I) divided by the total population size (N). Additionally, the term  $\alpha$  (R + D) represents the rate at which individuals lose their immunity and transition from the recovered (R) or disease (D) compartments back to the susceptible compartment (S).

Equation (3.18) represents the rate of change of infectious individuals. It considers the infection dynamics, likelihood of infection progressing to asymptomatic and symptomatic state. The term  $\lambda S \frac{I}{N}$  represents the rate at which susceptible individuals become infected, as mentioned earlier. The term  $\rho(\gamma + \pi)I$  capture the rate at which infectious individuals progress to asymptomatic and symptomatic state. It is the product of the timescale that infections are contagious  $(\rho)$ , the likelihood of infection progress to asymptomatic state of infectious individuals  $(\gamma)$ , and the power of infection of individuals  $(\pi)$ .

Equation (3.19) represents the rate of change of recovered individuals. It accounts for the individuals who have recovered from the disease and loss immunity. The term  $\rho\gamma I$  represents the rate at which infectious individuals become asymptomatic and transition to the recovered compartment (R). The term  $\alpha R$  represents the rate at which recovered individuals lose their immunity and transition back to the susceptible compartment (S).

Equation (3.20) represents the rate of change of disease individuals, representing those who are symptomatic with the disease. The term  $\rho\pi I$  represents the rate at which infectious individuals become symptomatic (disease) and transition to the disease compartment (D). The term  $\alpha D$  represents the rate at which symptomatic individuals lose their immunity and transition back to the susceptible compartment (S).

These equations provide insights into the dynamics of disease transmission, recovery, and disease within a single-age population. They highlight the interplay between the various compartments and the factors influencing the spread and control of infectious diseases. In this model, without accounting for birth and death, the total population remains constant, indicating that everyone is likely to be infected at least once during the course of the disease.

To gain further insights into the dynamics of the model, we can calculate key epidemiological measures that provide valuable information about disease transmission and impact. Two such measures are the force of infection and disease incidence, which can be computed using equations similar to those used in the post-infection single-age model. These measures will help us assess the intensity of disease transmission and the rate of new infections over time, enhancing our understanding of the epidemiological dynamics in the population.

#### **Identifying Steady States**

To analyze the steady states of the single age class model with absence of immunity, it is necessary to simplify the model. The original model is complex, and simplifying it would make it easier to identify the steady states. Following the approach used in the classical SIR model, we aim to determine the equilibria of the equations. This helps us understand when we have a disease-free equilibrium or a disease endemic state. In the single age class model, we begin by introducing the variable  $\tilde{R} = R + D$  to account for the loss of immunity. This modification leads to a new model formulation, as demonstrated below.

$$\frac{dS}{dt} = -\lambda S \frac{I}{N} + \mu \tilde{R},\tag{3.21}$$

$$\frac{dI}{dt} = \lambda S \frac{I}{N} - \rho(\gamma + \pi)I, \qquad (3.22)$$

$$\frac{d\tilde{R}}{dt} = \rho \gamma I - \alpha \tilde{R} \tag{3.23}$$

To analyze the steady states of the single age class model with absence of immunity, we consider two equilibrium points: the disease-free equilibrium and the disease-endemic equilibrium.

At the disease-free equilibrium, where the infected population I is zero, the susceptible population S reaches a value of  $\frac{\rho\gamma N}{\lambda}$ . This equilibrium represents the eradication of the disease.

At the disease-endemic equilibrium, where  $I \neq 0$ , we solve for the value of I by setting  $\frac{dS}{dt} = 0$ . The equation becomes:

$$-\lambda \frac{I}{N}S + \alpha \tilde{R} = 0$$

$$-\lambda \frac{I}{N}S + \alpha(N - S - I) = 0$$

Simplifying and substituting the value of S, we have:

$$-\lambda \frac{I}{N} \frac{\rho \gamma N}{\lambda} + \alpha N - \alpha \frac{\rho \gamma N}{\lambda} - \alpha I = 0$$

Solving for I, we obtain the steady state at the disease-endemic equilibrium:

$$I^* = \frac{\alpha N (1 + \frac{\rho \gamma}{\lambda})}{\rho \gamma + \alpha}$$

Therefore, we can calculate force of infection using  $I^*$  as:

$$F \approx \lambda I^* = \frac{\alpha N(\lambda + \rho \gamma)}{\rho \gamma + \alpha}$$

Additionally, the disease incidence rate can be defined as:

$$D \approx \rho \pi I^* = \rho \pi \frac{\alpha N (1 + \frac{\rho \gamma}{\lambda})}{\rho \gamma + \alpha}$$

By analyzing the relationship between the force of infection and disease incidence, we expect to see a linear relationship where an increase in the force of infection results in a proportional increase in disease incidence.

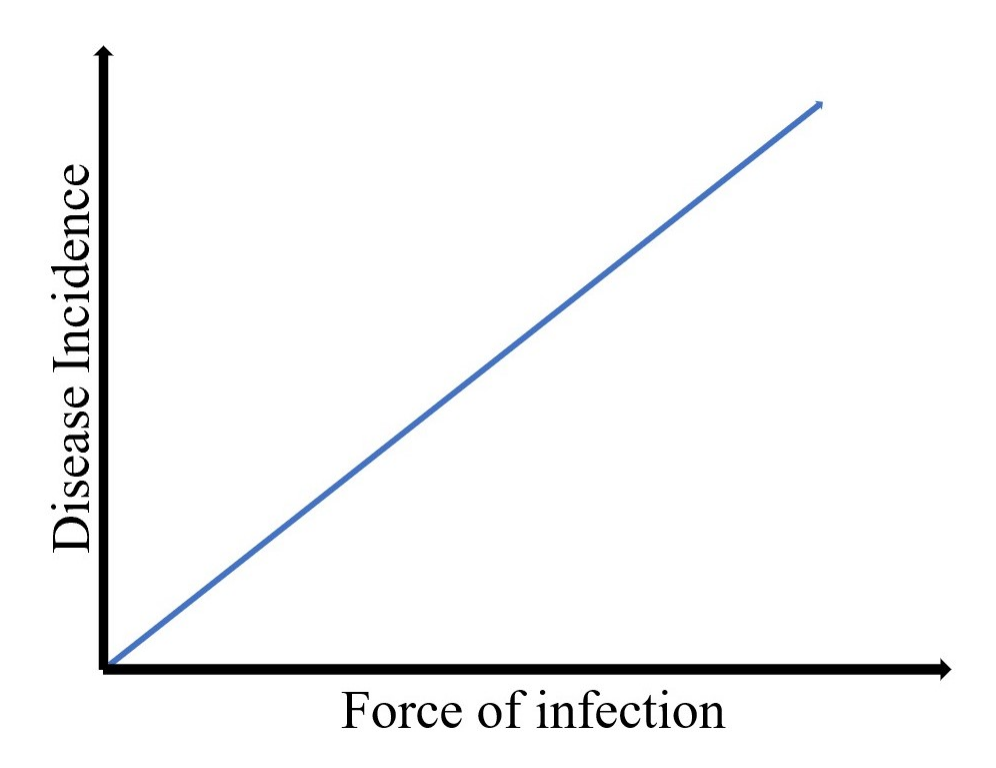


Figure 3.10: This graph illustrates the relationship between disease incidence and force of infection in the single age class absence of immunity model. As the force of infection increases, indicating a higher infection rate or increased contact between susceptible and infectious individuals, the disease incidence also increases. The relationship between these two variables is linear, highlighting the direct impact of the force of infection on the occurrence of new infections within the population.

Through our analysis of the single age class model with absence of immunity, we anticipate finding a direct relationship between the force of infection and disease incidence. Specifically, as the force of infection increases, we expect to observe a corresponding increase in the number of new cases of the disease. This phenomenon is expected due to the potential for individuals in the population to experience reinfection as a result of the loss of immunity, which can lead to an increase in the overall number of new cases of the disease. This is illustrated in the single age class model with absence of immunity

flow chart, where individuals may transition back to the susceptible compartment after a period of time, leading to an increased likelihood of infection and subsequent disease incidence.

# B. Age Structure Model with Absence of Immunity

The age structure model with absence of immunity follows a structure similar to the age structure model with immunity, but with some differences. It does not consider birth and death rates, focusing instead on the concept of loss of immunity. This model incorporates two age classes and four compartments (Susceptible, Infectious, Recovered, and Disease) to represent population dynamics.

The flow chart depicted in Figure 3.12 illustrates the transitions between compartments for each age class. Upon infection, individuals move from the susceptible compartment to the infectious compartment. Subsequently, they can transition to either the recovered or diseased compartments based on the disease outcome. Recovered individuals have the potential to lose their immunity and return to the susceptible compartment, while diseased individuals can also lose their immunity but remain in the diseased compartment.

The mathematical equations governing the age structure model without immunity are presented in Equations (3.24 - 3.31). These equations describe the rates of change for each compartment in each age class.

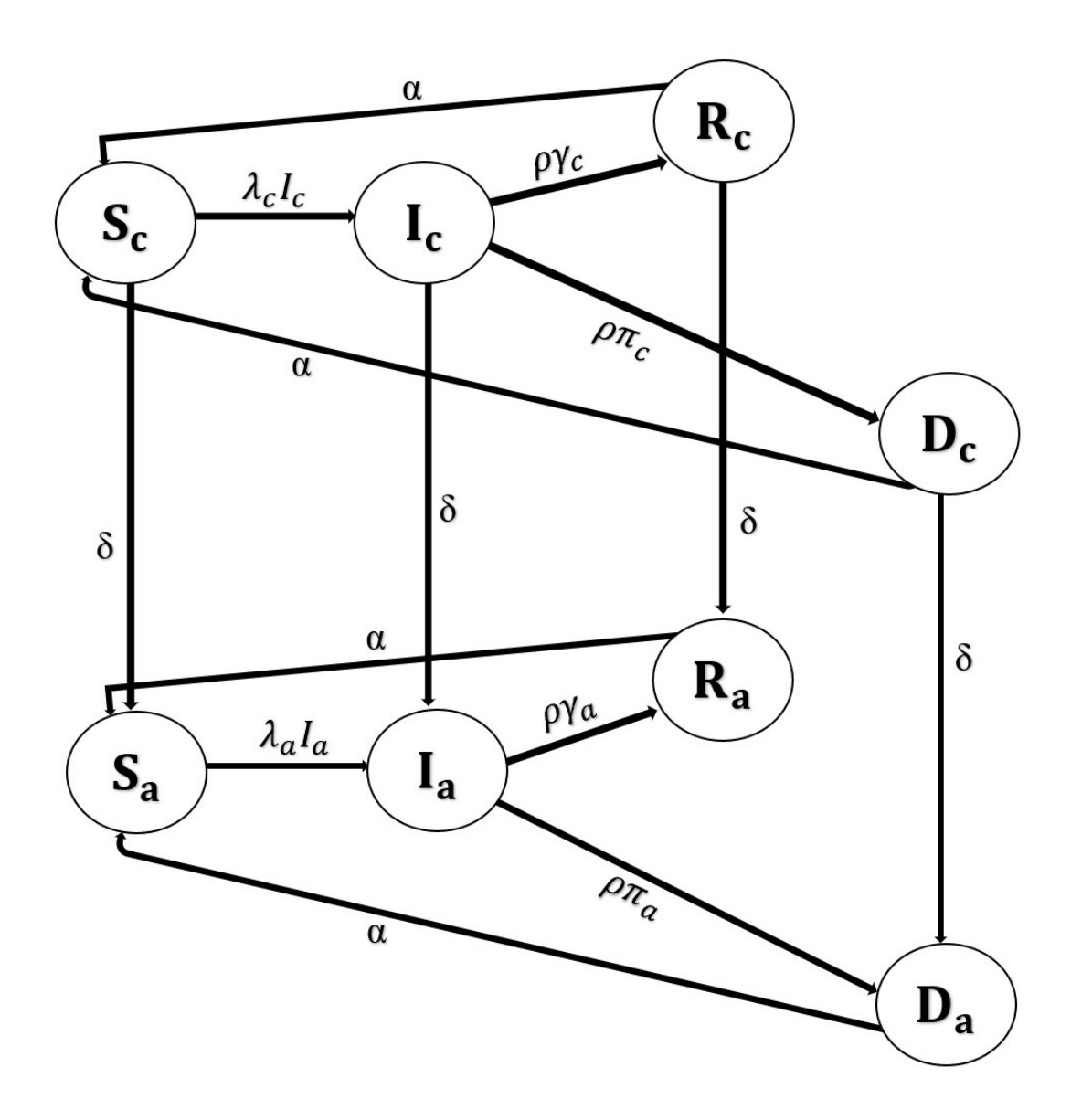


Figure 3.11: This model illustrates the spread of infectious diseases within a population using an age structure model that focus on absence of immunity. The population is divided into two age groups: children and adults, represented by the arrows flowing between the susceptible (S), infected (I), recovered (R), and disease (D) categories. The arrows indicate the movement of individuals as they transition between these compartments, capturing the transmission dynamics of the disease.

$$\frac{dS_c}{dt} = -\lambda_c \frac{I_c}{N} S_c + \alpha R_c + \alpha D_c - \delta S_c, \tag{3.24}$$

$$\frac{dS_a}{dt} = -\lambda_a \frac{I_a}{N} S_a + \alpha R_a + \alpha D_a + \delta S_c, \tag{3.25}$$

$$\frac{dI_c}{dt} = \lambda_c \frac{I_c}{N} S_c - \rho (\gamma_c + \pi_c) I_c - \delta I_c, \tag{3.26}$$

$$\frac{dI_a}{dt} = \lambda_a \frac{I_a}{N} S_a - \rho (\gamma_a + \pi_a) I_a + \delta I_a, \tag{3.27}$$

$$\frac{dR_c}{dt} = \rho \gamma_c I_c - \beta R_c - \delta R_c \tag{3.28}$$

$$\frac{dR_a}{dt} = \rho \gamma_a I_a - \beta R_a + \delta R_a \tag{3.29}$$

$$\frac{dD_c}{dt} = \rho \pi_c I_c - \alpha D_c - \delta D_c \tag{3.30}$$

$$\frac{dD_a}{dt} = \rho \pi_a I_a - \alpha D_a + \delta D_a \tag{3.31}$$

An age structure model, considering children and adults as distinct age classes, provides valuable insights into the transmission dynamics of a disease within a population. This model consists of compartments representing the susceptible, infected, recovered (asymptomatic), and diseased (symptomatic) populations.

In this simplified model, the total population is divided into two age classes: children and adults. Each age class has its own set of compartments, and the sum of individuals in each compartment within an age class adds up to the total population of that age class.

To capture important aspects of disease transmission, the model incorporates various parameters. The infection rate  $(\lambda_{c,a})$  represents the rate at which the disease spreads within each age class. The probabilities of transitioning to the asymptomatic and symptomatic states are denoted by  $\gamma_{c,a}$  and

 $\pi_{c,a}$ , respectively.

The parameters  $\alpha$  reflect the loss of immunity in symptomatic and asymptomatic infections within each age class. These parameters determine the duration of immunity after recovering from the disease.

The parameter  $\rho$  represents the contagious period of infected individuals, indicating the timeframe in which they can transmit the disease to susceptible individuals. The parameter  $\delta$  captures the transition rate between age classes, representing the movement of individuals from one age class to another as they age.

It is important to note that in this model, no birth or death processes are considered. As individuals transition from the child age class to the adult age class, the population of children eventually diminishes to zero. However, to refine the model, we assume a zero-transition rate between age classes, meaning children remain children indefinitely. This refinement allows us to examine the dynamics of disease transmission while considering a fixed population of children.

By simulating this refined model over a specified time period, we can gain valuable insights into the dynamics of disease transmission, the differential impact on different age groups, and the potential for re-infection or loss of immunity within the population. These insights can inform public health strategies, intervention planning, and efforts towards disease control and prevention.

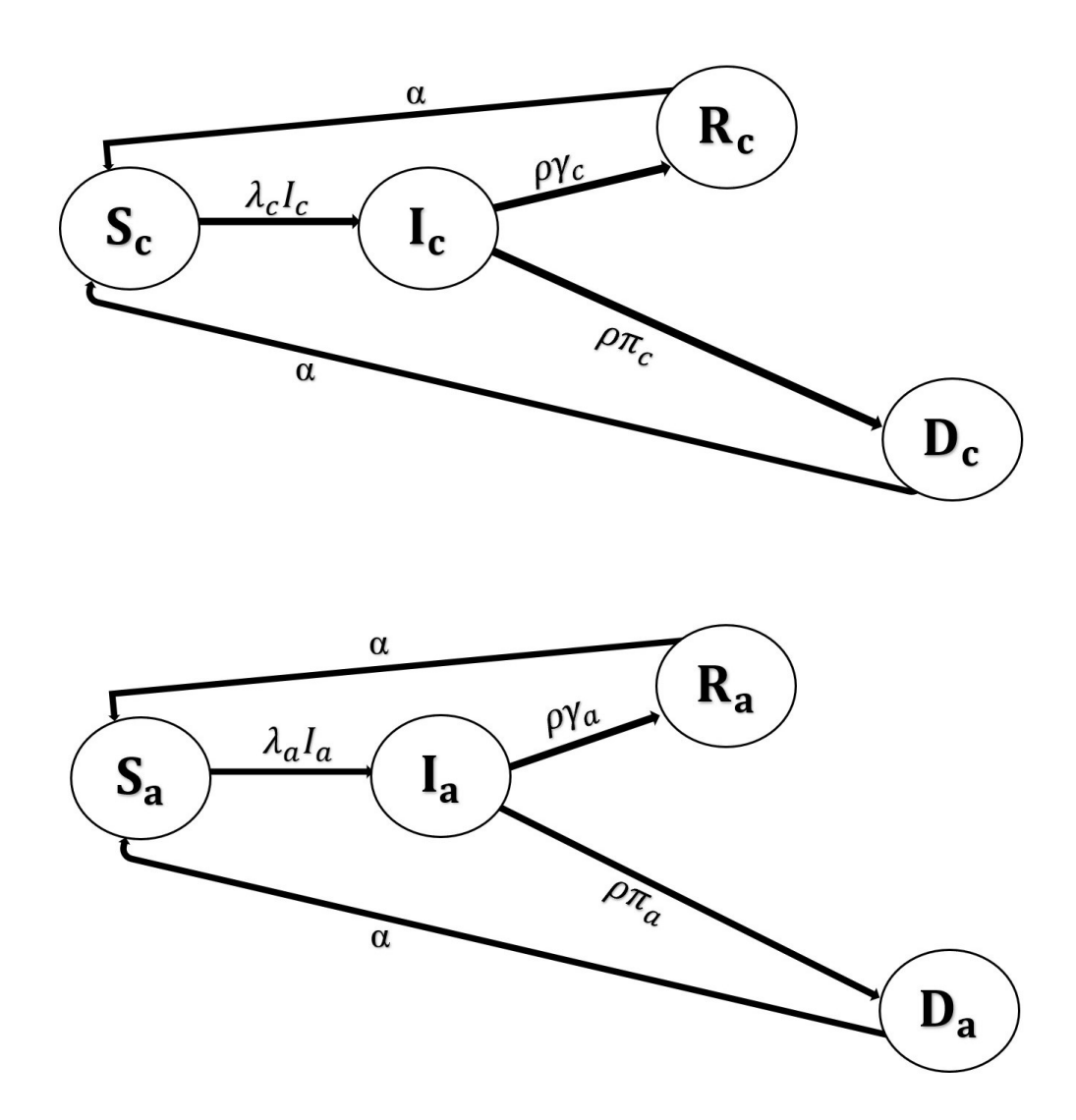


Figure 3.12: This model illustrates the spread of infectious diseases within a population using an age structure model that focus on absence of immunity without considering transition between age class. The population is divided into two age groups: children and adults, represented by the arrows flowing between the susceptible (S), infected (I), recovered (R), and disease (D) categories. The arrows indicate the movement of individuals as they transition between these compartments, capturing the transmission dynamics of the disease. This model illustrates that children class will remain children forever as well as the adult population.

$$\frac{dS_c}{dt} = -\lambda_c \frac{I_c}{N} S_c + \alpha R_c + \alpha D_c$$

$$\frac{dS_a}{dt} = -\lambda_a \frac{I_a}{N} S_a + \alpha R_a + \alpha D_a$$

$$\frac{dI_c}{dt} = \lambda_c \frac{I_c}{N} S_c - \rho (\gamma_c + \pi_c) I_c$$

$$\frac{dI_a}{dt} = \lambda_a \frac{I_a}{N} S_a - \rho (\gamma_a + \pi_a) I_a$$

$$\frac{dR_c}{dt} = \rho \gamma_c I_c - \beta R_c$$

$$\frac{dR_a}{dt} = \rho \gamma_a I_a - \beta R_a$$

$$\frac{dD_c}{dt} = \rho \pi_c I_c - \alpha D_c$$

$$\frac{dD_a}{dt} = \rho \pi_a I_a - \alpha D_a$$

Variable	Description	unit
λ	Infectious rate of susceptible population	1 people*days
$\alpha$	The timescale of loss of immunity	
$\pi$	Power of infection, likelihood of infection progress to symptomatic	days
$\gamma = (1 - \pi)$	Likelihhod of infection progress to asymptomatic state	$\begin{array}{c} \frac{1}{\text{days}} \\ \frac{1}{1} \\ \text{days} \\ \frac{1}{\text{days}} \\ \frac{1}{\text{days}} \\ \frac{1}{\text{days}} \\ \frac{1}{\text{days}} \end{array}$
ho	Timescale that Infections are contagious	$\frac{1}{\text{days}}$
$\delta$	Transition rate between age groups	days
t	Time	days
S	Number of susceptible people	people
I	Number of infected people	people
R	Number of recovered (asymptomatic) people	people
D	Number of disease (symptomatic) people	people
N	Total number of people	people

Table 3.2: This table presents the units associated with the variables and parameters utilized in absence of immunity SIRD (Susceptible-Infected-Recovered-Disease) models. The variables, representing population compartments such as susceptible (S), infected (I), recovered (R), and disease (D), are measured in absolute quantities or proportions. The parameters, including infection rates, power of infection, and loss of immunity rates, possess specific units that may vary depending on the particular disease and context being modeled.

# C. Single Age class Partial Immunity without Birth and Death

The single age class partial immunity model expands upon the SIRD framework, focusing on the dynamics of re-infection. It specifically accounts for scenarios where individuals can lose immunity after recovering from the disease, such as Covid-19.

This model introduces six compartments to represent different states of the population: susceptible (S), infected (I), recovered (R), disease (D), susceptible to re-infection  $(S^r)$ , and infected through re-infection  $(I^r)$ .

By investigating the flow of individuals among these compartments, as illustrated in Figure 3.13 and analyzing the mathematical equations (3.32 – 3.37) governing the model, we gain valuable insights into the complex dynamics of the disease.

This analysis allows us to explore the impact of partial immunity on disease transmission and progression within the population. We observe how individuals transition from susceptibility to infection, and potentially progress to a recovered or diseased state. Additionally, we consider the possibility of individuals who are asymptomatic and symptomatic from the disease becoming susceptible to re-infection, leading to a new cycle of infection.

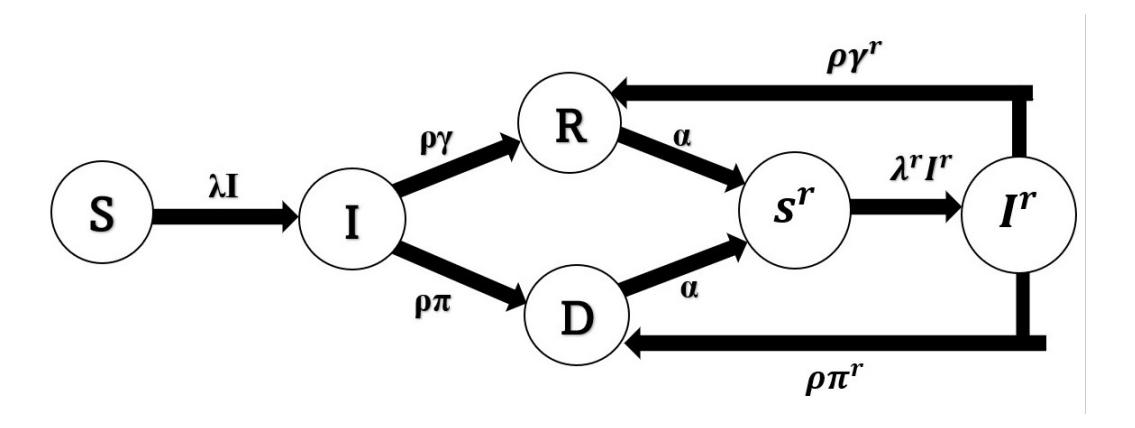


Figure 3.13: This model illustrates the dynamics of disease transmission and progression within a population, accounting for compartments such as susceptible, infected, recovered (asymptomatic), diseased (symptomatic), susceptible to re-infection, and infected through re-infection. The model offers valuable insights into the effects of partial immunity on disease spread and progression, providing a comprehensive understanding of the interplay between different compartments and the overall population dynamics.

$$\frac{dS}{dt} = -\lambda S \frac{I}{N} \tag{3.32}$$

$$\frac{dI}{dt} = \lambda S \frac{I}{N} - \rho(\gamma + \pi)I \tag{3.33}$$

$$\frac{dR}{dt} = \rho \gamma I - \alpha R + \rho^r \gamma^r I^r \qquad (3.34)$$

$$\frac{dD}{dt} = \rho \pi I - \alpha D + \rho^r \pi^r I^r \qquad (3.35)$$

$$\frac{dD}{dt} = \rho \pi I - \alpha D + \rho^r \pi^r I^r \tag{3.35}$$

$$\frac{dS^r}{dt} = \alpha(R+D) - \lambda^r \frac{I^r}{N} S^r \tag{3.36}$$

$$\frac{dI^r}{dt} = \lambda^r \frac{I^r}{N} S^r - \rho^r (\gamma^r + \pi^r) I^r$$
(3.37)

In the single age class partial immunity model, we utilize a set of mathematical equations to analyze the dynamics of various population compartments. These equations provide valuable insights into the changes occurring within the susceptible, infected, recovered, diseased, susceptible in the reinfection group, and infected in the reinfection group populations.

Equation (3.32) characterizes the rate of change of the susceptible population, depicting the decrease in susceptible due to disease transmission. The parameter  $\lambda$  represents the infection rate, indicating how quickly susceptible individuals become infected. The variable S denotes the susceptible population, I represents the infected population, and N signifies the total population size.

Equation (3.33) represents the rate of change of the infected population, highlighting its increase through new infections and decrease through recovery (asymptomatic) and disease progression (symptomatic). This equation enables us to understand the fluctuations in the number of individuals actively infected with the disease over time.

Equation (3.34) describes the rate of change of the recovered population, capturing its increase through recovery from the infection. However, it also accounts for the potential decrease in the recovered population due to loss of immunity and subsequent reinfection. This equation provides insights into the dynamics of individuals who have successfully recovered from the disease but remain susceptible to reinfection.

Equation (3.35) represents the rate of change of the diseased population, illustrating its increase through disease progression, as individuals transition from being infected to exhibiting symptoms. Similar to the recovered population, the diseased population can also decrease due to the loss of immunity leading to reinfection. This equation allows us to understand the dynamics of individuals affected by symptomatic disease and their potential for reinfection. Equation (3.36) focuses on the dynamics of individuals in the susceptible population in the reinfection group, who have previously been infected. It considers the possibility of reinfection, acknowledging that individuals in this group can become susceptible to the disease again. This equation explores how the susceptible population in the reinfection group changes over time, considering both natural population loss and reinfection dynamics.

Equation (3.37) provides insights into the dynamics of individuals who have been previously infected but are now susceptible to reinfection. It considers the possibilities of reinfection, recovery, and disease progression within this specific population subgroup. By examining this equation, we can understand how the number of individuals in the reinfection group who become reinfected or recover evolves over time.

Through the examination and analysis of these equations, we can gain a better understanding of how different population compartments interact and change over time in the context of absence or partial immunity. These mathematical representations allow us to explore the complex dynamics of disease transmission, recovery, reinfection, and disease progression, providing crucial insights into the behavior of infectious diseases within a single age class population.

# D. Age Structure Model Partial Immunity without Birth and Death

The age structure model, an extension of the single age class partial immunity model, provides a more comprehensive understanding of disease dynamics by considering the heterogeneity of age groups within the population. This model acknowledges that individuals of different ages may have distinct

levels of susceptibility, infection rates, asymptomatic and symptomatic cases, and re-infection dynamics.

In the age structure model, the population is divided into multiple age groups, each characterized by its own compartments representing the susceptible, infected, recovered (asymptomatic), diseased (symptomatic), susceptible to re-infection, and infected through re-infection populations. The transitions between these compartments are governed by age-specific parameters.

By examining the flow of individuals among these compartments, as depicted in Figure 3.15 and analyzing the system of equations (3.38 - 3.49) that describe the model, we gain a deeper understanding of the intricate dynamics of disease transmission and progression within different age groups.

Incorporating age structure into the partial immunity model enables us to explore the influence of age-related factors on disease dynamics. This includes comprehending the varying vulnerability of specific age groups to infection, assessing the potential for intergenerational transmission, and evaluating the effectiveness of age-targeted interventions. By accounting for age-specific parameters, we can develop more targeted strategies for disease control and prevention, tailored to the unique characteristics and requirements of different age groups in the population.

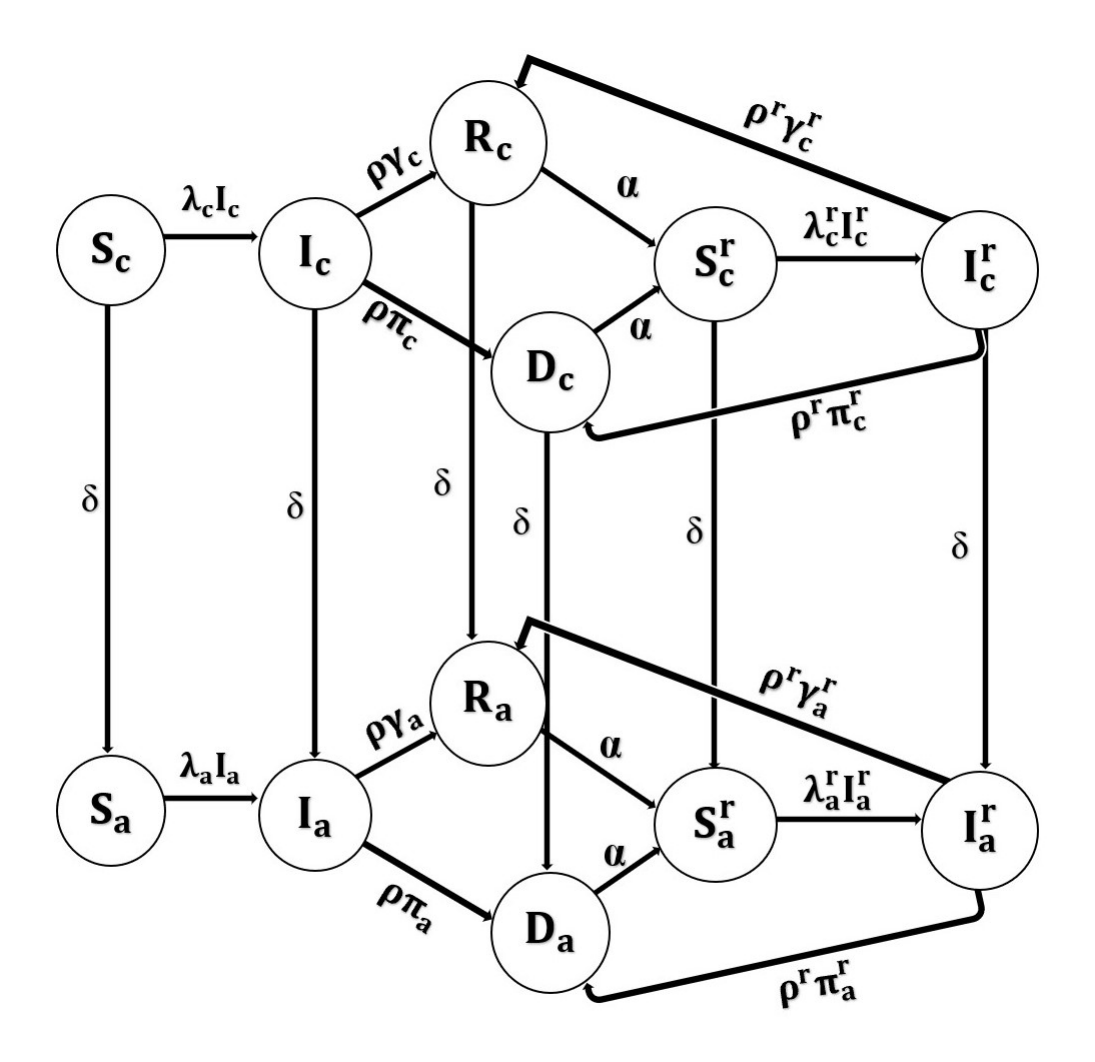


Figure 3.14: This model captures the dynamics of disease transmission and progression within a population that is divided into different age groups. The compartments include susceptible (S), infected (I), recovered (R), diseased (D), susceptible to re-infection  $(S^r)$ , and infected through re-infection  $(I^r)$  for each age group. By analyzing the transitions between these compartments and considering age-specific parameters, we gain insights into the interplay between age structure and partial immunity in shaping the spread and impact of the disease within the population.

$$\frac{dS_c}{dt} = -\lambda_c S_c \frac{I_c}{N} - \delta S_c \tag{3.38}$$

$$\frac{dS_a}{dt} = -\lambda_a S_a \frac{I_a}{N} + \delta S_c \tag{3.39}$$

$$\frac{dI_c}{dt} = \lambda_c S_c \frac{I_c}{N} - \rho(\gamma_c + \pi_c) I_c - \delta I_c$$
(3.40)

$$\frac{dI_a}{dt} = \lambda_a S_a \frac{I_a}{N} - \rho(\gamma_a + \pi_a) I_a + \delta I_c$$
(3.41)

$$\frac{dR_c}{dt} = \rho \gamma_c I_c - \alpha R_c + \rho^r \gamma_c^r I_c^r - \delta R_c$$
(3.42)

$$\frac{dR_a}{dt} = \rho \gamma_a I_a - \alpha R_a + \rho^r \gamma_a^r I_a^r + \delta R_c \tag{3.43}$$

$$\frac{dD_c}{dt} = \rho \pi_c I_c - \alpha D_c + \rho^r \pi_c^r I_c^r - \delta D_c$$
(3.44)

$$\frac{dD_a}{dt} = \rho \pi_a I_a - \alpha D_a + \rho^r \pi_a^r I_a^r + \delta D_c \tag{3.45}$$

$$\frac{dS_c^r}{dt} = \alpha (R_c + D_c) - \lambda_c^r \frac{I_c^r}{N} S_c^r - \delta S_c^r$$
(3.46)

$$\frac{dS_a^r}{dt} = \alpha (R_a + D_a) - \lambda_a^r \frac{I_a^r}{N} S_a^r + \delta S_c^r$$
(3.47)

$$\frac{dI_c^r}{dt} = \lambda_c^r \frac{I_c^r}{N} S_c^r - \rho^r (\gamma_c^r + \pi_c^r) I_c^r - \delta I_c^r$$
(3.48)

$$\frac{dI_a^r}{dt} = \lambda_a^r \frac{I_a^r}{N} S_a^r - \rho^r (\gamma_a^r + \pi_a^r) I_a^r + \delta I_c^r$$
(3.49)

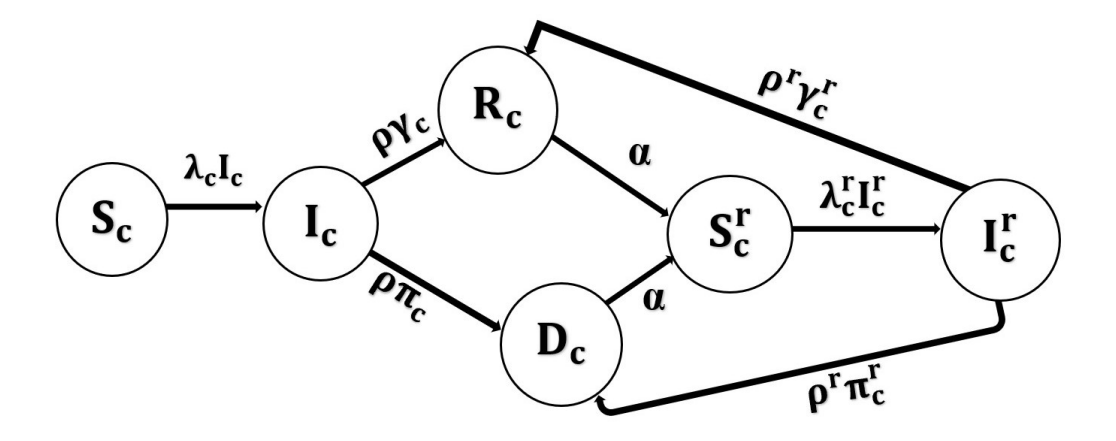
The age structure model with partial immunity builds upon the single age class model by introducing two distinct age classes: children and adults. The total population is now represented as the sum of individuals in both age classes, denoted as  $N = N_c + N_a$ . This extension enables us to capture the different dynamics and characteristics of disease transmission and progression within each age group.

In this model, we introduce the transition rate parameter  $\delta$ , which accounts for the movement of individuals between the two age classes. This parameter reflects the natural aging process and population dynamics, allow-

ing us to analyze how changes in age structure influence disease spread and progression.

The equations governing the age structure model with partial immunity are similar to those of the single age class model, but they are now differentiated for each age class. Variables and parameters such as the susceptible population (S), infected population (I), recovered population (R), diseased population (D), and the susceptible and infected populations in the reinfection group  $(S^r)$  and  $I^r$  are considered separately for each age class.

However, we acknowledge a limitation in the original model, which could result in the eventual depletion of the child population as they transition to adulthood. To overcome this issue, we refine the model by introducing a modification. In the refined model, we assume that children remain in the child age class indefinitely, with a transition rate of zero between age classes. This modification ensures the stability of the child population throughout the simulation, addressing the concern of population depletion.



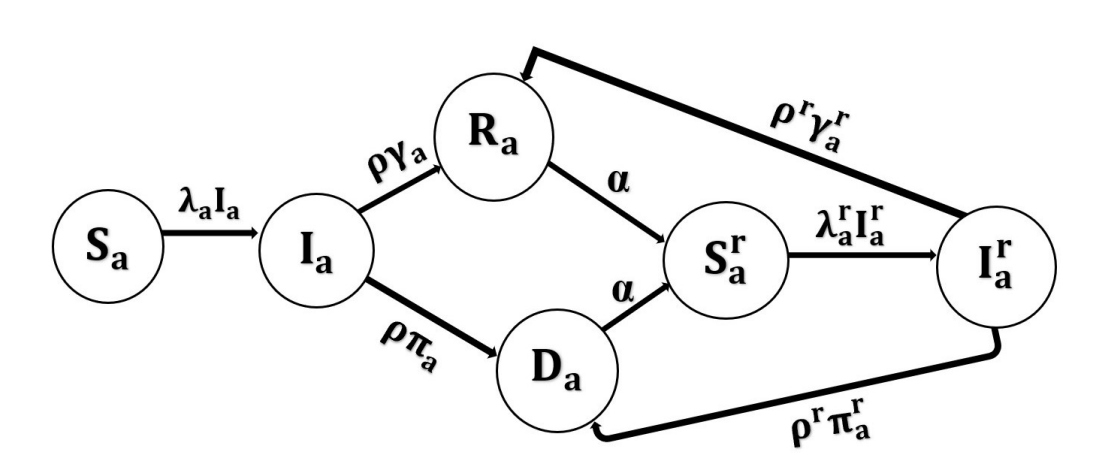


Figure 3.15: This model captures the dynamics of disease transmission and progression within a population that is divided into different age groups. The compartments include susceptible (S), infected (I), recovered (R), diseased (D), susceptible to re-infection  $(S^r)$ , and infected through re-infection  $(I^r)$  for each age group. By analyzing the transitions between these compartments and considering age-specific parameters, we gain insights into the interplay between age structure and partial immunity in shaping the spread and impact of the disease within the population. This is a refined model schematic where it does not considers the transition rate between age classes.

$$\frac{dS_c}{dt} = -\lambda_c S_c \frac{I_c}{N}$$

$$\frac{dS_a}{dt} = -\lambda_a S_a \frac{I_a}{N}$$

$$\frac{dI_c}{dt} = \lambda_c S_c \frac{I_c}{N} - \rho(\gamma_c + \pi_c) I_c$$

$$\frac{dI_a}{dt} = \lambda_a S_a \frac{I_a}{N} - \rho(\gamma_a + \pi_a) I_a$$

$$\frac{dR_c}{dt} = \rho \gamma_c I_c - \alpha R_c + \rho^r \gamma_c^r I_c^r$$

$$\frac{dR_a}{dt} = \rho \gamma_a I_a - \alpha R_a + \rho^r \gamma_a^r I_a^r$$

$$\frac{dD_c}{dt} = \rho \pi_c I_c - \alpha D_c + \rho^r \pi_c^r I_c^r$$

$$\frac{dD_a}{dt} = \rho \pi_a I_a - \alpha D_a + \rho^r \pi_a^r I_a^r$$

$$\frac{dS_c^r}{dt} = \alpha (R_c + D_c) - \lambda_c^r \frac{I_c^r}{N} S_c^r$$

$$\frac{dS_a^r}{dt} = \alpha (R_a + D_a) - \lambda_a^r \frac{I_a^r}{N} S_a^r$$

$$\frac{dI_c^r}{dt} = \lambda_c^r \frac{I_c^r}{N} S_c^r - \rho^r (\gamma_c^r + \pi_c^r) I_c^r$$

$$\frac{dI_a^r}{dt} = \lambda_a^r \frac{I_a^r}{N} S_a^r - \rho^r (\gamma_a^r + \pi_a^r) I_a^r$$

To further enhance our understanding of disease dynamics and population interactions, we can expand the age structure model with partial immunity to incorporate important demographic processes such as birth and natural deaths. By including these factors, we can investigate how population growth, mortality rates, and new births impact disease transmission patterns and overall population dynamics. This expanded model provides a more comprehensive framework for studying infectious diseases in realistic population settings, considering the complex interplay between epidemiological factors, age structure, and demographic processes.

## E. Single Age class Partial Immunity with Birth and Death

To enhance the realism of our model, we will now incorporate the important factors of births and deaths into the framework. This updated model recognizes that real-world populations are dynamic, with new individuals being born and existing individuals naturally passing away.

By considering the impact of births and deaths, we can capture the continuous renewal and replacement of individuals within a population. This becomes especially important when studying infectious diseases, as the population's composition changes over time due to the interplay between birth, death, and disease transmission.

Expanding on the previous model, we maintain the six compartments: susceptible (S), infected (I), recovered (R), disease (D), susceptible in the reinfection group  $(S^r)$ , and infected in the reinfection group  $(I^r)$ . However, we now recognize that the total population is subject to variations caused by births and deaths.

To illustrate the flow of individuals among these compartments and the influence of births and deaths, we can refer to the flow chart shown in Figure 3.16. Additionally, the mathematical equations (3.50 - 3.55) govern the model, accounting for the rates of change in each compartment while considering births and deaths.

By incorporating births and deaths into the model, we can more accurately reflect the dynamic nature of populations and the continuous renewal of individuals. This expanded framework enables us to investigate the impact of population growth, mortality rates, and new births on disease transmission patterns and overall population dynamics.

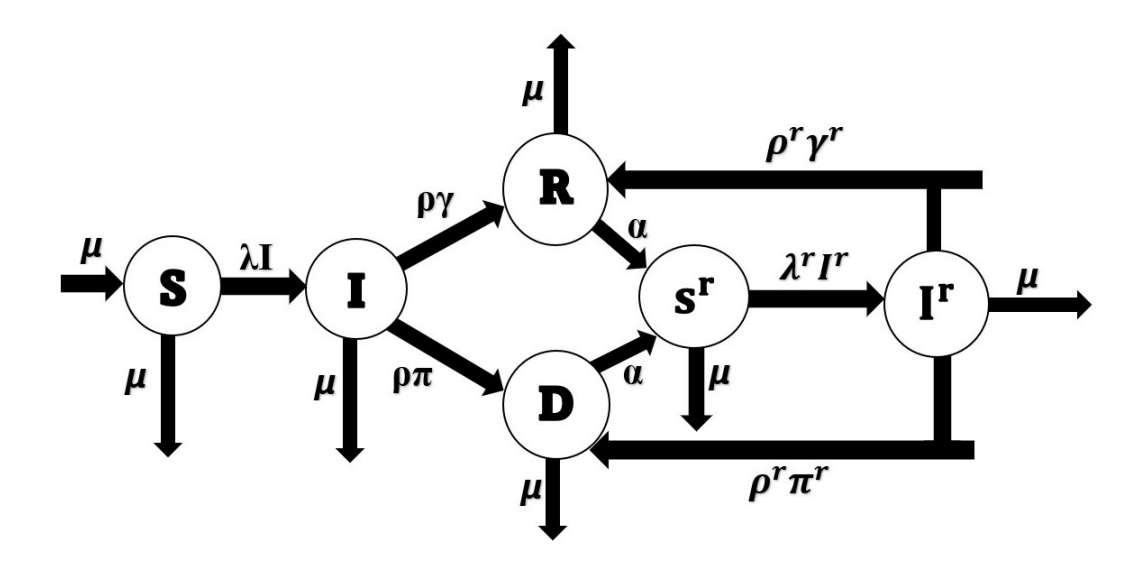


Figure 3.16: This flow diagram represents the movement of individuals among the different compartments in the single age class model. It shows the transitions between the susceptible (S), infected (I), recovered (R), disease (D), susceptible in the reinfection group  $(S^r)$ , and infected in the reinfection group  $(I^r)$  populations. Additionally, it highlights the influence of births and deaths on the overall population dynamics. The arrows indicate the direction of flow, and the labels on the arrows represent the corresponding transitions and processes. This diagram provides a visual representation of the interconnectedness and flow of individuals within the model, incorporating the effects of both disease transmission and population dynamics.

$$\frac{dS}{dt} = \mu N - \lambda S \frac{I}{N} - \mu S \tag{3.50}$$

$$\frac{dI}{dt} = \lambda S \frac{I}{N} - \rho(\gamma + \pi)I - \mu I \tag{3.51}$$

$$\frac{dR}{dt} = \rho \gamma I - \alpha R + \rho^r \gamma^r I^r - \mu R \tag{3.52}$$

$$\frac{dD}{dt} = \rho \pi I - \alpha D + \rho^r \pi^r I^r - \mu D \tag{3.53}$$

$$\frac{dS^r}{dt} = \alpha(R+D) - \lambda^r \frac{I^r}{N} S^r - \mu S^r$$
 (3.54)

$$\frac{dI^r}{dt} = \lambda^r \frac{I^r}{N} S^r - \rho^r (\gamma^r + \pi^r) I^r - \mu I^r$$
(3.55)

In this refined model, we observe a system of equations that builds upon the single age class model with partial immunity by incorporating birth and death processes. These additional equations consider the natural renewal of the population through births and the attrition of individuals through deaths.

Equation (3.50) describes the rate of change of the susceptible population, accounting for both disease transmission and population growth through births. It signifies that the susceptible population increases as a result of new births and decreases due to disease transmission and natural deaths. The infection rate, the number of susceptible and infected individuals, as well as natural deaths, influence the dynamics of the susceptible population.

Equation (3.51) represents the rate of change of the infected population, considering the contributions of new infections, recoveries, disease progression (symptomatic), and natural deaths. This equation allows us to understand how the number of actively infected individuals changes over time, considering both disease dynamics and population attrition.

Equation (3.52) captures the rate of change of the recovered population, emphasizing the impact of recoveries on its increase, and accounting for natural deaths and re-infection due to loss of immunity. This equation provides insights into the dynamics of individuals who have recovered from the disease and the potential for re-infection within the population.

Equation (3.53) reflects the rate of change of the diseased population, considering the increase through symptomatic disease progression, and the decrease through natural deaths and re-infection due to loss of immunity. It helps us understand the dynamics of individuals affected by symptomatic disease and their vulnerability to re-infection.

Equation (3.54) focuses on the rate of change of the susceptible population in the reinfection group, considering the dynamics of reinfection and natural deaths. It provides insights into the susceptibility to re-infection among individuals who have previously been infected.

Equation (3.55) represents the rate of change of the infected population in the reinfection group, accounting for the dynamics of reinfection, recoveries, disease progression (symptomatic), and natural deaths. This equation helps us understand how individuals in the reinfection group transition between different infection states over time.

By incorporating these refined equations into the model, we gain a more comprehensive understanding of the dynamics of an infectious disease within a population. The inclusion of birth and death processes allows for a more realistic representation of population renewal and attrition, enabling us to study disease dynamics and population stability in a more accurate and nuanced manner.

## F. Age Structure Model Partial Immunity with Birth and Death

The age structure model with partial immunity and incorporation of births and deaths is an advanced framework that considers the dynamic nature of real-world populations. By considering the continuous renewal and replacement of individuals through births and deaths, as well as age-specific dynamics and partial immunity, this model provides a more realistic depiction of disease dynamics.

In this expanded model, the population is divided into different age groups, such as children and adults. Each age group has its own compartments representing susceptible, infected, recovered (asymptomatic), diseased (symptomatic), susceptible to re-infection, and infected through re-infection populations. The transitions between these compartments are influenced by age-specific parameters, including infection rates, transition rates, likelihood of infection progress to asymptomatic and symptomatic state, and reinfection dynamics.

The flow of individuals among these compartments, as illustrated in Figure 3.17, is described by a system of equations (3.56 - 3.67). These equations capture the interactions between disease transmission, partial immunity, births, and deaths. They quantify the rate of change for each population compartment and account for the transitions between them. Additionally, they consider factors such as disease transmission from infected to susceptible individuals, the development and recovery of partial immunity, reinfection dynamics, and the impact of births and deaths on the overall population size.

By incorporating births and deaths into the age structure model with partial immunity, we gain a more accurate representation of population dynamics and their interaction with infectious diseases. This expanded framework enables us to examine the effects of population growth, mortality rates, and new births on disease transmission patterns, age-specific dynamics, and overall population dynamics. It provides valuable insights for understanding the complex interplay between disease dynamics, age structure, and population demographics, empowering decision-makers in public health interventions and policy planning.

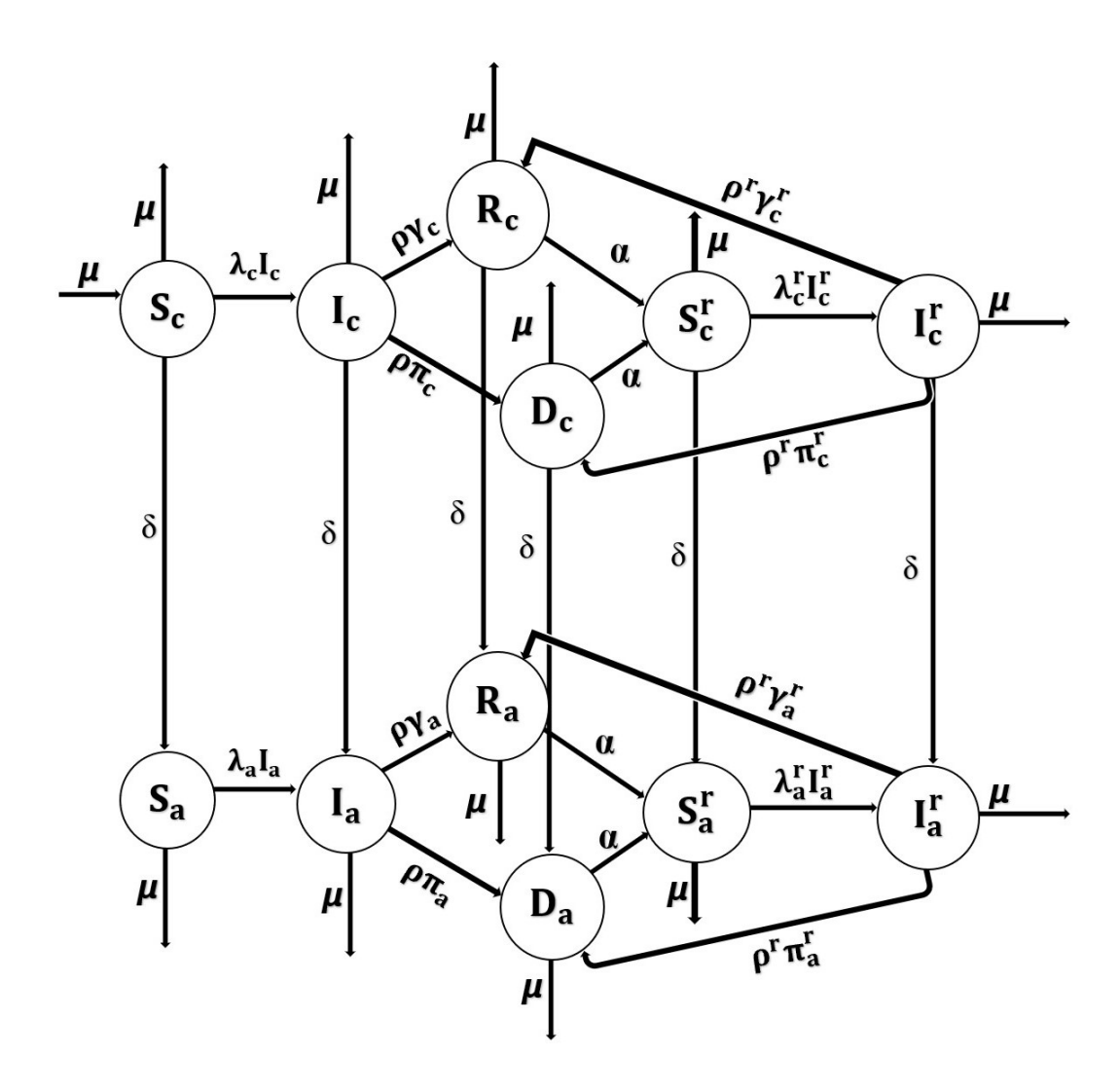


Figure 3.17: The flow diagram illustrates the dynamic movement of individuals among different compartments in the age structure model with partial immunity, accounting for births and deaths. The diagram showcases the transitions between susceptible, infected, recovered (asymptomatic), diseased (symptomatic), susceptible to re-infection, and infected through re-infection populations for each age group. This diagram visualizes the complex interactions and pathways within the model, highlighting the interplay between disease transmission, partial immunity, births, deaths, and population dynamics.

$$\frac{dS_c}{dt} = \mu N - \lambda_c S_c \frac{I_c}{N} - \mu S_c - \delta S_c \tag{3.56}$$

$$\frac{dS_a}{dt} = -\lambda_a S_a \frac{I_a}{N} - \mu S_a + \delta S_c \tag{3.57}$$

$$\frac{dI_c}{dt} = \lambda_c S_c \frac{I_c}{N} - \rho(\gamma_c + \pi_c) I_c - \mu I_c - \delta I_c$$
(3.58)

$$\frac{dI_a}{dt} = \lambda_a S_a \frac{I_a}{N} - \rho(\gamma_a + \pi_a) I_a - \mu I_a + \delta I_c$$
(3.59)

$$\frac{dR_c}{dt} = \rho \gamma_c I_c - \alpha R_c + \rho^r \gamma_c^r I_c^r - \mu R_c - \delta R_c$$
 (3.60)

$$\frac{dR_a}{dt} = \rho \gamma_a I_a - \alpha R_a + \rho^r \gamma_a^r I_a^r - \mu R_a + \delta R_c$$
 (3.61)

$$\frac{dD_c}{dt} = \rho \pi_c I_c - \alpha D_c + \rho^r \pi_c^r I_c^r - \mu D_c - \delta D_c$$
 (3.62)

$$\frac{dD_a}{dt} = \rho \pi_a I_a - \alpha D_a + \rho^r \pi_a^r I_a^r - \mu D_a + \delta D_c$$
(3.63)

$$\frac{dS_c^r}{dt} = \alpha (R_c + D_c) - \lambda_c^r \frac{I_c^r}{N} S_c^r - \mu S_c^r - \delta S_c^r$$
(3.64)

$$\frac{dS_a^r}{dt} = \alpha (R_a + D_a) - \lambda_a^r \frac{I_a^r}{N} S_a^r - \mu S_a^r + \delta S_c^r$$
(3.65)

$$\frac{dI_c^r}{dt} = \lambda_c^r \frac{I_c^r}{N} S_c^r - \rho^r (\gamma_c^r + \pi_c^r) I_c^r - \mu I_c^r - \delta I_c^r$$
(3.66)

$$\frac{dI_a^r}{dt} = \lambda_a^r \frac{I_a^r}{N} S_a^r - \rho^r (\gamma_a^r + \pi_a^r) I_a^r - \mu I_a^r + \delta I_c^r$$
(3.67)

The age structure model with partial immunity and incorporation of births and deaths represents an advanced framework that expands upon the single age class model by considering the specific dynamics of disease transmission and progression within different age groups. By dividing the population into children and adults, this model acknowledges the variations in susceptibility, infection rates, and recovery rates that can occur between these distinct age classes.

In this expanded model, a new parameter  $\delta$  is introduced to quantify the transition rate between the children and adult age classes. This parameter captures the natural aging process and the movement of individuals from one age class to another, reflecting the ongoing population dynamics.

The mathematical equations governing the age structure model with partial immunity and incorporation of births and deaths build upon the previous model but introduce additional differentiations for each age class. For example, we now have separate equations to track the rate of change of the susceptible population (S) in children  $(S_c)$  and adults  $(S_a)$ . Similarly, the equations for the infected population (I), recovered population (R), diseased population (D), and the susceptible and infected populations in the reinfection group  $(S^r)$  and  $I^r$ ) are tailored for each age class.

Upon closer examination of the system of equations, it becomes evident that the initial assumption of births occurring throughout the entire population may not accurately align with real-world dynamics. To address this discrepancy, we can refine the equations by considering that births only occur among adults, as they are the ones biologically capable of giving birth. Additionally, we assume that the natural death rate for children is zero.

To achieve a more realistic representation of the birth process, we introduce the concept of an equal birth and adult death rate, denoted as  $\mu$ . The value of  $\mu$  is determined by the transition rate between age classes,  $\delta$ , and the ratio of the children population,  $N_c$ , to the adult population,  $N_a$ . This modification ensures that the birth process aligns with the biological capacity for reproduction in the adult population and reflects the natural balance between births and adult deaths.

By incorporating these refinements, we can enhance the model's accuracy in mimicking real-world population dynamics, where births are limited

to adults and children have negligible natural death rates. This updated representation provides a more realistic portrayal of the birth process within the population, enabling us to gain deeper insights into the interplay between demographic factors and disease spread.

By incorporating the age-specific dynamics of disease transmission and accounting for the interplay between children and adults, the age structure model with partial immunity and incorporation of births and deaths provides a more comprehensive framework for analyzing infectious diseases. With this foundation, we can now shift our focus towards examining two important measures: the force of infection and disease incidence. These metrics enable us to assess the intensity and impact of disease transmission within each age class and the overall population, providing valuable insights into the dynamics of infectious diseases within an age-structured population.

$$\frac{dS_c}{dt} = \mu N_a - \lambda_c S_c \frac{I_c}{N} - \delta S_c$$

$$\frac{dS_a}{dt} = -\lambda_a S_a \frac{I_a}{N} - \mu S_a + \delta S_c$$

$$\frac{dI_c}{dt} = \lambda_c S_c \frac{I_c}{N} - \rho(\gamma_c + \pi_c) I_c - \delta I_c$$

$$\frac{dI_a}{dt} = \lambda_a S_a \frac{I_a}{N} - \rho(\gamma_a + \pi_a) I_a - \mu I_a + \delta I_c$$

$$\frac{dR_c}{dt} = \rho \gamma_c I_c - \alpha R_c + \rho^r \gamma_c^r I_c^r - \delta R_c$$

$$\frac{dR_a}{dt} = \rho \gamma_a I_a - \alpha R_a + \rho^r \gamma_a^r I_a^r - \mu R_a + \delta R_c$$

$$\frac{dD_c}{dt} = \rho \pi_c I_c - \alpha D_c + \rho^r \pi_c^r I_c^r - \delta D_c$$

$$\frac{dD_a}{dt} = \rho \pi_a I_a - \alpha D_a + \rho^r \pi_a^r I_a^r - \mu D_a + \delta D_c$$

$$\frac{dS_c^r}{dt} = \alpha (R_c + D_c) - \lambda_c^r \frac{I_c^r}{N} S_c^r - \delta S_c^r$$

$$\frac{dS_a^r}{dt} = \alpha (R_a + D_a) - \lambda_a^r \frac{I_a^r}{N} S_a^r - \mu S_a^r + \delta S_c^r$$

$$\frac{dI_c^r}{dt} = \lambda_c^r \frac{I_c^r}{N} S_c^r - \rho^r (\gamma_c^r + \pi_c^r) I_c^r - \delta I_c^r$$

$$\frac{dI_a^r}{dt} = \lambda_a^r \frac{I_a^r}{N} S_a^r - \rho^r (\gamma_a^r + \pi_a^r) I_a^r - \mu I_a^r + \delta I_c^r$$

Examining Force of infection and Disease incidence of partial immunity models

### 1. Single Age Structure Models

Our analysis builds upon the absence of immunity model by incorporating partial immunity dynamics, enabling us to capture the occurrence of multiple infections and account for birth and natural deaths. This extension includes notable improvements, particularly in the calculation of the average force of infection and the modification of disease incidence calculations to

accommodate re-infection dynamics. These refinements enhance our understanding of disease transmission within a single age class, allowing us to gain more comprehensive insights into the spread of the disease.

The average force of infection serves as a key measure in understanding the rate at which susceptible individuals become infected with the disease. It considers both the transmission rate  $(\lambda)$  and the re-infection transmission rate  $(\lambda^r)$ . By summing two terms, namely the transmission rate multiplied by the number of infected individuals (I), and the re-infection transmission rate multiplied by the number of re-infected individuals  $(I^r)$ , we obtain a comprehensive estimation of the force driving the spread of the disease. This approach allows us to consider both initial infections and subsequent re-infections, providing a more accurate representation of disease transmission dynamics.

To normalize the average force of infection, we divide the sum by the product of the total population size (N) and the time interval (T) over which the calculations are performed. This normalization accounts for the population size and the duration of the analysis, ensuring that the force of infection is expressed in a meaningful way. The resulting equation becomes:

$$\tilde{F} = \frac{\int_0^T (\lambda I + \lambda^r I^r) dt}{NT}$$
(3.68)

Similarly, we modify the calculation of disease incidence, which represents the number of new symptomatic individuals occurring within a specific time period, to incorporate re-infection disease incidence. The disease incidence now comprises two components: the product of the power of infection rate  $(\rho\pi)$  and the number of infected individuals (I), and the product of the re-infection power of infection rate  $(\rho\pi^r)$  and the number of re-infected indi-

viduals from the disease. The equation for disease incidence becomes:

$$\tilde{D} = \frac{\int_0^T (\rho \pi I + \rho \pi^r I^r) dt}{NT}$$
(3.69)

Furthermore, when we extend these concepts to the age structure model with partial immunity and incorporate births and deaths, we can examine age-specific force of infection and disease incidence, allowing us to gain a deeper understanding of how disease transmission and its impact vary across different age groups.

### 2. Age Structure Models

In addition to extending the absence of immunity model to incorporate partial immunity dynamics, we can further enhance our analysis by applying the concepts of force of infection and disease incidence to an age structure model. The age structure model recognizes the variations in susceptibility, infection rates, and recovery rates that can occur between different age groups, providing a more refined understanding of disease transmission dynamics.

In the age structure model, the force of infection is calculated separately for each age class. We consider the transmission rates specific to children  $(\lambda_c)$  and adults  $(\lambda_a)$ , as well as the re-infection transmission rates  $(\lambda_c^r)$  and  $(\lambda_a^r)$  for each age class. By multiplying these transmission rates by the respective number of infected individuals (I) and (I) in each age class, we obtain age-specific contributions to the force driving the spread of the disease. Summing these contributions provides a comprehensive estimation of the force of infection in the age structure model, accounting for both initial infections and re-infections within different age groups.

To normalize the age structure model force of infection, we follow the same procedure as in the single age class model. The sum of the age-specific force of infection terms is divided by the product of the total population size (N) and the time interval (T) over which the calculations are performed. This normalization ensures that the force of infection in the age structure model is expressed in a meaningful way, considering the population size and the duration of the analysis.

$$\tilde{F} = \frac{\int_0^T (\lambda_c I_c + \lambda_a I_a + \lambda_c^r I_c^r + \lambda_a^r I_a^r) dt}{NT}$$
(3.70)

Similarly, we can modify the calculation of disease incidence in the age structure model to incorporate re-infection disease incidence. Disease incidence represents the number of new symptomatic individuals occurring within a specific time period in each age class. We incorporate two components: the product of the power of infection rate  $(\rho\pi)$  and the number of infected individuals (I), and the product of the re-infection power of infection rate  $(\rho\pi^r)$  and the number of re-infected individuals from the disease. By summing these age-specific components, we obtain the overall disease incidence in the age structure model, accounting for both initial infections and re-infections across different age groups.

$$\tilde{D} = \frac{\int_0^T (\rho(\pi_c I_c + \pi_a I_a) + \rho^r(\pi_c^r I_c^r + \pi_a I_a))dt}{NT}$$
(3.71)

By applying the concepts of force of infection and disease incidence to the age structure model, we gain a more nuanced understanding of disease transmission dynamics within different age groups. This enhanced analysis allows us to capture age-specific variations in susceptibility, transmission rates, and disease burden, enabling us to develop targeted public health strategies and interventions to control the impact of the disease on the population, particularly considering the potential for re-infections.

Having extended the absence of immunity model to incorporate partial immunity dynamics and applied the age structure model to analyze disease transmission, we can now examine the results obtained from these enhanced approaches. By considering multiple infections, birth and natural deaths, and age-specific factors, our analysis provides a comprehensive understanding of disease transmission dynamics and its impact on different population groups.

Variable	Description	$\operatorname{unit}$
λ	Infectious rate of susceptible population	1 people*days
$\lambda^r$	Re-nfectious rate of susceptible population	people*days
$\mu$	Birth and Death rate	<u>1</u>
$\pi$	Likelihood of infection progress to symptomatic state	$\begin{array}{c} \text{days} \\ \hline 1 \\ \text{days} \\ \end{array}$
$\pi^r$	Likelihood of re-infection progress to symptomatic state	$\frac{1}{\text{davs}}$
$\gamma = (1 - \pi)$	Likelihhod of infection progress to asymptomatic state	$\frac{1}{\text{days}}$
$\gamma^r = (1 - \pi^r)$	Likelihhod of re-infection progress to asymptomatic state	$\frac{1}{\text{days}}$
ho	Timescale that infections are contagious	$\frac{1}{\text{days}}$
$ ho^r$	Timescale that re-infections are contagious	$\frac{1}{\text{davs}}$
t	Time	days
S	Number of susceptible people	people
I	Number of infected people	people
R	Number of recovered (asymptomatic) people	people
D	Number of disease (symptomatic) people	people
$S^r$	Number of re-infected susceptible people	people
$I^r$	Number of re-infected people	people
N	Total number of people	people

Table 3.3: In the table, the units of the variables and parameters in both the partial immunity model without births and deaths and the partial immunity model with births and deaths are provided. The variables, such as susceptible (S), infected (I), recovered (R), diseased (D), susceptible in the reinfection group  $(S^r)$ , and infected in the reinfection group  $(I^r)$ , are measured in population count (number of individuals). The parameters are expressed as per capita rates, representing the rate of occurrence per individual per unit of time. These units provide a clear understanding of the measurement scale and rate at which the variables and parameters are considered in the partial immunity models, facilitating the interpretation and application of the models in the context of infectious disease dynamics.

### 3.3.3 Results

Our study focuses on exploring and comparing two models: the single age class models and the age structure models. These models are designed to examine the dynamics of disease transmission and share certain parameter values and initial conditions. By investigating these models in parallel, we aim to gain a comprehensive understanding of the impact of different modeling approaches on our analysis and insights into disease spread. The comparison between these models allows us to assess the influence of age-specific factors

and population structure on disease transmission dynamics. Through this comparative analysis, we can derive valuable findings that can inform decision-making and contribute to the development of targeted strategies to mitigate the spread and impact of Covid-19.

# Single age class with Absence of Immunity

In our investigation of the single age class model with immunity, our objective is to examine the influence of varying infection rates (0.1 and 2.0) on disease dynamics. Within this model, individuals can experience two outcomes following infection: they either become asymptomatic or progress to a symptomatic state. The probability of progressing to the asymptomatic state is 0.95, while the probability of transitioning to the symptomatic state is 0.05. To maintain population equilibrium, we assume a timescale of 0.01 for the loss of immunity post-infection, for both asymptomatic and symptomatic cases. By conducting simulations over a 10-year period, we can observe the dynamics of immunity over time. Additionally, we consider a contagious timescale of 0.15, representing the duration during which individuals are infectious and can transmit Covid-19.

To apply these models to a real-world scenario, our focus is specifically on the city of San Francisco, utilizing population data from 2021. With an estimated population of approximately 815,201 individuals, we initialize the simulation with around 100 infected individuals, assuming no individuals are classified as recovered or diseased at the beginning.

By incorporating these parameters and contextualizing the models for San Francisco, we can simulate and analyze the spread of the disease, monitor the progression of immunity, and derive insights into the potential for endemic stability within the city. This approach enables us to assess the impact of different transmission rates on disease dynamics, providing valuable information for understanding and managing the spread of the disease in the context of San Francisco.

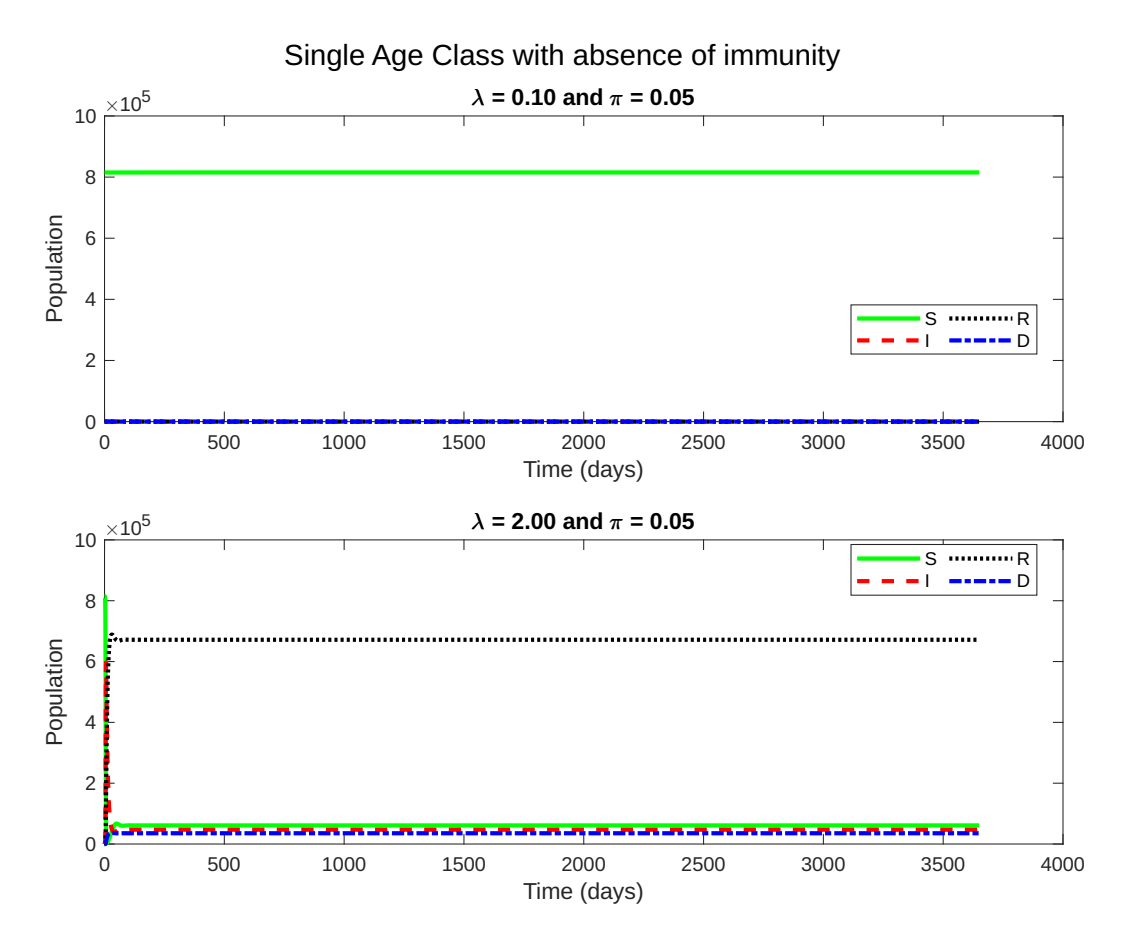


Figure 3.18: The figure displays the simulation results from a single age class model, demonstrating the influence of varying infection rates on the spread of a disease within a population. When the infection rate is low, the number of infections remains relatively limited, gradually increasing over time. The majority of infected individuals recover promptly, resulting in a small proportion of symptomatic cases. However, as the infection rate increases, the number of infections experiences a rapid upsurge, leading to a larger pool of infected individuals within the population. Despite the higher overall number of infections, the proportion of symptomatic cases remains relatively small, indicating that a significant portion of infected individuals either experience asymptomatic infections or develop mild symptoms. Additionally, it is worth noting that the model reaches a steady state, where the infection dynamics stabilize over time. This suggests that the disease has reached an equilibrium within the population, with new infections and recoveries balancing each other out. Furthermore, the results reveal an interesting observation: at higher infection rates, the number of symptomatic cases is low. This phenomenon is an indication of endemic stability, where the disease persists in the population at a relatively stable level, with a lower proportion of symptomatic cases over time.

Our research findings indicate that when the infection rate among the susceptible population is set to a very low value, the impact on the overall population is minimal. In such scenarios, the transmission of Covid-19 occurs slowly, resulting in a low number of infections and a small proportion of symptomatic cases. Infected individuals tend to recover quickly, leading to a short duration of infection.

However, increasing the infection rate among the susceptible population leads to a notable rise in the number of infections within a shorter timeframe. This higher infection rate results in a larger number of individuals contracting Covid-19, including a higher proportion of asymptomatic cases. Our model simulations indicate that a steady state is eventually reached, where Covid-19 becomes contained within the population. This can be attributed to the high level of infection and a reduced number of symptomatic cases, indicating a state of endemic stability. It is worth noting that our model assumes the hypothesis that the probability of progressing to a symptomatic state,  $\pi$ , is the same for initial infections and reinfections.

It is important to acknowledge that our models have certain limitations. They do not incorporate demographic factors such as birth and death rates, assuming a constant population size throughout the simulation. Additionally, the development of long-term immunity to Covid-19 is not considered in our simulations. Instead, we focus on the possibility of reinfection due to the loss of immunity after recovery. This simplification allows us to specifically analyze the dynamics of disease transmission and isolate the impact of changes in the infection rate on the spread of Covid-19.

# Age Structure with Absence of Immunity

In our investigation of the two-age class model with absence of immunity, we explore various infections rate of susceptible population, similar to the single age class model and immunity analysis. To account for age-specific dynamics, we introduce a distinction between children and adults by assuming different power of infection values: a lower value for children ( $\pi_c$ ) and higher values for adults ( $\pi_a$ ). Specifically, we consider transmission rates of  $\pi_c = 0.005$  and  $\pi_a = 0.05$ . By incorporating these different power of infection values for adults, we aim to understand how the level of infection contributes to the stability of the disease within the population.

Furthermore, we account for different likelihood of infection progress to asymptomatic state between children and adults. The likelihood of infection for children is set to be approximately 0.995, while for adults, we consider values of 0.95. This variation in likelihood of infection allows us to examine the impact of different recovery dynamics on the overall disease dynamics. Additionally, since this model considers loss of immunity, we set the loss of immunity rate for both asymptomatic and symptomatic individuals in both age groups to be 0.01.

To simulate the age transition from children to adults, we set the transition rate to be around 0.001 for children transitioning to adults, and 0 for adults transitioning to other age groups, as this model focuses on the children-to-adults transition.

In the context of San Francisco, we adapt the population data from 2021. Based on available information, the population of children between 0 and 2 years old in San Francisco was approximately 23,996, while the adult

population was around 791,205. We use these population figures to initialize the model, while maintaining similar initial conditions for the other compartments as in the single age class model.

By considering these parameters and population data, our goal is to gain insights into the dynamics of the disease and its endemic stability in a population with distinct age groups.

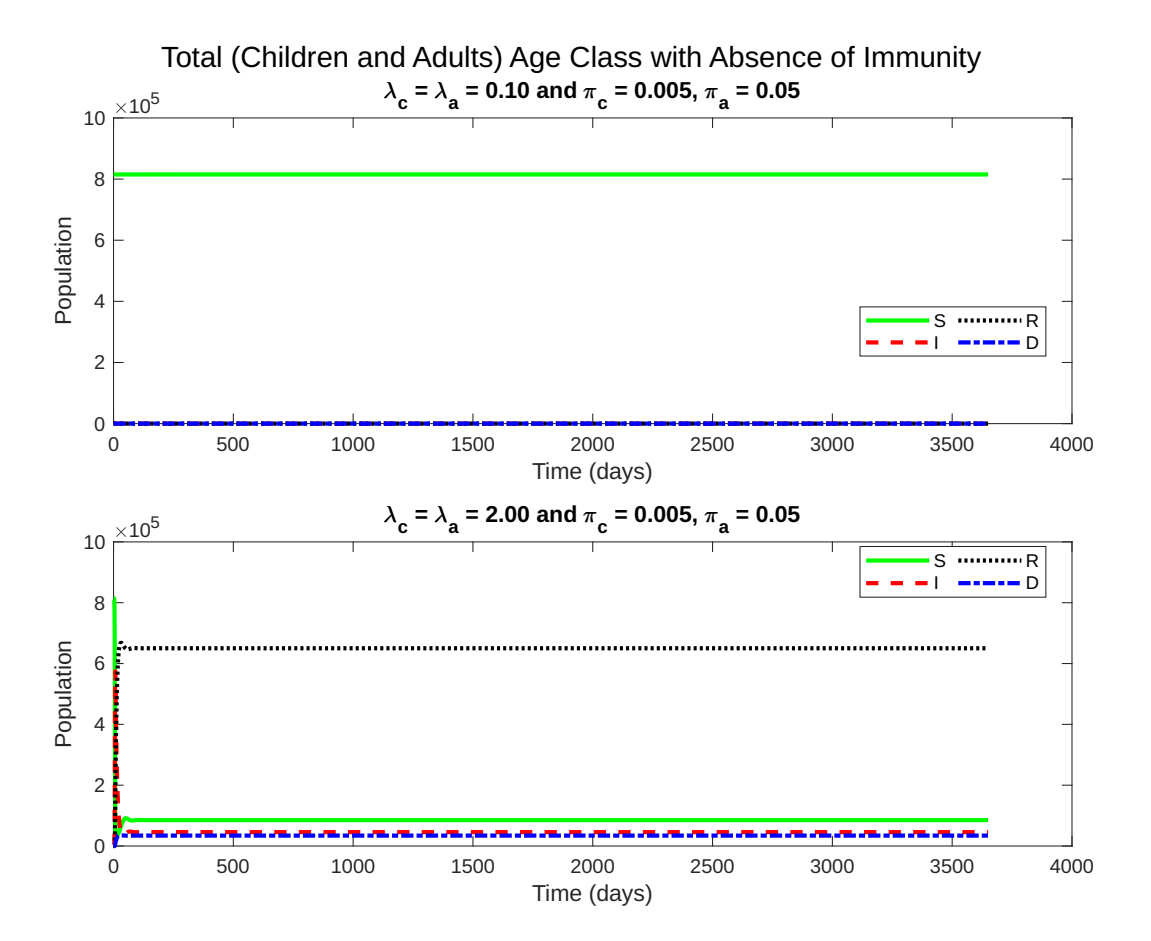


Figure 3.19: In this study, we investigate the impact of infection rates on the dynamics of Covid-19 within a population that includes both children and adults. Using an age structure model that does not consider immunity, we analyze important parameters such as the infection rate among susceptible individuals, the probability of infection progressing to symptomatic or asymptomatic states, the duration of immunity loss following infection for both symptomatic and asymptomatic cases, and initial population values based on San Francisco's demographics. Our findings demonstrate an equilibrium state that reflects the patterns observed in real-world Covid-19 outbreaks. Specifically, when infection rates are low, no significant outbreaks occur. However, as the infection rates increase, outbreaks become evident and spread within the population becomes more pronounced. It is important to note that our model does not incorporate the presence of immunity, which can significantly influence disease dynamics. Additionally, the specific results are based on the parameters and initial population values used in our study, which are specific to the context of San Francisco.

Our analysis demonstrates that lower infection rates have minimal im-

pact on the population, as they do not trigger outbreaks of Covid-19. Conversely, higher infection rates have a profound impact, leading to significant outbreaks and a decrease in the total number of susceptible individuals. These findings suggest that the population reaches a steady state, indicating the potential for an endemic stability in the future.

However, to gain a more comprehensive understanding of the Covid-19 dynamics, it is crucial to delve deeper into the age structure model. By conducting separate simulations for children and adults, we can acquire valuable insights into how the virus affects each age group. Such a focused analysis will provide us with a more nuanced perspective on the transmission patterns, susceptibility, and potential risks associated with different segments of the population.

# Of immunity Children Adults $\lambda_c = \lambda_a = 0.10 \text{ and } \pi_c = 0.005, \pi_a = 0.05$ $\lambda_c = \lambda_a = 0.10 \text{ and } \pi_c = 0.005, \pi_a = 0.05$ $\lambda_c = \lambda_a = 0.10 \text{ and } \pi_c = 0.005, \pi_a = 0.05$ $\lambda_c = \lambda_a = 0.10 \text{ and } \pi_c = 0.005, \pi_a = 0.05$ $\lambda_c = \lambda_a = 0.00 \text{ and } \pi_c = 0.005, \pi_a = 0.05$ $\lambda_c = \lambda_a = 0.00 \text{ and } \pi_c = 0.005, \pi_a = 0.05$ $\lambda_c = \lambda_a = 0.00 \text{ and } \pi_c = 0.005, \pi_a = 0.05$ $\lambda_c = \lambda_a = 0.00 \text{ and } \pi_c = 0.005, \pi_a = 0.05$ $\lambda_c = \lambda_a = 0.00 \text{ and } \pi_c = 0.005, \pi_a = 0.05$

Age structure model absence

Figure 3.20: This figure illustrates the outcomes of the age structure model (Susceptible-Infected-Recovered-Disease) when considering the dynamics of Covid-19 in the absence of immunity. The model incorporates the specified initial conditions and parameter values to simulate the spread of the disease. The figure is divided into two sections, with the left side representing the simulation results for the children population and the right side depicting the simulation results for the adult population. In the simulation for the children population, we observe consistent patterns across different infection rates. There are no outbreaks observed in this population, and the number of children remains constant throughout the simulation period. This indicates that the transition from the children age class to the adult age class does not occur in this model, as the children population remains unaffected by the disease dynamics. On the other hand, the simulation for the adult population closely aligns with the overall population results. The infection rates used in the simulation correspond to the occurrence of outbreaks, mirroring the dynamics observed in the total population. This suggests that the behavior and infection patterns within the adult population heavily influence the overall trends and patterns in the age structure model. The dynamics observed in the adult population have a significant impact on the spread and progression of the disease throughout the entire population.

Our analysis of simulations using an age structure model has yielded intriguing findings when comparing the dynamics of Covid-19 in adults and the total population, which includes both children and adults. These observations provide valuable insights and emphasize the significance of considering agespecific factors when managing the pandemic effectively.

Examining the simulations of the children population, we consistently observe a distinctive pattern. Regardless of the infection rates tested, no outbreaks occur among children, and their population size remains constant throughout the simulation period. This suggests that the transition from the children age class to the adult age class does not take place in this specific model. The absence of outbreaks among children indicates either a lower susceptibility to Covid-19 at a younger age or a different disease progression that does not result in noticeable outbreaks.

These findings contribute valuable insights into the dynamics of Covid19. The age structure model implies that every individual in the population is susceptible to contracting the virus at some point in their lives, regardless of age. However, the simulations for children indicate a lower susceptibility or milder symptoms, which aligns with real-world observations of children experiencing less severe disease outcomes compared to adults.

In contrast, the simulations for adults closely align with the overall population results. The infection rates used in these simulations lead to outbreaks, reflecting the dynamics observed in the total population. This indicates that the behavior and infection patterns within the adult population strongly influence the overall trends and patterns observed in the age structure model. The high susceptibility and potential for disease transmission among adults significantly contribute to the overall disease dynamics.

These insights underscore the importance of implementing tailored strategies and interventions that consider the unique vulnerabilities and behaviors of different age groups in effectively managing the ongoing Covid-19 pandemic.

While children may exhibit lower susceptibility or milder symptoms, it is crucial to recognize the role of adults in disease transmission and implement targeted measures to protect vulnerable individuals, such as older adults or those with underlying health conditions.

Furthermore, it is essential to refine the model to achieve endemic stability. In the current model, the simulations for children do not reach endemic stability. Therefore, it is crucial to consider the necessary conditions required to achieve endemic stability. One of the potential considerations is increasing the infection rate, as this has shown the presence of infected individuals and the attainment of an endemic stability state in the simulations.

# Single age class Partial Immunity without Birth and Death

This refined model introduces the concept of re-infection and incorporates it into the dynamics of the disease. Following the initial infection and recovery (asymptomatic), individuals become susceptible to re-infection, although the likelihood of re-infection is lower compared to the first infection. Specifically, we use parameter values of  $\pi = 0.05$  for the likelihood of first infection and  $\pi^r = 0.0125$  for the likelihood of re-infection.

The model retains similar parameters for the probability of infection progressing to asymptomatic and symptomatic states as the previous single age class model with absence of immunity. These parameters govern the likelihood of infection progress to asymptomatic state and transmission probabilities between infected and susceptible individuals.

The remaining parameters and initial conditions are consistent with the previous single age model without immunity, capturing the population dynamics and initial states of susceptible, infected, recovered (asymptomatic), and diseased (symptomatic) individuals.

By incorporating re-infection dynamics with a diminished power of infection after recovery, this refined model allows us to explore the possibility of multiple infections. This is particularly important for understanding the long-term dynamics and stability of diseases such as COVID-19, where waning immunity and re-infection have been observed.

Through extensive analysis and simulations using this single age class re-infection model, we can gain valuable insights into how the transmission rate and the power of infection after re-infection influence the overall disease dynamics. This expanded model provides a more comprehensive understanding of the complex interplay between transmission, recovery, and re-infection processes, offering insights into the potential impact on susceptible, infected, recovered (asymptomatic), and diseased (symptomatic) populations.

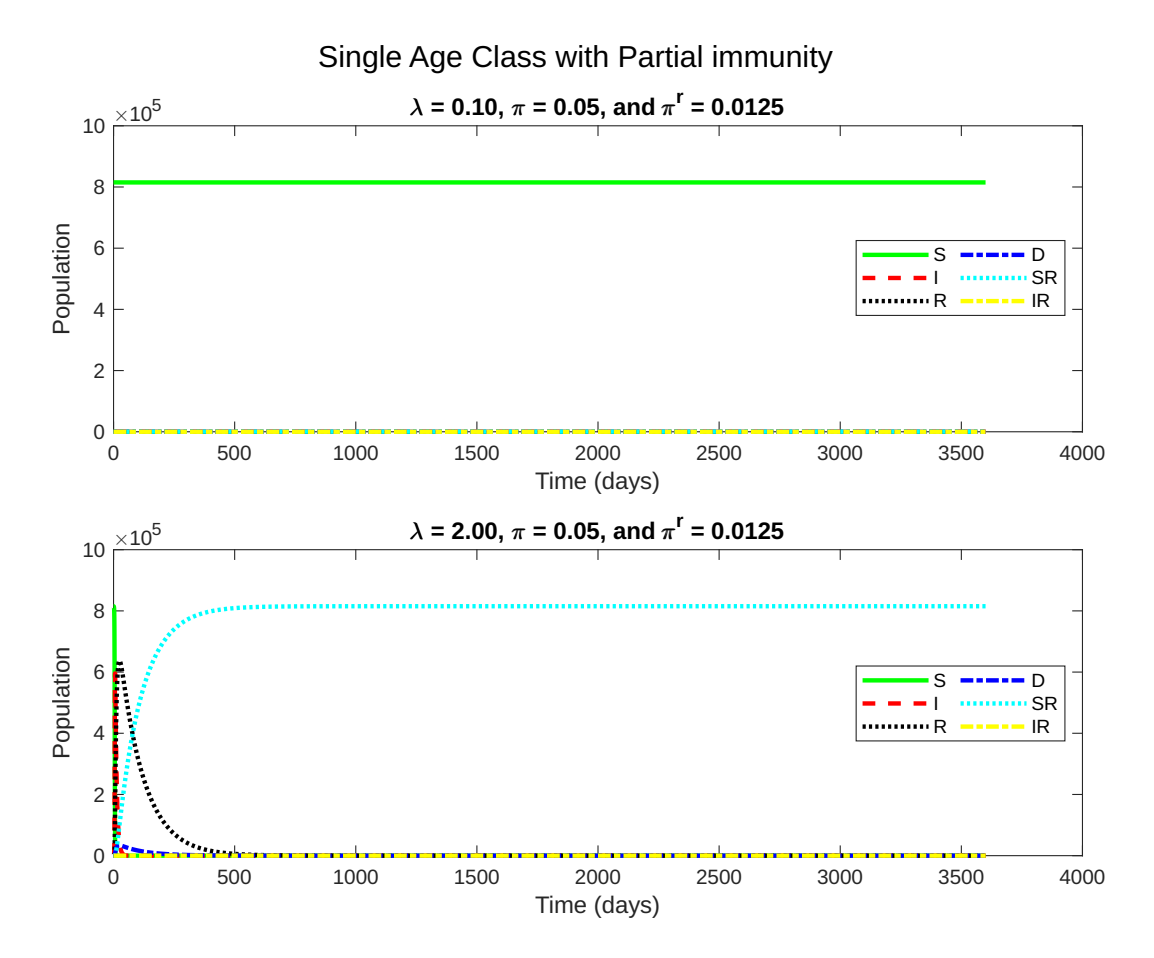


Figure 3.21: This figure presents a simulation of a single age class model with partial immunity, specifically focusing on re-infection dynamics and excluding the consideration of birth and death processes. At low infection rates, the impact on the population is minimal, with only a small number of individuals in the infected, recovered, re-infected susceptible, and disease compartments. However, as the infection rate increases, a transition occurs to a steady state where the disease spreads extensively, resulting in a higher number of re-infections. The higher infection rate leads to a gradual decrease in the susceptible population until it reaches zero, indicating that the disease has spread to the majority of the population. These findings underscore the significant influence of infection rates on the dynamics of re-infection and highlight the potential for disease spread in populations with higher levels of contagion.

In our analysis of the single age class model with partial immunity, we made interesting observations regarding the dynamics of different compartments and their responses to varying infection rates. At low infection rates, the population remains largely unaffected, with minimal numbers in the infected, recovered, re-infected susceptible, and disease compartments. It's important to note that the model does not consider the birth process, resulting in a constant total population size throughout the simulation.

However, as the transmission rate increases, there is a significant shift in the model dynamics. A transition occurs from an absence of infection to a steady state where the disease spreads extensively, leading to re-infections. The higher transmission rate increases the chances of individuals coming into contact with infected individuals, resulting in a larger number of people acquiring the disease. Consequently, the susceptible, infected, asymptomatic, symptomatic, and re-infected populations gradually diminish over time until they reach zero.

Simultaneously, the population of re-infected susceptible individuals grows as those who have previously recovered become susceptible to re-infection, highlighting the loss of immunity and the potential for re-infection within the model. This indicates that the disease has been eradicated from the population since there are no infected individuals or re-infections present. However, it's important to note that if the disease were to re-emerge, these re-infected susceptible individuals could lose their immunity and become susceptible again.

The infected population initially experiences a rapid increase as more individuals become infected due to the higher transmission rate. However, as the susceptible population diminishes and a significant portion of the population recovers to the disease, the infected population eventually reaches its peak and starts to decline. This decline occurs due to the combined effects of asymptomatic and symptomatic disease.

The number of asymptomatic individuals shows an intriguing pattern, initially increasing and subsequently decreasing. This pattern arises from the interplay between recovery (asymptomatic), symptomatic disease, and reinfection dynamics. Initially, as the disease spreads and individuals recover, the number of recoveries rises. However, as re-infections occur and the susceptible population decreases, the number of recoveries starts to decline.

Our findings highlight the importance of considering re-infection dynamics and the potential loss of immunity when studying the spread and impact of diseases. Specifically, in the re-infection model, as the transmission rate increases, the disease eventually spreads throughout the entire population, establishing a steady state where everyone becomes infected and is susceptible to re-infection. These observations provide valuable insights into the dynamics of diseases and their long-term implications.

Additionally, we observed that the simulation did not achieve endemic stability. To attain endemic stability, one of the considerations was to increase the infection rate, which ultimately resulted in the simulation reaching an endemic state.

### Age Structure Partial Immunity without Birth and Death

In our investigation of the two-age class model with partial immunity, we examine the impact of different infection rates on the susceptible population. Building upon the single age class model and absence of immunity analysis, we introduce a distinction between children and adults by utilizing different power of infection values. This differentiation allows us to explore the stability of the disease within the population.

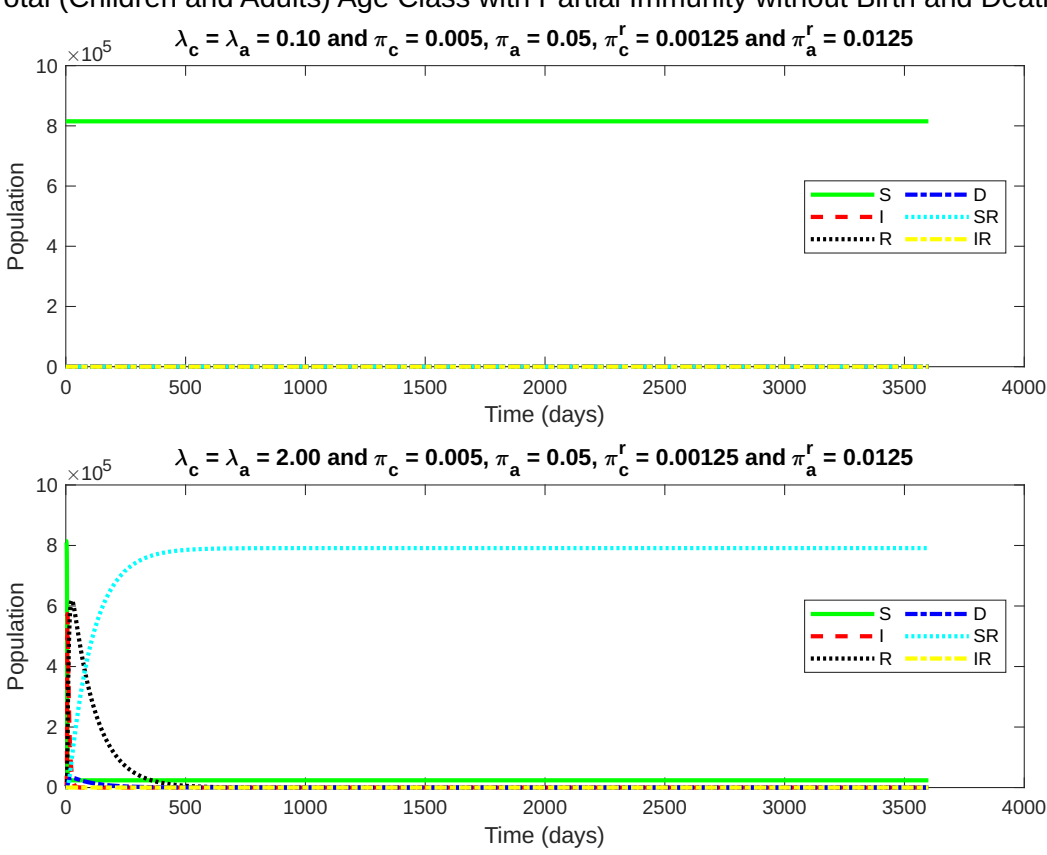
To account for age-specific dynamics, we set a lower power of infection  $(\pi_c = 0.005)$  for children and a higher power of infection  $(\pi_a = 0.05)$  for adults. Additionally, we consider the re-infection power of infection values  $(\pi_c^r = 0.00125 \text{ and } \pi_a^r = 0.0125)$  to capture the possibility of re-infection after recovery.

The likelihood of infection progressing to the asymptomatic state varies between children and adults, with a value of approximately 0.995 for children and 0.95 for adults. This discrepancy in recovery dynamics enables us to examine the overall disease dynamics and its implications.

To simulate the transition from children to adults, we set the transition rate to be 0.001 for children transitioning to adults, while adults do not transition to other age groups, as our focus lies on the children-to-adults transition.

Taking into account the population data from San Francisco in 2021, we initialize the model using the recorded figures. The population of children aged 0 to 2 years old in San Francisco was approximately 23,996, while the adult population was around 791,205. These population values serve as the foundation for our model initialization, while maintaining consistent initial conditions for the other compartments.

By considering these parameters and population data, our objective is to gain valuable insights into the disease dynamics and understand its potential for endemic stability within a population comprising distinct age groups.



Total (Children and Adults) Age Class with Partial Immunity without Birth and Death

Figure 3.22: This figure illustrates total age class model with partial immunity no birth and death processes demonstrate a similar trend to the single age class model, with consistent disease dynamics. However, a notable difference arises in the susceptible population. Unlike the single age class model where the susceptible population reaches zero, the two-age class model maintains a non-zero susceptible population due to the presence of two distinct age groups with varying power of infection values. This highlights the importance of age-specific dynamics in understanding the persistence of the disease and the potential for continued transmission within the population.

The results of our analysis exhibit a similar trend to the single age class model, indicating that the dynamics of the disease remain consistent. However, an interesting observation emerges regarding the susceptible population. In contrast to the single age class model where the susceptible population eventually reaches zero, in the two-age class model, we find that the susceptible population

tible population does not decline to zero. This deviation from the single age class model can be attributed to the presence of two distinct age groups with different power of infection values.

Similarly, we observed that the simulation did not achieve endemic stability. To attain endemic stability, one of the considerations was to increase the infection rate, which ultimately resulted in the simulation reaching an endemic state.

# Age structure model partial immunity without births and deaths

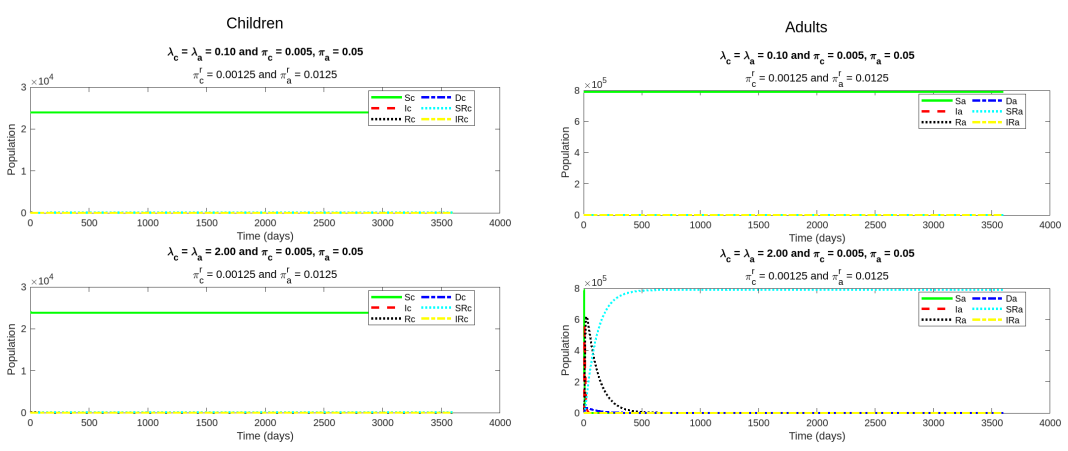


Figure 3.23: The simulation results of the age structure model with partial immunity, without considering birth and death rates and separating children and adults, reveal similar patterns as absence of immunity. On the other hand, the simulation results for the adult population resemble those of the total population model, showing similar trends and dynamics. These findings align with our existing knowledge of Covid-19 dynamics and provide further evidence to support our understanding. The simulation results demonstrate the stability and reliability of our understanding of the disease's behavior within different age groups. In particular, the simulation of the adult population shows a steady state, indicating that the disease has been eradicated from that age group.

Our analysis confirms that the simulation results for the children population in the two-age class model align closely with both the absence of immunity and immunity models. Similarly, the simulation results for the adult population resemble those of the total population model. Therefore, our analysis does not introduce any new significant findings that deviate from previous observations.

In the simulation of the children population, we consistently observe the absence of outbreaks regardless of the infection rates tested. The population size of children remains constant throughout the simulation, indicating either a lower susceptibility or a different disease progression in this age group compared to adults.

Similarly, the simulation results for the adult population mirror those of the total population model, indicating that the behavior of the adult population strongly influences the overall trends observed in the age structure model. These outcomes align with our existing understanding of Covid-19 dynamics.

To achieve endemic stability in the model, it is crucial to refine the model by incorporating interactions between the two age classes. By considering contact and potential disease transmission between children and adults, we can enhance our understanding of transmission patterns within the population. Additionally, identifying the necessary conditions for achieving endemic stability requires a comprehensive analysis of factors such as infection rates, population demographics, and intervention strategies.

While our analysis may not introduce novel findings, it reinforces and corroborates the patterns observed in previous models, highlighting the stability and reliability of our understanding of Covid-19 dynamics within different age groups. However, the ultimate goal is to achieve endemic stability. Increasing the infection rate alone does not lead to endemic stability in the model incorporating partial immunity without considering birth and death rates.

Adjusting parameters such as the time scale of immunity loss, the power of infection for subsequent infections, and the subsequent infection rate does not result in significant changes either.

To establish the necessary conditions for endemic stability, analytical calculations and evaluations of the model are essential. These calculations can help determine the specific requirements for achieving endemic stability, providing valuable insights into the dynamics of disease transmission and control.

Our analysis reinforces the need for ongoing research and refinement of models to improve our understanding of disease dynamics and inform effective strategies for managing infectious diseases like Covid-19.

# Single age class Partial Immunity with Birth and Death

In our analysis of the partial immunity model with consideration of birth and death dynamics, we enhance the previous model by incorporating the natural processes of population growth and mortality. By introducing birth and death rates into the model, we aim to capture the realistic scenario where new individuals enter the population through births, while existing individuals depart through natural deaths.

By including birth and death rates of 0.005, which represent equal rates of new births and natural deaths, we are able to explore the impact of these factors on the dynamics of the disease. New births contribute to the susceptible population, introducing a continuous influx of individuals who are vulnerable to the disease. On the other hand, natural deaths reduce the total population and have implications for all compartments of the model, including the susceptible, infected, recovered, and diseased populations.

Through the incorporation of birth and death rates, our analysis provides a more comprehensive understanding of the long-term implications of disease transmission, recovery, and population dynamics. We can observe how the interplay between these factors influences the stability and trends of the susceptible, infected, recovered, and diseased populations over time. This refined model enables us to evaluate the potential impacts of the disease on population growth, as well as the overall health and well-being of the population.

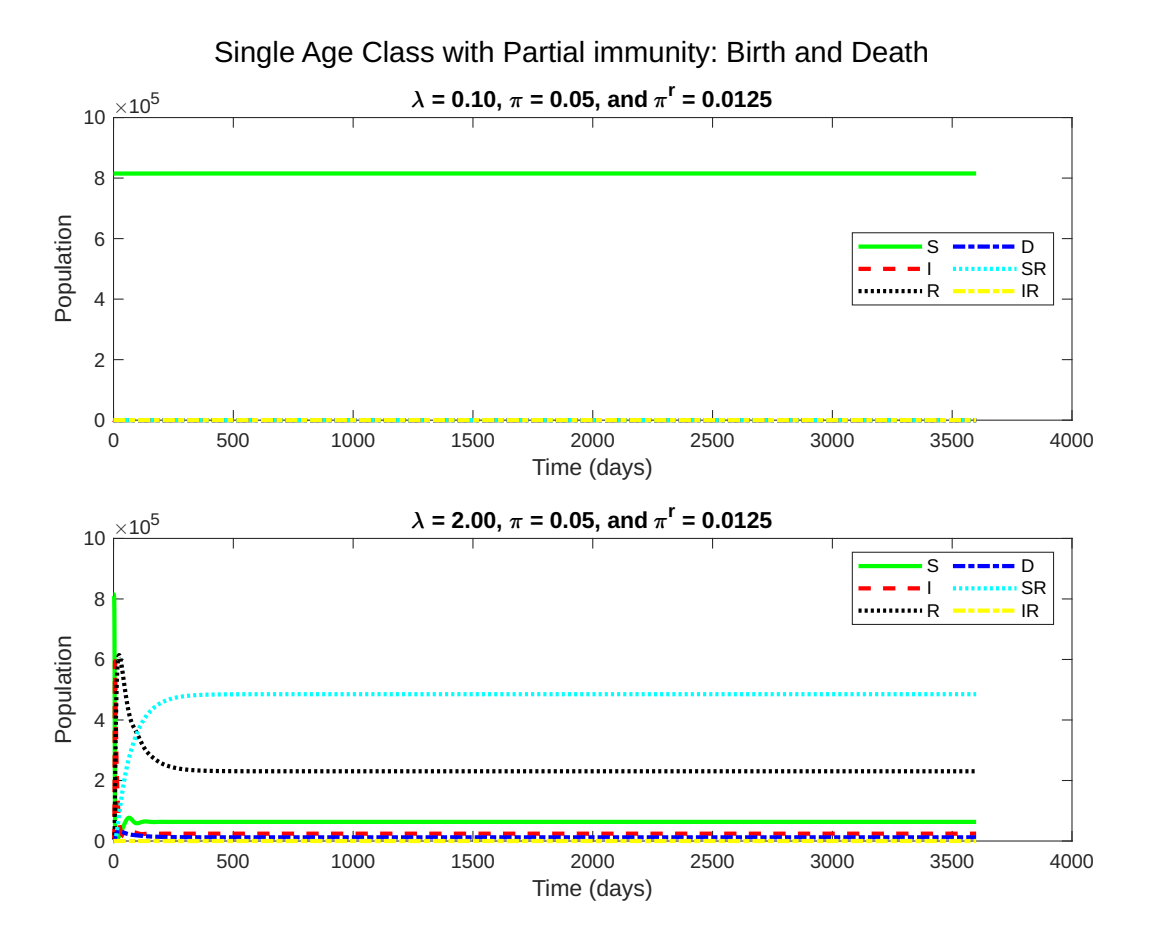


Figure 3.24: The analysis of partial immunity with birth and death dynamics in the age structure model reveals intriguing patterns and dynamics. The incorporation of birth processes introduces a dynamic interaction between disease transmission and population growth, leading to fluctuations in the susceptible population before reaching a stable state. Additionally, the population of re-infected susceptible individuals initially increases but eventually stabilizes. Furthermore, the simulation results indicate that the model has reached a steady state with a low number of symptomatic cases, suggesting an endemic state. This suggests that the population has acquired immunity, and those who were previously infected have developed protection against further infections. As a result, the re-infected population eventually diminishes and reaches zero, indicating that only individuals who have never been infected with Covid-19 before are susceptible to the disease.

In our analysis of the single age class model with partial immunity, birth, and death dynamics, we have uncovered intriguing patterns that provide new insights into the dynamics of the disease. While we still observe similar overall trends as in previous models, the inclusion of birth and death processes introduces additional complexities and dynamics to the epidemic dynamics.

One notable distinction is the behavior of the susceptible population. As the infection rate increases and the disease spreads, the susceptible population initially decreases, consistent with our previous findings. However, the introduction of birth processes means that new individuals are continuously added to the population. Consequently, when the susceptible population reaches a lower value, it starts to increase again due to the birth of newborn individuals. This interplay between disease transmission and population growth creates a dynamic feedback loop that influences the course of the epidemic. The continuous addition of new susceptible individuals can sustain the spread of the disease and potentially lead to fluctuations in the susceptible population over time.

Regarding the re-infected susceptible population, we observe an initial increase followed by a relatively stable phase. As individuals who have recovered from the disease become susceptible to re-infection, the population of re-infected susceptible gradually rises. However, it eventually reaches a point where it stabilizes. The decrease in the re-infected susceptible population can be attributed to natural deaths or a reduction in the number of individuals becoming re-infected. The re-infected transmission rate, which determines the probability of re-infection, plays a significant role in shaping the dynamics of the re-infected susceptible population. Different re-infected transmission rates can result in varying levels of susceptibility to re-infection and influence the overall spread and persistence of the disease.

Importantly, we observe that the re-infected population eventually goes

to zero, indicating that individuals who have been infected with Covid-19 once or more acquire some level of immunity. However, those who have not been previously infected remain susceptible to infection. This highlights the dynamic nature of partial immunity and the finite duration of protection against re-infection. Over time, individuals who have been re-infected may lose their immunity, making them susceptible to subsequent infections.

The findings from studying the interplay of different age classes in the model can provide a deeper understanding of the disease dynamics. By dividing the population into multiple age classes, we can investigate how different age groups interact, potentially leading to variations in disease transmission, susceptibility, and re-infection dynamics. This understanding can inform the development of targeted strategies for disease control and prevention, tailored to the specific dynamics of different age groups within the population.

### Age Structure Partial Immunity with Birth and Death

In this enhanced version of the age structure model, we incorporate the dynamics of birth and death, which were absent in the previous model with partial immunity. By including these factors, our objective is to create a more realistic simulation that better captures the complexities of population dynamics in the context of disease transmission. In this updated model, only adults contribute to the birth process, resulting in a birth rate of  $\mu \cdot N_a$ , where  $\mu$  is defined as  $\delta \cdot \frac{N_c}{N_a}$ . Additionally, we assume a death rate of zero for children.

The introduction of birth and death dynamics allows us to investigate how these natural population processes interact with the dynamics of disease transmission and collectively shape the overall population structure. New births contribute to the susceptible population, introducing individuals who are vulnerable to the disease. Conversely, natural deaths reduce the total population size and have an impact on all compartments of the model, including the susceptible, infected, recovered, and diseased populations.

By considering these demographic factors, we can explore how changes in birth and death rates influence disease dynamics and population outcomes. The birth rate affects the rate at which susceptible individuals are added to the population, potentially increasing the pool of individuals who can contract the disease. On the other hand, natural deaths decrease the overall population size, which can have implications for disease spread and the recovery of the population.

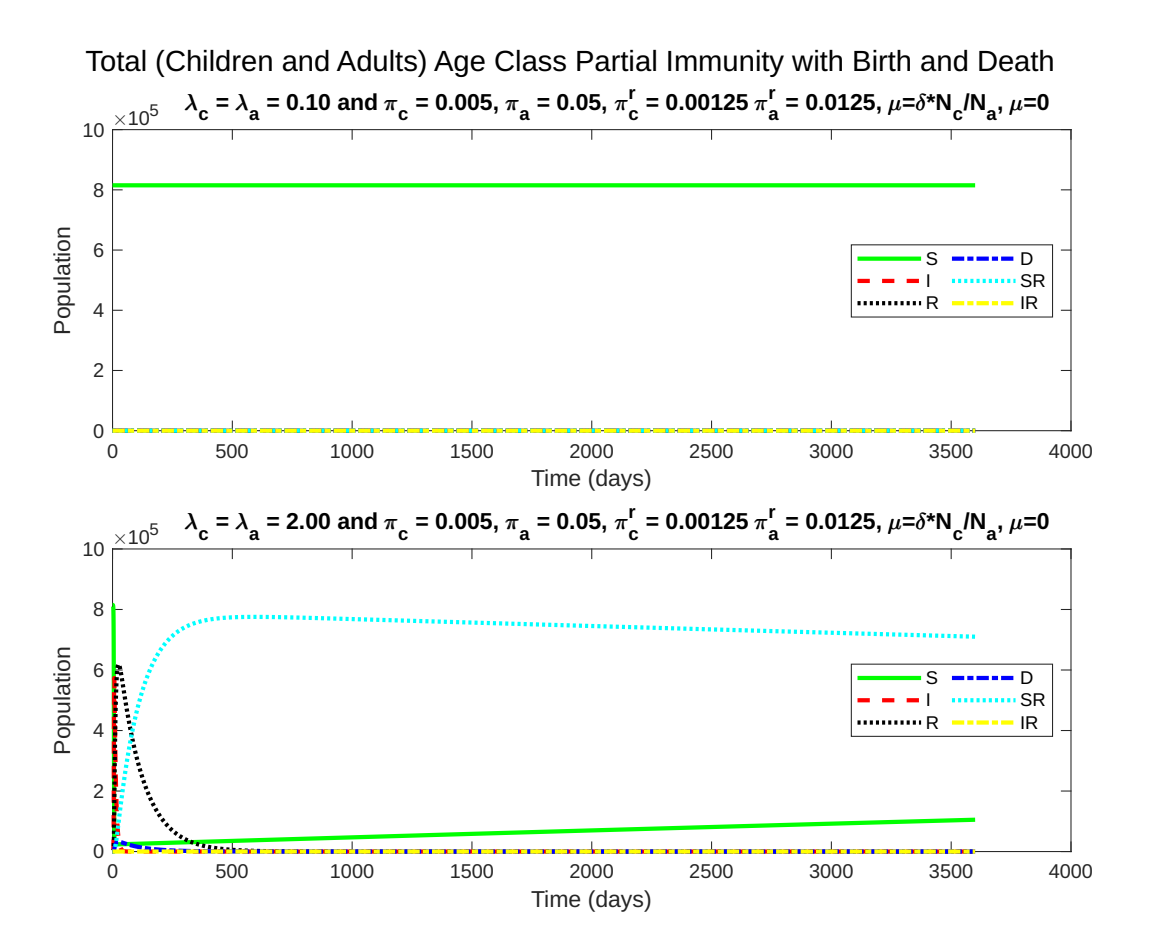


Figure 3.25: The figure depicting the age structure model with partial immunity, where birth is represented by  $\mu = \delta \frac{N_c}{N_a}$  and  $\mu_c = 0$ , reveals interesting dynamics. Similar to previous models, we observe the occurrence of an outbreak as we increase the infection rate. However, a distinctive feature emerges in this model: the disease is eventually eradicated, as both the infected and re-infected populations converge to zero. This signifies that there is no active disease present in the population, and individuals have acquired immunity.

The age structure model with partial immunity, incorporating birth dynamics represented by  $\mu = \delta \frac{N_c}{N_a}$  and  $\mu_c = 0$ , exhibits intriguing dynamics that deepen our understanding of disease spread and immunity acquisition. Similar to previous models, an outbreak occurs as we increase the infection rate, resulting in a rise in the number of infected individuals. However, a notable distinction arises in this model: the disease ultimately gets eradicated,

leading to both the infected and re-infected populations converging to zero.

This implies a complete absence of the disease in the population and signifies the acquisition of immunity by individuals.

The eradication of the disease in this model can be attributed to multiple factors. First, the interplay between transmission dynamics and immunity acquisition plays a pivotal role. As the infection rate rises, susceptible individuals become infected, leading to a surge in the infected population. However, as infected individuals recover, they develop partial immunity, reducing their susceptibility to re-infection. This gradual accumulation of immunity across the population acts as a protective barrier, gradually depleting the pool of susceptible individuals and impeding the further spread of the disease.

Additionally, the introduction of birth dynamics into the model contributes to the ultimate eradication of the disease. The birth rate, determined by  $\mu = \delta \frac{N_c}{N_a}$ , adds new susceptible individuals to the population. However, as the disease spreads and immunity is acquired, the susceptible population gradually diminishes over time. This decline in susceptibility, coupled with the absence of re-infection, eventually leads to the complete eradication of the disease.

It is important to note that this model does not exhibit a steady state, as the disease is ultimately eradicated rather than reaching an equilibrium. This highlights the dynamic nature of disease dynamics and the potential for disease elimination through immunity acquisition. To achieve endemic stability, we increase the infection rate and observe the behavior of the model. When this is done, we observe that the model attains endemic stability.

# Age structure model partial immunity with birth and death

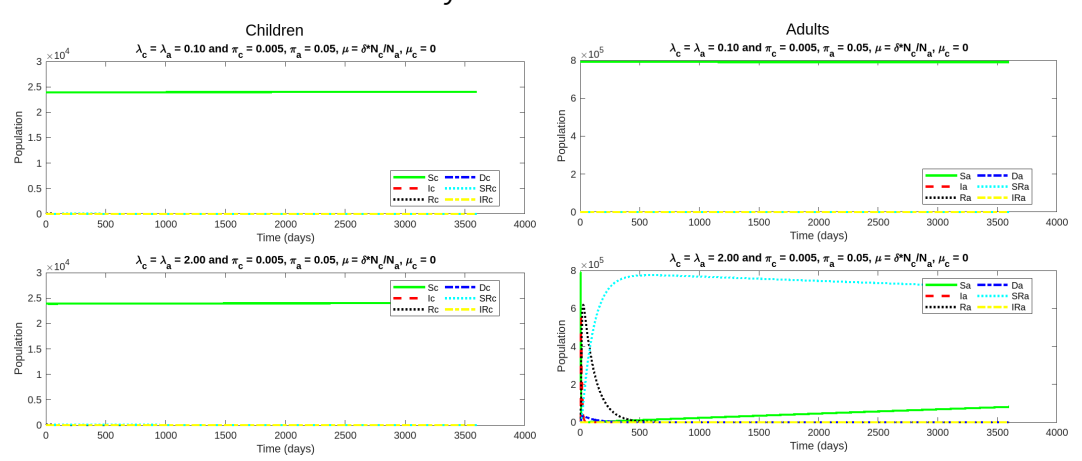


Figure 3.26: The figure presented depicts the dynamics of disease transmission in the age structure model with partial immunity and birth/death dynamics. In this model, we set  $\mu_c = 0$  to exclude children from the analysis, and  $\mu = \delta \frac{N_c}{N_c}$ , where  $\mu$  represents the birth rate in relation to the number of adults  $(N_a)$  and the proportion of infected individuals  $(N_c)$ . Interestingly, when examining the simulation results for children, we observe no outbreak as we increase the infection rates. This suggests that the disease transmission dynamics among children do not contribute significantly to the overall spread of the disease. Consequently, the impact of the disease on the child population may be relatively limited in this particular model configuration. In contrast, when focusing on the adult population, we observe similar results as those observed in the total population. This implies that adults play a crucial role in influencing the dynamics of the disease. The susceptibility of adults to Covid-19 appears to be higher, leading to a greater likelihood of outbreaks occurring among this age group. The interplay between infection rates, susceptibility, and the interactions among adults contribute to the observed disease dynamics in the age structure model.

The dynamics of disease transmission in an age structure model with partial immunity and birth/death dynamics, where  $\mu_c = 0$  and  $\mu * N_a$ , with  $\mu = \delta \frac{N_c}{N_a}$ . This model configuration allows us to gain valuable insights into the role of different age groups in influencing the spread and impact of the disease.

When we focus on the simulation results for children, we observe an intriguing finding: there is no outbreak as we increase the infection rates.

This suggests that the transmission dynamics among children alone do not contribute significantly to the overall spread of the disease in this particular model. It is important to note that the absence of an outbreak in children does not mean they are immune or unaffected by the disease. It simply indicates that the transmission patterns and interactions within the child population are not driving the observed outbreak dynamics.

In contrast, the simulation results for adults reveal a different scenario. We observe similar trends in the dynamics of the disease as those observed in the total population, suggesting that adults have a more pronounced influence on the disease dynamics compared to children. This finding implies that adults are more susceptible to Covid-19, leading to a higher likelihood of outbreaks occurring among this age group. The interplay between infection rates, susceptibility levels, and interactions among adults play a significant role in shaping the observed disease dynamics in the age structure model.

We observe similar pattern that the model does not attain endemic stability. In order to achieve this, we need to consider increasing the infection rate. When done so, we observe that the model reaches an endemic stability with very few number of infected people.

## Single Age Class Models Force of Infection and Disease Incidence

In our analysis of the force of infection and disease incidence, we compare the average values between the single age class and two-age class models. This comparison allows us to understand the factors that contribute to the disease reaching an endemic state in the population under absence of immunity and partial immunity. By examining these metrics, we can gain valuable in-

sights into the conditions required for the disease to establish a stable presence within the population.

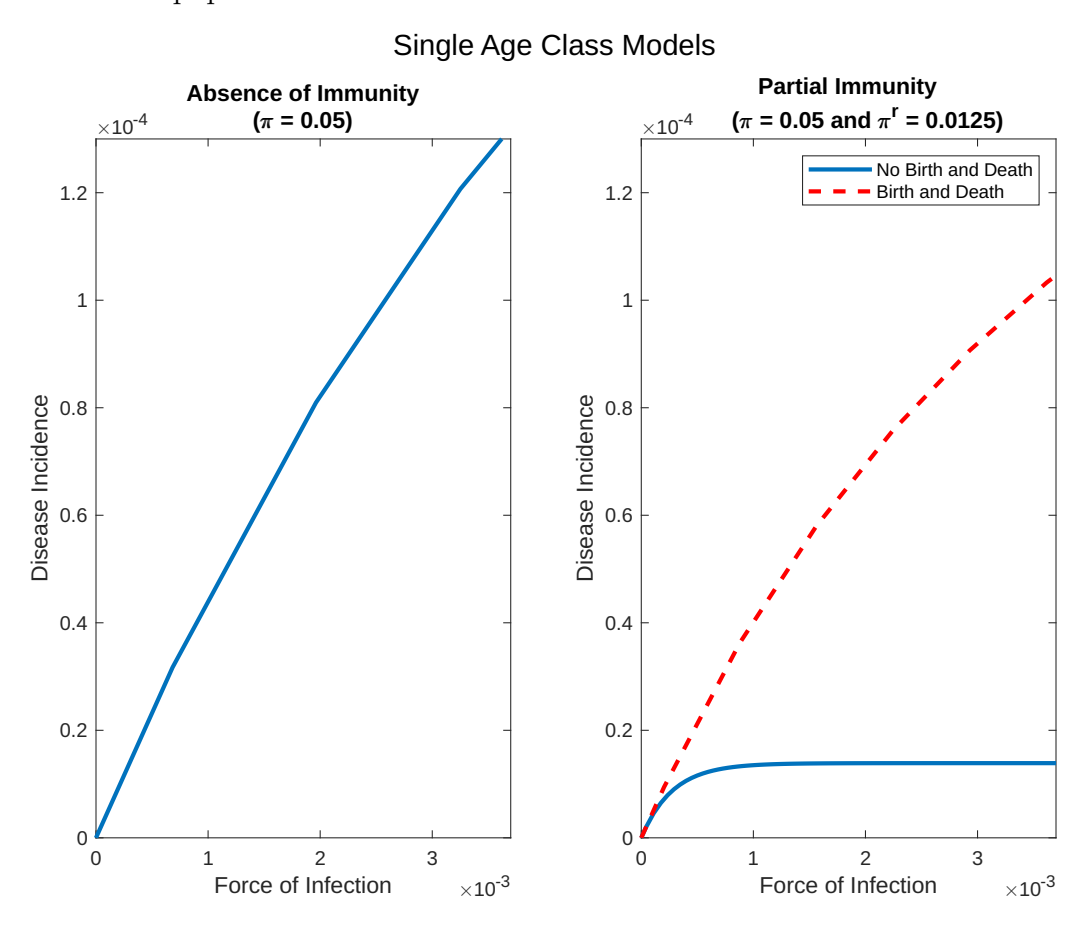


Figure 3.27: The figure illustrates the impact of immunity and birth/death processes on disease dynamics. Without immunity, increasing infection rates lead to a rise in disease incidence, eventually reaching a plateau indicating endemic stability. Partial immunity significantly reduces disease incidence, and considering birth/death processes further decreases it. In the partial immunity model without birth/death, the disease is eradicated, and everyone becomes re-infected susceptible. This absence of reinfection cycles leads to a constant number of symptomatic individuals and endemic stability.

In our study of the single age class model without immunity, we have made interesting observations regarding the relationship between the infection rate, force of infection, disease incidence, and disease stability.

We found that as the infection rate increases in the absence of im-

munity, there is a corresponding rise in the force of infection. The force of infection represents the rate at which susceptible individuals become infected per unit time and is influenced by factors such as contact patterns and disease infectiousness. With a higher infection rate, more individuals come into contact with infected individuals, leading to an increased force of infection.

This increase in the force of infection also results in a higher disease incidence, which measures the number of new cases within a specific population over time. As more individuals become infected due to the increased force of infection, the disease incidence rises. However, we observed that this upward trend eventually reaches a plateau, indicating the attainment of endemic stability. At this point, the disease becomes endemic within the population, and the incidence remains relatively constant over time.

Moving on to the partial immunity model, where individuals have acquired partial immunity through previous infections, we noticed a greater decrease in the magnitude of disease incidence compared to the model without immunity. The presence of partial immunity reduces the susceptibility of previously infected individuals, resulting in a dampening of disease incidence and mitigating the overall impact of the disease.

When we introduced birth and death dynamics into the partial immunity model, we observed a slight decrease in the magnitude of disease incidence. The interplay between births and deaths influenced disease dynamics, leading to a smaller decrease in disease incidence compared to the partial immunity model without these dynamics. The introduction of births contributes to a susceptible population, increasing the pool of individuals at risk of infection, while deaths reduce the overall population size, limiting the spread of the

disease. Thus, considering birth and death processes slightly decreases the magnitude of disease incidence.

It is worth noting that in our previous analysis of the partial immunity model without birth and death processes, we observed the eradication of the disease, indicating that everyone in the population had acquired immunity. However, when birth and death dynamics were incorporated, the disease persisted, although at a reduced magnitude. This suggests the existence of a continuous cycle of infection and partial immunity, leading to a constant number of symptomatic individuals and establishing endemic stability.

These findings highlight the importance of understanding the interplay between infection rates, force of infection, disease incidence, and the influence of immunity, birth, and death processes. Such understanding can provide valuable insights for public health interventions and strategies aimed at controlling the spread of diseases and safeguarding vulnerable populations.

#### Age Structure Models Force of Infection and Disease Incidence

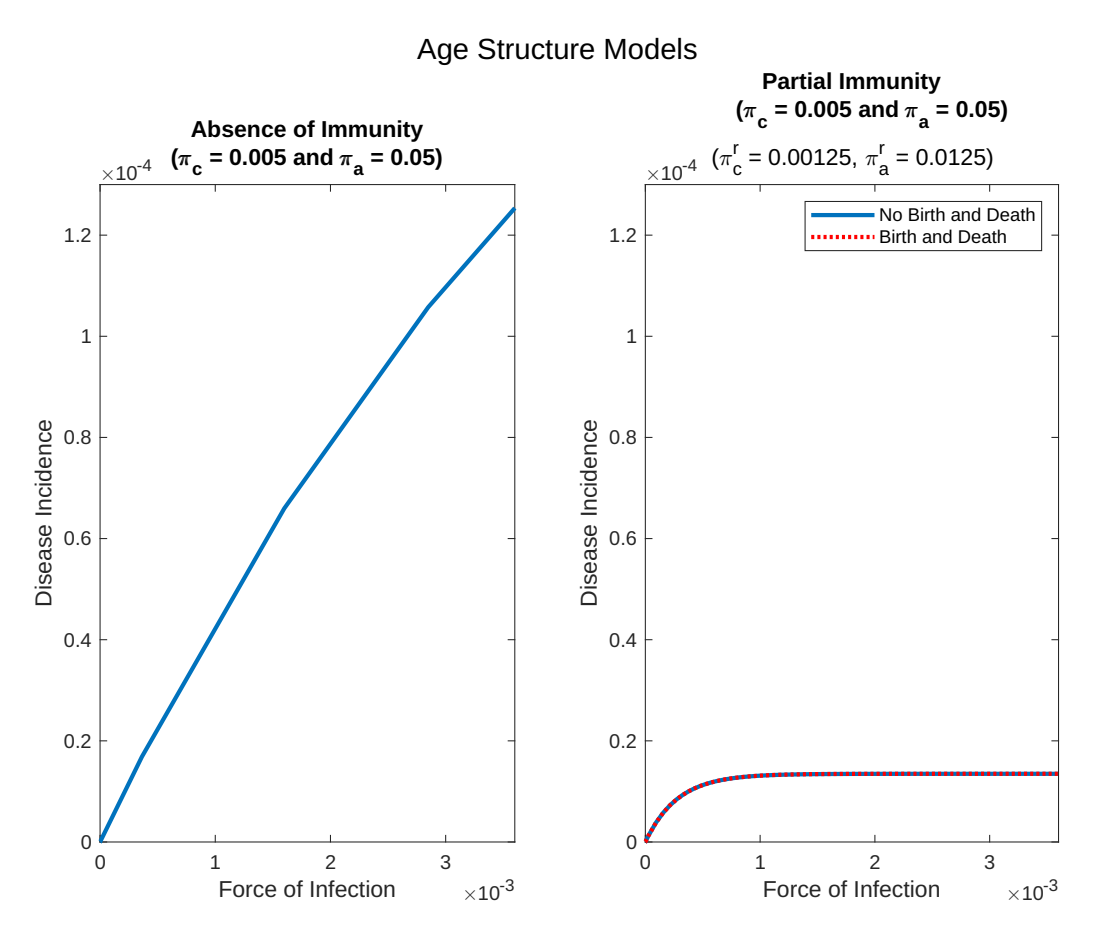


Figure 3.28: This figure depicts the effects of immunity and demographic factors on the dynamics of COVID-19 within an age structure model. The left panel represents the absence of immunity, where disease incidence initially increases with the infection rate and eventually reaches a plateau, indicating endemic stability. Notably, without immunity, the peak of disease incidence is considerably higher. In the right panel, we explore the scenario of partial immunity and consider two cases: one without incorporating birth and death processes and the other with their inclusion. When birth and death processes are not considered, the presence of partial immunity acquired from previous infections leads to a reduction in the peak of disease incidence. This highlights the role of immunity in mitigating the impact of the disease. However, when birth and death processes are included in the model, the results align with the scenario of partial immunity without considering these demographic factors. This suggests that there is no active disease present in the population, and symptomatic cases reach an endemic stability. The inclusion of birth and death processes further contributes to the overall dynamics of the disease by accounting for changes in population size over time.

Our investigation into the impact of partial immunity on disease dynamics within an age structure model has yielded fascinating insights, particularly when considering the incorporation of birth and death processes.

In line with the single age class model, we confirm that as the infection rate increases, there is an initial surge in disease incidence, indicating a higher number of new cases in the population. However, as the infection rate continues to rise, we observe a plateau in the peak of disease incidence, indicating the attainment of endemic stability. This suggests that the disease has reached a state where the incidence remains relatively constant over time.

When examining the scenario of partial immunity, we discover distinct outcomes depending on whether we include birth and death processes in the model. Without considering these demographic factors, we observe a significantly greater reduction in the peak of disease incidence compared to the absence of immunity model. This reduction is attributed to the presence of individuals who have acquired partial immunity through previous infections, leading to a lower susceptibility to the disease and dampened disease incidence. The decline in the peak of disease incidence highlights the role of partial immunity in mitigating the disease's impact.

However, when we incorporate birth and death processes into the model, the results align with the scenario of partial immunity without considering these demographic factors. This suggests the absence of active disease in the population, with symptomatic cases reaching endemic stability. The inclusion of birth and death processes further contributes to the overall dynamics by accounting for changes in population size over time.

Furthermore, our findings indicate that due to a lower power of infection

and subsequent infection rate among children, a higher proportion of infected children become asymptomatic, leading to a lower number of symptomatic cases in the population.

These insights underscore the complexity of disease dynamics within an age structure model and emphasize the interplay between immunity, birth and death processes, and disease incidence. They highlight the importance of considering these factors in understanding and managing the spread of infectious diseases. The knowledge gained from this analysis can inform the development of targeted strategies and interventions to effectively control and mitigate the impact of diseases like COVID-19 in populations with diverse age structures.

### 3.4 Discussion

### 3.4.1 Immunity

Polio, primarily affecting children under 5, exhibits distinct characteristics in its transmission dynamics and disease burden. Our analysis of polio dynamics revealed several important findings. When the infection rate is low, the impact on the population is minimal, resulting in a low number of infections and symptomatic cases. However, as the infection rate increases, the disease burden intensifies, leading to more infections within a shorter time frame.

The interplay between population dynamics, such as new births and natural deaths, also influences the spread of polio. In scenarios with equal birth and death rates, the susceptible population initially decreases as more individuals become infected and recover. However, over time, the susceptible population gradually increases due to new births, while the number of infected individuals reaches a steady state. This equilibrium is crucial for understanding the long-term dynamics of polio.

In the refined model considering births from the adult population and no deaths among children, we observed the eradication of polio as the number of infected individuals eventually reduced to zero. Interestingly, the analysis indicated that children were less likely to become symptomatic when infected with polio compared to adults. The model highlighted the importance of asymptomatic cases among children, contributing to the reduction in disease incidence. However, it also demonstrated that children who were not infected during childhood remained susceptible as they transitioned into adulthood,

indicating the potential for re-emergence of polio.

Furthermore, the age structure model provided valuable insights into the interaction between age groups and disease dynamics. Children exhibited a higher susceptibility to polio, with a relatively low number of symptomatic cases even at higher infection rates. Conversely, adults had a greater likelihood of experiencing symptomatic disease and potential paralysis. This age-specific analysis shed light on the differential impacts of polio within each age group.

Analyzing historical data, we observed that the prevalence of polio was lower in the past when children were exposed to the disease at a younger age due to poor sanitation. This exposure led to the development of immunity, resulting in a larger population with polio immunity. However, improvements in sanitation reduced children's exposure to polio, leading to a larger susceptible population. As these individuals grew up and became adults, they were more likely to experience symptomatic disease and paralysis due to their lack of previous exposure and immunity.

These findings have significant implications for polio control strategies. Vaccination programs targeting children under 5 are crucial in reducing polio transmission and protecting vulnerable populations. Additionally, ensuring high vaccination coverage among adults can help prevent symptomatic cases and long-term consequences. Population immunity plays a critical role, and maintaining high immunization coverage and hygiene practices are key in controlling the spread of polio and protecting vulnerable individuals.

### 3.4.2 Absence of Immunity and Partial Immunity

When studying the spread of Covid-19, it becomes evident that a single age class model is insufficient to capture the complexity of the disease dynamics. In reality, interactions between individuals of different ages play a crucial role. Children, for instance, have shown to be less susceptible to the virus compared to adults. Their immune systems are often more resilient, allowing them to mount effective defenses against the virus and resulting in a higher likelihood of asymptomatic infections. This characteristic has significant implications for disease transmission, as asymptomatic individuals can unknowingly spread the virus to others, contributing to the overall spread of the disease.

To create a more accurate model that mimics real-world scenarios, it is essential to consider factors such as birth and death rates. Births introduce new susceptible individuals into the population, while deaths remove individuals from the population altogether. These factors are particularly relevant in the context of Covid-19, as they contribute to the overall dynamics of the disease.

Incorporating birth and death rates into the model allows us to observe the long-term effects of the disease. Over time, as individuals are infected and recover, they develop partial immunity, which reduces their likelihood of being re-infected and experiencing severe symptoms. This gradual acquisition of immunity, coupled with the ongoing birth and death processes, can lead to disease eradication. As the number of infected individuals decreases, the disease reaches a state of endemic stability, where the occurrence of symptomatic cases becomes less frequent.

By incorporating an age structure model, we gain valuable insights into the differential impact of Covid-19 on different age groups. It becomes evident that the likelihood of infection progressing to a symptomatic state increases with age. Adults, who generally have more developed immune systems but may also have underlying health conditions, are more prone to experiencing severe symptoms and complications. Therefore, they contribute significantly to the overall incidence of the disease.

Interestingly, when considering re-infection, the likelihood of progressing to a symptomatic state is lower compared to initial infection. This suggests that individuals who have already been infected and experienced symptoms have built some level of immunity, which provides a degree of protection upon subsequent exposure to the virus. Consequently, their re-infection is more likely to result in a milder course of illness or even an asymptomatic infection. This phenomenon contributes to a decrease in disease incidence as the epidemic progresses.

Breaking down the analysis by age groups, we find that children have a lower likelihood of progressing to a symptomatic state upon subsequent reinfection compared to adults. This can be attributed to their robust immune responses, which enable them to effectively control the virus and minimize the severity of symptoms. As a result, the overall disease incidence is significantly reduced, as a larger proportion of infections in the population are asymptomatic or mild among children.

## Chapter 4

### Conclusion

In recent years, infectious diseases have posed significant challenges to global public health. Understanding the dynamics of disease transmission is essential for developing effective control strategies and mitigating the impact of these diseases on populations. Our analysis of polio, bubonic plague during the Second Pandemic, and COVID-19 sheds light on the complex interplay between biological factors, population dynamics, and historical context in shaping disease burden and transmission.

Polio, a viral disease primarily affecting children under 5, exhibits distinct characteristics in its transmission dynamics. Our study reveals that when the infection rate is low, the impact on the population is minimal, with a low number of infections and symptomatic cases. This finding underscores the importance of maintaining low infection rates through vaccination programs targeting children under 5. By protecting this vulnerable age group, we can reduce transmission and prevent the long-term consequences of the disease.

Furthermore, our analysis highlights the role of population dynamics, including birth and death rates, in shaping polio transmission. In scenarios

where birth and death rates are equal, the susceptible population initially decreases as more individuals become infected and recover. However, over time, the susceptible population gradually increases due to new births. This equilibrium between births and infections is critical in understanding the long-term dynamics of polio and the potential for disease eradication.

In the refined model considering births from the adult population and no deaths among children, we observe the eventual eradication of polio as the number of infected individuals reduces to zero. This finding underscores the importance of vaccination efforts targeting children and maintaining high immunization coverage among adults to prevent the re-emergence of the disease.

Moving on to the bubonic plague during the Second Pandemic, our study supports the notion that both rodent and human transmission contributed to its spread. The inclusion of rodents, particularly rats, as significant players in the transmission dynamics of the disease is a crucial finding. The Lynch-Oster model, which incorporates both rodent and human transmission, demonstrates superior fit to observed mortality patterns compared to other models. This suggests that rodents played a significant role in the transmission dynamics of the bubonic plague.

However, it is important to acknowledge the limitations and uncertainties associated with modeling infectious diseases. Our study was based on specific assumptions and available data, which may introduce inherent biases. Different modeling approaches and parameterizations may yield alternative results, and therefore, the choice of model should consider not only the goodness of fit but also biological plausibility and prior knowledge about the disease.

The contradiction with Dean et al.'s paper highlights the complexity of

modeling plague transmission and underscores the need for further research. Divergent findings among studies may arise due to variations in data sources, model assumptions, or methodological approaches. To gain a more comprehensive understanding of the transmission dynamics during the Second Pandemic, additional data are needed. This includes information on ecological factors that affect rodent populations, the dynamics of ectoparasites, and detailed historical records that provide insights into human behavior and movement patterns.

Turning to COVID-19, our analysis reveals that a single age class model is insufficient to capture the complexity of disease dynamics. Interactions between individuals of different ages play a crucial role, with children exhibiting a lower susceptibility to the virus compared to adults. This characteristic has significant implications for disease transmission, as asymptomatic children can unknowingly spread the virus to others.

To create a more accurate model that mimics real-world scenarios, it is essential to consider factors such as birth and death rates. Births introduce new susceptible individuals into the population, while deaths remove individuals from the population altogether. These factors contribute to the overall dynamics of the disease and its long-term effects.

Incorporating an age structure model into our analysis provides valuable insights into the differential impact of COVID-19 on different age groups. Adults, who generally have more developed immune systems but may also have underlying health conditions, are more prone to experiencing severe symptoms and complications. This underscores the need for targeted interventions and protective measures for this age group.

Furthermore, our analysis demonstrates that individuals who have already been infected and experienced symptoms have built some level of immunity, resulting in a lower likelihood of progressing to a symptomatic state upon subsequent re-infection. This phenomenon contributes to a decrease in disease incidence as the epidemic progresses.

The findings highlight the importance of ongoing vaccination efforts, surveillance, hygiene practices, and targeted interventions based on age-specific factors in controlling the spread of COVID-19. Maintaining high immunization coverage, particularly among vulnerable populations, is crucial for reducing disease transmission and protecting individuals from severe illness.

Analysis of polio, bubonic plague, and COVID-19 underscores the complexity of infectious diseases and the need for comprehensive approaches to understanding and controlling their transmission. By considering factors such as age-specific susceptibility, population dynamics, and historical context, we can develop more accurate models and inform evidence-based interventions. Ongoing research, data collection, and collaboration among scientists and public health professionals are essential for advancing our understanding of these diseases and enhancing global preparedness for future outbreaks.

# Bibliography

- A Costa, M Pires, R Resque, and SSMS Almeida. Mathematical modeling of the infectious diseases: key concepts and applications. *Journal of Infectious Diseases and Epidemiology*, 7(5):209, 2021.
- [2] Katharine R Dean, Fabienne Krauer, Lars Walløe, Ole Christian Lingjærde, Barbara Bramanti, Nils Chr Stenseth, and Boris V Schmid. Human ectoparasites and the spread of plague in europe during the second pandemic. Proceedings of the National Academy of Sciences, 115(6):1304– 1309, 2018.
- [3] Mirjam Kretzschmar and Jacco Wallinga. Mathematical models in infectious disease epidemiology. Modern infectious disease epidemiology: Concepts, methods, mathematical models, and public health, pages 209–221, 2010.
- [4] Michael Y Li. An introduction to mathematical modeling of infectious diseases, volume 2. Springer, 2018.
- [5] Nicholas C Grassly and Christophe Fraser. Mathematical models of infectious disease transmission. *Nature Reviews Microbiology*, 6(6):477–487, 2008.

- [6] Roy M Anderson and Robert M May. Infectious diseases of humans: dynamics and control. Oxford university press, 1991.
- [7] Waleed M Sweileh. Global research activity on mathematical modeling of transmission and control of 23 selected infectious disease outbreak. Globalization and Health, 18(1):1–14, 2022.
- [8] Lee A Segel and Leah Edelstein-Keshet. A Primer in Mathematical Models in Biology, volume 129. Siam, 2013.
- [9] Johannes Müller. Mathematical models in biology. *Technical University Munich, Centre for Mathematical Sciences*, 2004.
- [10] Linda JS Allen. The sir model for spread of disease: The differential equation model. *Mathematics Magazine*, 80(4):233–245, 2007.
- [11] Jason Brownlee. Markov chain monte carlo (MCMC) for probability, 2019.
- [12] Mark Pinsky and Samuel Karlin. An introduction to stochastic modeling. Academic press, 2010.
- [13] StatLect. Metropolis-hastings algorithm. https://www.statlect.com/fundamentals-of-statistics/Metropolis-Hastings-algorithm, n.d.
- [14] Roger D. Peng. Advanced statistical computing. https://bookdown.org/rdpeng/advstatcomp/, 2019. Accessed: April 16, 2023.
- [15] Kathryn A Glatter and Paul Finkelman. History of the plague: An ancient pandemic for the age of covid-19. *The American journal of medicine*, 134(2):176–181, 2021.

- [16] Xavier Vallès, Nils Chr Stenseth, Christian Demeure, Peter Horby, Paul S Mead, Oswaldo Cabanillas, Mahery Ratsitorahina, Minoarisoa Rajerison, Voahangy Andrianaivoarimanana, Beza Ramasindrazana, et al. Human plague: An old scourge that needs new answers. PLoS neglected tropical diseases, 14(8):e0008251, 2020.
- [17] Christopher John Duncan and Susan Scott. What caused the black death? Postgraduate medical journal, 81(955):315–320, 2005.
- [18] Ruifu Yang. Plague: recognition, treatment, and prevention. *Journal of clinical microbiology*, 56(1):e01519–17, 2018.
- [19] Thomas Butler. Plague into the 21st century. Clinical Infectious Diseases, 49(5):736–742, 2009.
- [20] MJ Keeling and CA Gilligan. Bubonic plague: a metapopulation model of a zoonosis. Proceedings of the Royal Society of London. Series B: Biological Sciences, 267(1458):2219–2230, 2000.
- [21] Luke C. Mattfeld, Philip A. Eckhoff, and John S. Brownstein. A data-driven comparison of plague models. *Epidemics*, 25:70–79, 2018.
- [22] Zhe Sun, Lei Xu, Boris Schmid, Katharine Dean, Zhibin Zhang, Yan Xie, Xiye Fang, Shuchun Wang, Qiyong Liu, Baolei Lyu, et al. Data from: Human plague system associated with rodent diversity and other environmental factors. Zenodo, 2019.
- [23] PG Coleman, Brian D Perry, and Mark EJ Woolhouse. Endemic stability—a veterinary idea applied to human public health. The Lancet, 357(9264):1284–1286, 2001.

- [24] Svetlana Bunimovich-Mendrazitsky and Lewi Stone. Modeling polio as a disease of development. *Journal of theoretical biology*, 237(3):302–315, 2005.
- [25] Akio Nomoto. Molecular aspects of poliovirus pathogenesis. *Proceedings* of the Japan Academy, Series B, 83(8):266–275, 2007.
- [26] Man Mohan Mehndiratta, Prachi Mehndiratta, and Renuka Pande. Poliomyelitis: historical facts, epidemiology, and current challenges in eradication. The Neurohospitalist, 4(4):223–229, 2014.
- [27] Muhammad Suleman Rana, Rana Jawad Asghar, Muhammad Usman, Aamer Ikram, Muhammad Salman, Massab Umair, Syed Sohail Zahoor Zaidi, Muhammad Anas, and Nadeem Ullah. The resurgence of wild poliovirus in pakistan and afghanistan: A new setback for polio eradication. Journal of Infection, 85(3):334–363, 2022.
- [28] Leslie Roberts. Africa battles out-of-control polio outbreaks. Science (New York, NY), 375(6585):1079–1080, 2022.
- [29] Nete Munk Nielsen, Peter Aaby, Jan Wohlfahrt, Kåre Mølbak, and Mads Melbye. The polio model. does it apply to polio? *International Journal* of epidemiology, 31(1):181–186, 2002.
- [30] Centers for Disease Control and Prevention. About polio, 2021.
- [31] Stuart Blume and Ingrid Geesink. A brief history of polio vaccines. *Science*, 288(5471):1593–1594, 2000.
- [32] Shiva Moein, Niloofar Nickaeen, Amir Roointan, Niloofar Borhani, Zarifeh Heidary, Shaghayegh Haghjooy Javanmard, Jafar Ghaisari, and

- Yousof Gheisari. Inefficiency of sir models in forecasting covid-19 epidemic: a case study of isfahan. *Scientific Reports*, 11(1):1–9, 2021.
- [33] Ian Cooper, Argha Mondal, and Chris G Antonopoulos. A sir model assumption for the spread of covid-19 in different communities. *Chaos, Solitons & Fractals*, 139:110057, 2020.
- [34] Saloni Dattani, Fiona Spooner, Sophie Ochmann, and Max Roser. Polio.

  Our World in Data, 2022.
- [35] LN Nkamba, JM Ntaganda, H Abboubakar, JC Kamgang, and Lorenzo Castelli. Global stability of a sveir epidemic model: Application to poliomyelitis transmission dynamics. 2017.
- [36] A EZRA. Spate of polio outbreaks worldwide puts scientists on alert.

  Nature, 609, 2022.
- [37] Dimitra Klapsa, Thomas Wilton, Andrew Zealand, Erika Bujaki, Eugene Saxentoff, Catherine Troman, Alexander G Shaw, Alison Tedcastle, Manasi Majumdar, Ryan Mate, et al. Sustained detection of type 2 poliovirus in london sewage between february and july, 2022, by enhanced environmental surveillance. *The Lancet*, 400(10362):1531–1538, 2022.
- [38] Isobel M Blake, Rebecca Martin, Ajay Goel, Nino Khetsuriani, Johannes Everts, Christopher Wolff, Steven Wassilak, R Bruce Aylward, and Nicholas C Grassly. The role of older children and adults in wild poliovirus transmission. Proceedings of the National Academy of Sciences, 111(29):10604–10609, 2014.

- [39] Aktar Saikh and Nurul Huda Gazi. The effect of the force of infection and treatment on the disease dynamics of an sis epidemic model with immigrants. Results in Control and Optimization, 2:100007, 2021.
- [40] Marwan Al-Raeei. Numerical simulation of the force of infection and the typical times of sars-cov-2 disease for different location countries. Modeling Earth Systems and Environment, 8(1):1443–1448, 2022.
- [41] Nils Chr Stenseth, Bakyt B Atshabar, Mike Begon, Steven R Belmain, Eric Bertherat, Elisabeth Carniel, Kenneth L Gage, Herwig Leirs, and Lila Rahalison. Plague: past, present, and future. *PLoS medicine*, 5(1):e3, 2008.
- [42] Jenny Howard. Plague was one of history's deadliest diseases—then we found a cure. National Geographic, https://www.nationalgeographic.com/science/health-and-human-body/human-diseases/the-plague/. Accessed, 7, 2020.
- [43] David JD Earn, Junling Ma, Hendrik Poinar, Jonathan Dushoff, and Benjamin M Bolker. Acceleration of plague outbreaks in the second pandemic. Proceedings of the National Academy of Sciences, 117(44):27703–27711, 2020.
- [44] Björn P Zietz and Hartmut Dunkelberg. The history of the plague and the research on the causative agent yersinia pestis. *International journal of hygiene and environmental health*, 207(2):165–178, 2004.
- [45] Kidsdata.org. Child population by age and gender. https://www.kidsdata.org/topic/34/child-population-age-gender/table, 2023. Accessed on May 5, 2023.

[46] Stephen M Kissler, Christine Tedijanto, Edward Goldstein, Yonatan H Grad, and Marc Lipsitch. Projecting the transmission dynamics of sarscov-2 through the postpandemic period. *Science*, 368(6493):860–868, 2020.

#### **VITA**

Author: Vivian John Goshashy

Place of Birth: Dar-es-salaam, Tanzania

Undergraduate Schools Attended: Edmonds Community College,

Central Washington University

Degrees Awarded: Associate Degree, 2018, Edmonds Community College

Bachelor of Science, 2021, Central Washington University

Honors and Awards: Merit Scholarship Award, 2019-2021, Central Wash-

ington University

Graduate Assistantship, Mathematics Department,

2021-2023, Eastern Washington University

Graduated Cum Laude, Central Washington Univer-

sity, 2021